FZD-535

The sorption of uranium(VI) and neptunium(V) onto surfaces of selected metal oxides and alumosilicates studied by *in situ* vibrational spectroscopy

Katharina Müller

Mai 2010

Wissenschaftlich-Technische Berichte
FZD-535 2010 · ISSN 1437-322X

WISSENSCHAFTLICH-TECHNISCHE BERICHTE

Forschungszentrum
Dresden Rossendorf

Wissenschaftlich-Technische Berichte
FZD-535
2010

KATHARINA MÜLLER

The sorption of uranium(VI) and neptunium(V) onto surfaces of selected metal oxides and alumosilicates studied by *in situ* vibrational spectroscopy

Forschungszentrum Dresden Rossendorf

Acknowledgements

The research in this thesis was performed at the Institute of Radiochemistry at the Forschungszentrum Dresden-Rossendorf e.V. It was funded mainly by the Deutsche Forschungsgemeinschaft. I would like to express my deepest gratitude to all who have contributed to this work.

At first, grateful thanks are due to Prof. Dr. G. Bernhard for the scientific supervision, for introducing me to the exciting field of radiochemistry and for his efforts during the completion process.

I would like to express my sincere gratitude to my supervisor Dr. H. Foerstendorf for the patience, the practical advice and constant encouragement. I thank for valuable discussions and critical comments on the manuscripts. I could not have imagined a better scientific guidance.

I gratefully acknowledge the efforts of Dr. V. Brendler for the introduction to thermodynamic modeling using EQ3/6, many fruitful discussions and his excellent support.

Appreciation is due to R. Steudtner for TRLFS analysis, scientific discussion and a humorous PhD time.

I highly appreciate the enormous experimental support from T. Meusel, K. Stolze and R. Husar.

I wish to thank Dr. S. Tsushima for valuable discussions on quantum chemistry.

I acknowledge the assistance of Dr. A. Ikeda and Dr. K. Takao and the advice of Dr. G. Geipel during the preparation of the Np stock solutions.

I am pleased to thank K. Heim and B. Li for their technical assistance in FT-IR spectroscopy, U. Schaefer and A. Ritter for ICP-MS, C. Eckardt for BET measurements, S. Weiß for PCS, C. Nebelung for α-, γ-spectrometry and the introduction to LSC, M. Eilzer for photo-acoustic measurements and IT support, A. Rumpel, H. Heim, and S. Henke for introducing me to important aspects of radiation protection, B. Hiller and D. Falkenberg for the construction of the small N_2 box and the technical assistance concerning glove box use, C. Kirmes for administrative support, Dr. N. Baumann for the preparation of the TiO_2 sample S5, Dr. K. Großmann for CLSM TRLFS measurements, T. Günther for AFM measurements, the PhD students of the Institute of Radiochemistry for the friendly atmosphere and their helpful attitude.

Thanks are due to Prof. Dr. G. Lefèvre for the review of my PhD thesis and for valueable discussions. Furthermore, I thank to Dr. T. Payne and Dr. J. Comarmond for providing the TiO_2 samples.

I thank the FZD for advanced vocational training opportunities.

I send my warmest thanks to my friends for their understanding, amity and support during the last four exciting years. I thank Uwe for corrections on the manuscript.

Finally, my heartfelt appreciation goes to Volker for his love and inspiration, and to my parents and my brother who have helped me to carry on for one decade in the academic and research field.

Katharina Müller
April 2010

Contents

List of abbreviations and symbols

Abbreviations:

AES	Auger electron spectroscopy
AFM	Atomic force microscopy
AMTIR	Amorphous material which transmits IR radiation
ATR FT-IR	Attenuated total reflection Fourier transform – infrared
BET	Brunauer-Emmet-Teller
CLSM	Confocal laser scanning microscopy
CV	Cyclic voltammetry
DFT	Density functional theory
ESR	Electron spin resonance
EXAFS	Extended x-ray absorption fine structure
FZD	Forschungszentrum Dresden-Rossendorf e.V.
GI-XAFS	Grazing incidence - x-ray absorption fine structure
IRE	Internal reflection element
IRS	Internal reflection spectroscopy
ICP-MS	Inductively coupled plasma mass spectroscopy
IEP	Isoelectric point
IRC	Institute of Radiochemistry at FZD
KRS-5	Thallium bromoiodide
LIPAS	Laser-induced photoacoustic spectroscopy
LSC	Liquid scintillation counting
MOX	Mixed oxide fuel
MQ-water	Milli Q water
μ-XAFS	Micro-focus option of x-ray absorption fine structure
μ-XRD	Micro-focus option of x-ray diffraction
μ-XRF	Micro-focus option of x-ray fluorescence
NIR	Near infrared
NMR	Nuclear magnetic resonance
NEA	Nuclear Energy Agency
OECD	Organization for Economic Co-operation and Development
OD	Optical density
PCS	Photon correlation spectroscopy
PWR	Pressurized water reactor
PZC	Point of zero charge
SCM	Surface complexation model
SEM	Scanning electron microscopy

SIT	Specific ion interaction theory
SNF	Spent nuclear fuel
TDB	Thermochemical database (NEA)
TMA-OH	Tetramethylammonium hydroxide
TRLFS	Time-resolved laser-induced fluorescence spectroscopy
UV	Ultra-violet
Vis	Visible
XAS	X-ray absorption spectroscopy
XANES	X-ray absorption near-edge structure
XPS	X-ray photoelectron spectroscopy
XRD	X-ray diffraction

Symbols and their units:

α	Absorptivity of the sample	
d_e	Effective thickness	µm
d_P	Penetration depth	µm
Kd	Distribution coefficient	
λ	Wavelength	nm
n	Index of refraction	
R	Retardation	
θ	Internal reflection angle	degree
υ	Wavenumber	cm^{-1}

Summary

The migration behavior of actinides and other radioactive contaminants in the environment is controlled by prominent molecular phenomena such as hydrolysis and complexation reactions in aqueous solutions as well as the diffusion and sorption onto minerals present along groundwater flow paths. These reactions significantly influence the mobility and bioavailability of the metal ions in the environment, in particular at liquid-solid interfaces. Hence, for the assessment of migration processes the knowledge of the mechanisms occurring at interfaces is crucial. The required structural information can be obtained using various spectroscopic techniques.

In the present study, the speciation of uranium(VI) and neptunium(V) at environmentally relevant mineral – water interfaces of oxides of titania, alumina, silica, zinc, and alumosilicates has been investigated by the application of attenuated total reflection Fourier-transform infrared (ATR FT-IR) spectroscopy. Moreover, the distribution of the hydrolysis products in micromolar aqueous solutions of U(VI) and Np(V/VI) at ambient atmosphere has been characterized for the first time, by a combination of ATR FT-IR spectroscopy, near infrared (NIR) absorption spectroscopy, and speciation modeling applying updated thermodynamic databases.

From the infrared spectra, a significant change of the U(VI) speciation is derived upon lowering the U(VI) concentration from the milli- to the micromolar range, strongly suggesting the dominance of monomeric U(VI) hydrolysis products in the micromolar solutions. In contradiction to the predicted speciation, monomeric hydroxo species are already present at pH $\geq$ 2.5 and become dominant at pH 3. At higher pH levels (> 6), a complex speciation is evidenced including carbonate containing complexes.

For the first time, spectroscopic results of Np(VI) hydrolysis reactions are provided in the submillimolar concentration range and at pH values up to 5.3, and they are comparatively discussed with U(VI). For both actinides, the formation of similar species is suggested at pH $\leq$ 4, whereas at higher pH, the infrared spectra evidence structurally different species. At pH 5, the formation of a carbonate-containing dimeric complex, that is $(NpO_2)_2CO_3(OH)_3^-$, is strongly suggested, whereas carbonate complexation occurs only under more alkaline conditions in the U(VI) system.

The results from the experiments of the sorption processes clearly demonstrate the formation of stable U(VI) surface complexes at all investigated mineral phases. This includes several metal oxides, namely TiO_2, Al_2O_3, and SiO_2, serving as model systems for the elucidation of more complex mineral systems, and several alumosilicates, such as kaolinite, muscovite and biotite. From a multiplicity of *in situ* experiments, the impact of sorbent characteristics and variations in the aqueous U(VI) system on the sorption processes was considered.

A preferential formation of an inner-sphere complex is derived from the spectra of the TiO_2 and SiO_2 phases. In addition, since the *in situ* FT-IR experiments provide an online monitoring of the absorption changes of the sorption processes, the course of the formation of the U(VI) surface complexes can be observed spectroscopically. It is shown that after prolonged sorption time on TiO_2, resulting in a highly covered surface, outer-sphere complexation predominates the sorption processes. The prevailing crystallographic modification, namely anatase and rutile, does not significantly contribute to the spectra, whereas surface specific parameters, e.g. surface area or porosity are important.

A significant different surface complexation is observed for Al_2O_3. The formation of inner-spheric species is assumed at low U(VI) surface coverage which is fostered at low pH, high ionic strength and short contact times. At proceeded sorption the surface complexation changes. From the spectra, an outer-spheric coordination followed by surface precipitation or polymerization is deduced. Moreover, in contrast to TiO_2, the appearance of ternary U(VI) carbonate complexes on the γ-Al_2O_3 surface is suggested.

The first results of the surface reactions on more complex, naturally occurring minerals (kaolinite, muscovite and biotite) show the formation of U(VI) inner-sphere sorption complexes. These findings are supported by the spectral information of the metal oxide surfaces.

In this work, first spectroscopic results from sorption of aqueous Np(V) on solid mineral phases are provided. It is shown that stable inner-sphere surface species of NpO_2^+ are formed on TiO_2. Outer-sphere complexation is found to play a minor role due to the pH independence of the sorption species throughout the pH range 4 – 7.6. The comparative spectroscopic experiments of Np(V) sorption onto TiO_2, SiO_2, and ZnO indicate structurally similar bidentate surface complexes.

The multiplicity of IR spectroscopic experiments carried out within this study yields a profound collection of spectroscopic data which will be used as references for future investigations of more complex sorption systems in aqueous solution. Furthermore, from a methodological point of view, this study comprehensively extends the application of ATR FT-IR spectroscopic experiments to a wide range in the field of radioecology.

The results obtained in this work contribute to a better understanding of the geochemical interactions of actinides, in particular U(VI) and Np(V/VI), in the environment. Consequently, more reliable predictions of actinides migration which are essential for the safety assessment of nuclear waste repositories can be performed.

1. Introduction

For decades, there has been an intense debate on the most appropriate approach to manage spent fuel from nuclear power reactors. On the one hand, the waste can be directly disposed in deep geologic repositories, on the other hand, it can be reprocessed to recover and recycle the plutonium and uranium and disposing only the residual waste from the recycling process.

For disposal purposes, the waste produced is divided into two categories – heat-generating waste and non-heat-generating waste. Heat-generating waste includes spent fuel from light water and other nuclear reactors, vitrified high-level waste, and core instrumentation and residues from fuel element cladding after reprocessing. In 2040, Germany will possess 22,000 metric tons of heat-generating waste for final disposal in deep geologic formations [1].

Uranium (U) is a constituent of high-level nuclear waste arising from the nuclear spent fuel. Furthermore, it is found at elevated concentrations in the environment at facilities of former uranium mining and milling sites, e.g. in Saxony and Thuringia (Germany), and in subsurface dumps and sites with radioactive and/or heavy metal containing inventory [2, 3]. Neptunium (Np) is one of the most important components of nuclear waste to consider for the long-term safety assessment of nuclear waste repositories. Although its concentration in spent fuel is relatively low at the beginning of storage (0.5 kgT^{-1} spent nuclear fuel (SNF) in a pressurized water reactor (PWR); Fig. 1-1, left), the radioactive decay of ^{241}Am with a half life of 432.7 years causes enrichment of ^{237}Np with time. Due to its long half life (2.14×10^6 years) the hazardous isotope ^{237}Np becomes the major contributor of the total radiation in 10^5 years. (cf. Fig. 1-1, right) [4-6].

For the long-term storage of nuclear waste, the assessment of water contamination, depending on retention and migration processes of radionuclides in the geosphere, is of primary environmental concern. The migration behavior of (radioactive) contaminants, i.e. their mobility and bioavailability in the environment is strongly affected by molecular reactions occurring in and among solid, aqueous, and gas phases [7].

Hence, in the safety assessment of potential underground disposals, great attention must be paid to the geochemistry and migration behavior of both elements. Geochemical reactions,

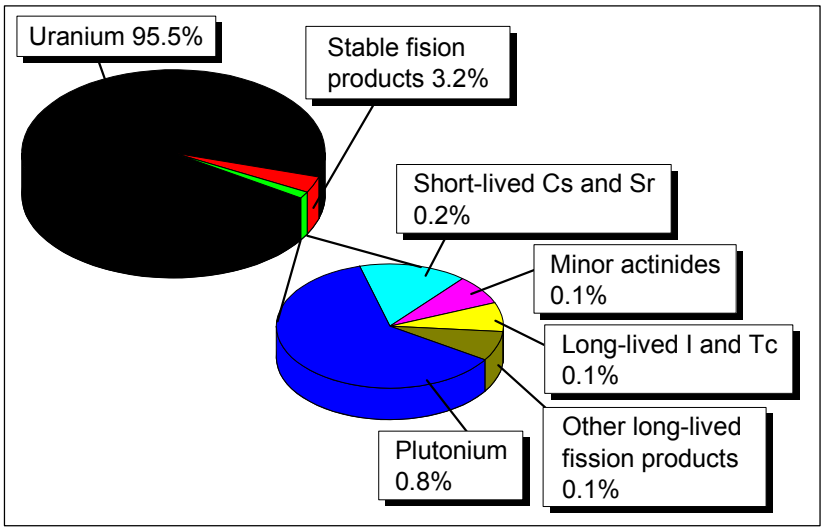

Fig. 1-1: Composition of SNF of a standard PWR with UO_2 fuel and irradiated up to a burn-up of 33 GWd/t. Extended burn-ups or the use of mixed oxide fuel (MOX) increases the amount of minor actinides (Np, Am, Cm) produced [8].

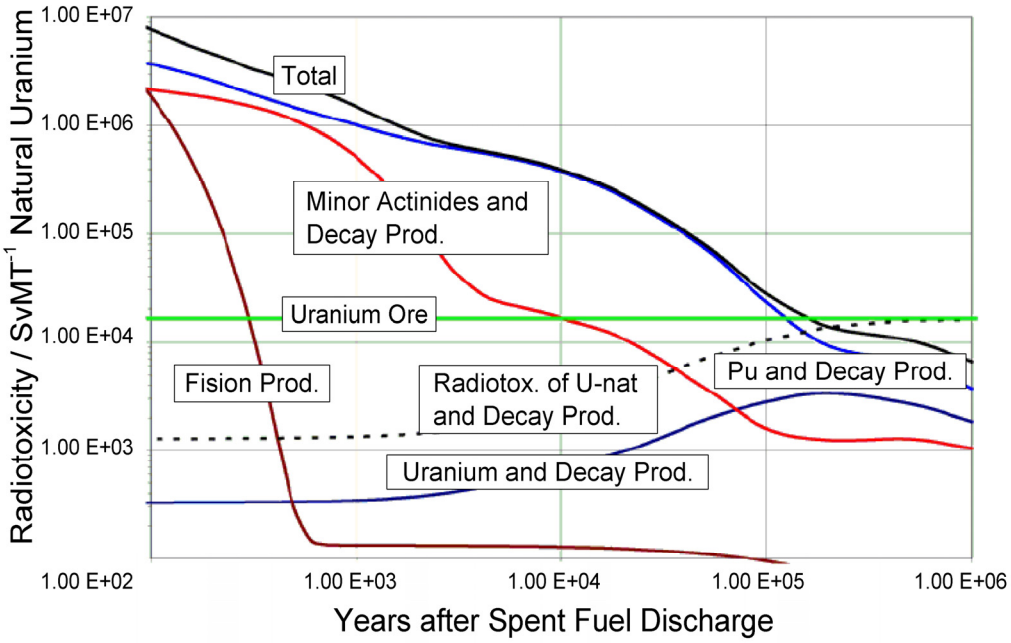

Fig. 1-2: Radiotoxicity evolution in time and its components [8].

such as complexation in solution, sorption onto mineral and biological phases, surface precipitation and colloid formation, are primarily defined by the oxidation state and the distribution of appropriate aqueous species of U and Np [9].

The current knowledge of thermodynamic constants of actinyl species in aqueous solution is based on data mainly resulting from potentiometry and solubility measurements, performed at concentrations in the millimolar range [10-12]. But the elucidation of the molecular structures of the detected species by spectroscopic techniques is still insufficient, in particular at a reduced concentration level relevant to environmental conditions.

The molecular reactions of actinides at the solid-water interface play an important role in the retardation of radionuclide migration in the environment. In recent years, the sorption

behavior of U and Np onto synthetic and naturally occurring minerals has been intensively studied, see [13] for an overview. The vast majority of these studies provide macroscopic results presenting sorption capacities of the substrates and the effect of selective parameters on the sorption behavior. Modeling of the sorption behavior has also been performed. However, for a better understanding of the sorption mechanisms, structural information on a molecular level of the type of surface complex is still needed and can be derived from spectroscopic and microscopic experiments.

The aim of this work is to contribute to a comprehensive understanding of the molecular processes and structures of the uranium and neptunium species present in aqueous solution and at the mineral-water interface. For this approach, vibrational spectroscopy was chosen as a methodic focus, since this technique potentially provides molecular information which can be directly derived from the spectral data obtained.

The speciation of the hexavalent cations of U and Np in aqueous solution is studied as a function of several parameters, such as pH, concentration, and the presence of carbonate. For the first time, ATR FT-IR and NIR spectroscopy are applied to low concentrated actinyl(V/VI) solutions, since they are useful tools for the identification of aqueous molecular species. The results are comparatively discussed with predictions based on currently accepted thermodynamic data.

For the elucidation of molecular processes of hexavalent U and pentavalent Np at the solid-water interface, metal oxides of alumina, silica, titanium and zinc are chosen as model substrates. Furthermore, the sorption mechanisms are studied on alumosilicates, e.g. kaolinite, biotite and muscovite, exemplarily for complex mineral surfaces as found in environmental scenarios. For the first time, the U(VI) surface speciation is intensively investigated using a variety of minerals, and as a function of several sorption parameters. The experiences from the characterization of aqueous Np species and surface U(VI) species are used for the very first *in situ* IR spectroscopic study of the molecular Np(V) sorption reactions.

With the obtained spectroscopic results an increased confidence in the thermodynamic data and an improvement of migration modeling of both actinides can be achieved. Furthermore, the obtained data may serve as analogue for the elucidation of the environmental behavior of more complex actinide systems, e.g. plutonium which simultaneously exists in several oxidation states. The results obtained at a lower concentration level are more relevant for the specific conditions occurring in the near and far field of radioactive waste repositories.

The findings are expected to contribute to a more reliable safety assessment.

2. Speciation of uranium and neptunium in the environment

In this study, the speciation of the actinides uranium (U) and neptunium (Np) has been investigated in solution and on mineral surfaces. In the following sections, some general chemical and physical information on both actinides is provided, and their reactions in aqueous solutions under distinct conditions and at the mineral-water interface are described.

2.1 Properties of uranium and neptunium

Interrupting the series of the 6d transition elements, the actinides, also known as 5f elements, appear in the last row of the periodic table, because of the completion of the 5f orbitals. The chemical similarity to the lanthanides (4f elements) was recognized nearly 50 years ago and provided the framework for the design of chemical methods for the isolation and identification of the heavier actinides [14]. In comparison to the 4f series, the 5f electrons are shielded to a larger extent from the nucleus of the atom resulting in a smaller energy difference between the 5f, 6d and 7s electrons than in the lanthanide series. Consequently, the number of oxidation states of the actinides is generally increased [15]. Tab. 2-1 depicts the possible oxidation states of several actinides in light grey, the most stable ones of environmental relevance are shown in dark grey.

Actinide ions of the same oxidation state have essentially the same molecular structures. In acidic solutions, four structural species are possible. The spherical ions of An^{3+} and An^{4+} exhibit strong affinity to solvation, hydrolysis and polymerization. For the higher oxidation states, the effective charge on the simple ion is reduced by formation of the dioxygenated species, referred to as actinyl ions (AnO_2^{n+}). These ions are stable entities and travel as a unit through a great variety of chemical transformations [15]. The stabilities of the aqua ions of U and Np are summarized in Tab. 2-2.

Tab. 2-1: Chemical and physical properties of actinides [15-18].

	Th	Pa	U	Np	Pu	Am	Cm
Atomic number	90	91	92	93	94	95	96
Electr. config. (g)	$5f^0 6d^2 7s^2$	$5f^2 6d^1 7s^2$	$5f^3 6d^1 7s^2$	$5f^4 6d^1 7s^2$	$5f^6 7s^2$	$5f^7 7s^2$	$5f^7 6d^1 7s^2$
Ox. states / species							
II (An^{2+})							
III (An^{3+})							
IV (An^{4+})							
V (AnO_2^{+})							
VI (AnO_2^{2+})							
VII (AnO_2^{3+})							

Vibrational spectroscopy showed that the free actinyl ions exist as linear, or almost linear molecule groups, sharing the same $D_{\infty h}$ symmetry [19]. Hence, the very stable and less radioactive ion UO_2^{2+} can serve as an analog for the hexavalent ions of Np, Pu, and Am. Similar, the NpO_2^{+} ion is a stable reference system for the pentavalent ions of Pu and Am [20].

A major advantage associated with the use of these oxidation state analogs is that macro concentrations of the analogs can be studied since the oxidation state distribution is not a function of the concentration as it is, e.g. for plutonium. The primary requirements for choice of the cations used as oxidation state analogs are: that they are in the same oxidation state, are hard acid cations, and have a radius similar to the ion of interest [21].

2.2 Reactions in aqueous solution

Water is the dominant transport medium for the migration of actinides through environmental compartments. Most natural waters are relatively mild, i.e. typically, they are near neutral (pH 5 – 9) with a wide range of redox potentials (−300 – 500 mV) and low salinities (ionic strength ≤ 1 M) [22]. The water conditions determine the predominating

Tab. 2-2: Stability of the aqua ions of U and Np [15].

Aqua ions	Color (in 1 M $HClO_4$)	Stability
U^{3+}	red	Aqueous solutions generate hydrogen on standing
U^{4+}	green	Stable to water, but slowly oxidized by air to UO_2^{2+}
UO_2^{+}	mauve	Disproportionates to U^{4+} and UO_2^{2+}
UO_2^{2+}	yellow	Stable, difficult to reduce
Np^{3+}	blue to purple	Stable to water, but readily oxidized to Np^{4+}
Np^{4+}	yellow-green	Stable to water, but slowly oxidized by air to NpO_2^{+}
NpO_2^{+}	green	Stable, disproportionates only at high acidities
NpO_2^{2+}	pink to red	Stable, easy to reduce
NpO_2^{3+}	dark green	Observed only in alkaline solutions

actinide oxidation state and the stable species. For instance, Fig. 2-1 shows the Porbaix diagram (Eh vs pH) for U and Np in water, exemplifying the complexity of U and Np redox chemistry. The normal range of natural waters is outlined in the diagrams and overlaps with the stability fields of U and Np in different oxidation states.

In most ocean and groundwater environments, U is present in the hexavalent state. U(III) is unstable under most conditions and oxidizes easily to U(IV), while U(V) disproportionates esily to U(IV) and U(VI). The redox behaviour of Np is different. The pentavalent Np is expected to be the most stable oxidation state in groundwaters and in the ocean. Np(III) and Np(VI) are on the edges of the water stability region and can exist under strongly reducing or oxidizing conditions, respectively. However, in aquatic environments such as streams, brines and bogs, the predominance of the tetravalent oxidation states are predicted [22]. For the investigation of the speciation of such redoxsensitive compounds a precautionary approach must be taken to the predominant oxidation state. Using appropriate analytical techniques the distribution of the redox species should be monitored during the whole experimental time scale. In this work particular attention was paid to the reduction of Np(VI) to Np(V) in aqueous solution (cf. section 4.2) and to photocatalytic processes of sorbed U(VI) on the TiO_2 surface (cf. section 5.3).

In natural waters, complexation of the actinide ions is an important factor has a strong influence on their speciation. By altering the charge and composition of actinide ions in solution, complexation with carbonate significantly increases actinide solubility, and largely

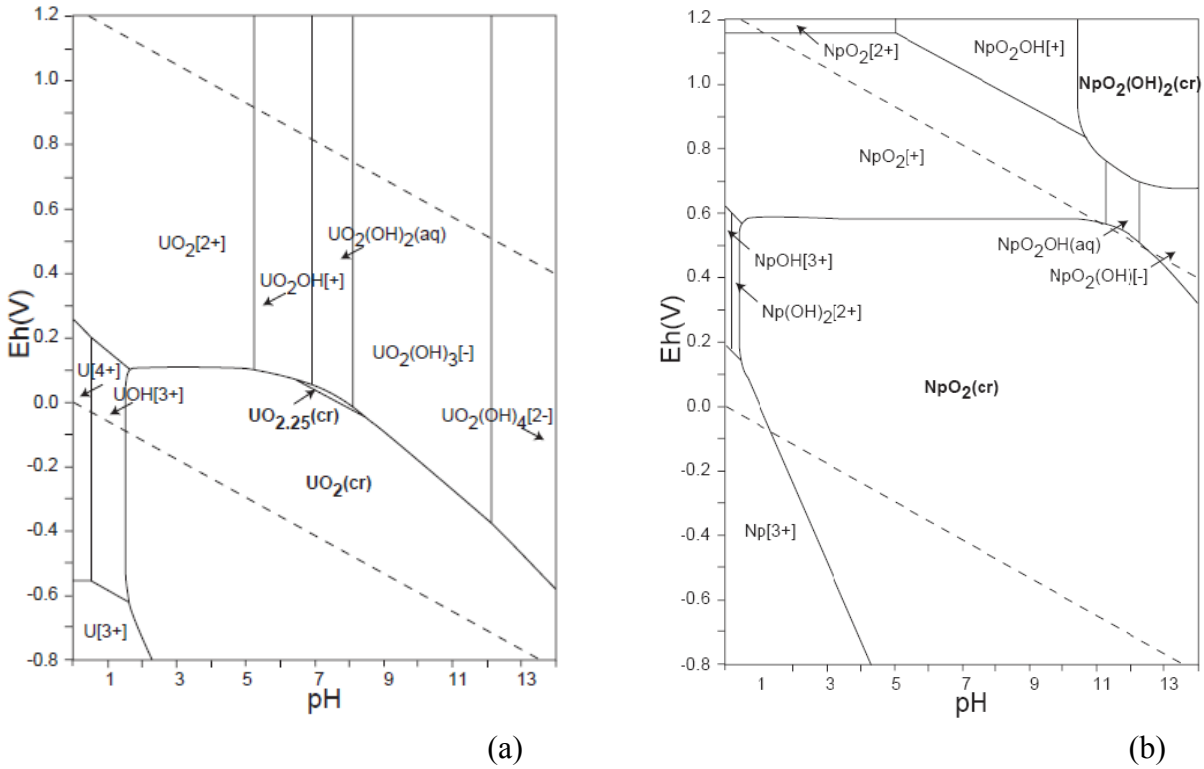

Fig. 2-1: Pourbaix diagrams for U (a) and Np (b) based on updated NEA TDB [11]. The area between the two dashed diagonal lines indicates the stability field of water at 298.15 K and 10^5 Pa [23].

Tab. 2-3: Comparison of thermodynamic complex formation constants of Np(V/VI), U(VI) and Pu(VI) [11].

Log K	NpO_2^+	NpO_2^{2+}	UO_2^{2+}	PuO_2^{2+}
AnO_2OH^+	2.70	8.40	8.75	8.40
$AnO_2CO_3(aq)$	4.96	9.32	9.94	9.50
$AnO_2SO_4(aq)$	0.44	3.28	3.15	3.38
$AnO_2HPO_4(aq)$	2.95	6.20	7.24	-
AnO_2F^+	1.20	4.57	5.16	4.56
AnO_2Cl^+	-0.40	0.40	0.17	0.23

affects actinide sorption [24]. The complexation strength is a figure of merit describing the effectivity of a ligand to compete with water in the coordination sphere of an actinide ion. Actinide ions are “hard” Lewis acids and consequently form strong complexes with highly ionic “hard” ligands, such as carbonate and hydroxide [25]. The relative tendency of actinides to form complexes generally follows the trend: An(IV) > AnO_2^{2+} ≥ An(III) > AnO_2^+[25]. As an example the formation constants of similar complexes of pentavalent Np and of the hexavalent cations of U, Np and Pu are compared in Tab. 2-3. The complexation behavior of the hexavalent ions is very similar, whereas Np(V) shows distinctly reduced complexation in comparison to Np(VI).

The speciation of the hexavalent ions of Np and U in aqueous solution is basically controlled by hydrolysis reactions and carbonate complexation with a strong dependence on the concentration level and pH range [24, 26]. Hydrolysis begins at pH 3 and several hydroxo, carbonate, and / or mixed species can simultaneously be present in solution. At low micromolar AnO_2^{2+} concentrations, monomeric hydroxo species, e.g. $AnO_2(OH)^+$ are expected, while at higher concentration polymeric species, e.g. $(AnO_2)_2(OH)_2^{2+}$ or $(AnO_2)_3(OH)_5^+$ are formed [21, 27, 28]. Actinyl(VI) carbonate systems are usually quite complex, since they often consist of several different complex ions in rapid equilibria with one another. There is little doubt about the compositions of the three monomeric complexes $AnO_2(CO_3)$, $AnO_2(CO_3)_2^{2-}$, $AnO_2(CO_3)_4^{3-}$ [21, 24]. Polymeric species are found to play a major role at high ionic strength and high metal ion concentration [24]. In contrast, the speciation of the pentavalent form of Np is not that sophisticated. Np(V) hydrolyzes in solution solely at pH > 9. In the presence of carbonate, different monomeric complexes are formed, e.g. $NpO_2(CO_3)^-$, $NpO_2(CO_3)_2^{3-}$, $NpO_2(CO_3)_3^{5-}$ [29-31]. There is no evidence for the formation of polymeric species.

A detailed understanding of the chemical equilibria and the formation constants, that correspond to actinide species, may allow thermodynamic modeling of radionuclide speciation and solubility in aqueous environments [11]. The Organization for Economic Co-operation and Development, Nuclear Energy Agency (OECD NEA) initiated a series of detailed expert reviews on the chemical thermodynamics of key elements in nuclear technology and waste management. Up to now, several volumes of the thermochemical database (NEA TDB), including uranium and neptunium, have been published [10-12].

For the U(VI) hydrolysis species 65 references from 1947 to 1991 and 15 further references from 1992 to 2002 were reviewed by Grenthe et al. [10] and Guillaumont et al. [11]. Stability constants of approximately 50 studies were taken into account, to some extent they were re-evaluated and re-interpreted, i.e. using chemical models thought to be more realistic. Re-evaluation was applied to correct for known systematic errors and to extrapolate to standard state conditions. Namely, the extrapolation to infinite dilution was based on the Specific Ion Interaction Theory (SIT) approach [32]. Furthermore, uncertainties of the 95% confidence level are provided in the reviews, but these assignments are often based on a subjective choice, that is, the scientific expertise of the reviewers [11]. It must also be mentioned that in the first NEA database, published in 1992, most values for the determination of stability constants of U(VI) hydroxo complexes arise from non-structural experiments [10], such as potentiometry providing more than 90% of the used raw data, and a few data sets coming from solubility measurements, ion-exchange, liquid-liquid-extraction, or calorimetry. Colorimetry and spectrophotometry were applied only to a very small extent. In the updated NEA TDB from 2003, new experimental methods, in particular some spectroscopic studies, were considered in addition to the "traditional" thermodynamic methods [33-36].

In contrast to the thoroughly studied U(VI) hydrolysis and carbonate complexation, less data is available for Np(VI). This is clearly demonstrated by a cumulative view on the related NEA TDB volumes. Namely, the Np(VI) thermodynamic data only rely on 3 and 13 original references reviewed by Lemire et al. in 2001, for the aqueous hydroxide and carbonate systems, respectively; none of them offering any structural information [12]. For Np(VI) hydrolysis, only one work (Cassol et al., 1972) was integrated in the NEA data pool. The data result from acidity measurements of Np(VI) hydrolysis at concentrations in the range of 0.3 – 80 mM (1 M ClO_4^-) in the absence of atmospheric CO_2 [37]. Lemire et al. point out that there are no reliable data available which support thermodynamic parameters for $NpO_2(OH)_2(aq)$ or for neutral or anionic polymeric Np(VI) hydrolysis species, although such species may well exist [12]. In case of Np(VI) carbonate complexation, the authors suggest thermodynamic values in analogy to the better known U(VI) species with large uncertainties. They also provide maximum formation constant values, rather than proposing no value at all. However, there is satisfactory experimental information available for only two Np(VI) complexes in aqueous carbonate/bicarbonate media, namely $NpO_2(CO_3)_3^{4-}$ and $(NpO_2)_3(CO_3)_6^{6-}$ [12]. The thermodynamic data of Np(VI) mixed hydroxo carbonate complexes only result from a very few original publication and are additionally extrapolated from U(VI) [38]. In 2003, data of Np(VI) hydrolysis and carbonate complexation was retained in the updated NEA TDB since new data was not available [11].

For the Np(V) hydrolysis constants in the NEA TDB of 2001, Lemire et al. reviewed several data mainly arising from solubility and potentiometric measurements and the consensus is that both $NpO_2OH(aq)$ and $NpO_2(OH)_2^-$ can be considered as hydrolysis species. Although there might be evidence for an additional anionic hydrolysis species in strongly

basic solutions no reliable values of the formation constants are evaluated [12]. In the update from 2003, the hydrolysis constants were retained unchanged [11]. An analysis of the literature data concerning Np(V) behaviour in aqueous solutions was carried out by Kaszuba and Runde, evidencing the reduced stability of $NpO_2OH(aq)$, and that $NpO_2(OH)_2^-$ and the mixed Np(V) hydroxo carbonate species become important at high pH [6].

2.3 Reactions at the solid-water interface

The solubility of an actinide species provides an upper limit for the contaminant concentration in the aqueous solution and is considered as a first barrier to actinide transport. As a second barrier, the reaction of actinides at the mineral/rock-water interface is expected. When the actinide concentrations are far below the solubility limits, the interfacial processes dominate the migration [40]. Actinide sorption onto mineral surfaces depends on several factors, e.g. actinide's speciation and concentration, the flow rate and the chemistry of the water and the mineral composition [22]. Furthermore, different mechanisms can occur at the mineral/rock-water interface, including physical adsorption, ion-exchange, chemisorption, surface precipitation, sorption of colloidal actinide phases, electron transfer (oxidation state changes), coordination changes (number and/or type of ligands around the sorbed species), relaxation or reconstruction of the surface structure, dissolution of the substrate, diffusion into crystal lattice and the formation of solid solutions [7, 14, 41].

Physisorption or formation of an outer-sphere complex occurs when a charged complex retains its hydration shell and is hydrogen bonded or attracted to the surface via long-range forces, i.e. electrostatic and van-der-Waals attraction (Fig. 2-2a). Electrostatic adsorption is frequently rapid and reversible, e.g. ion-exchange reactions [14, 42]. Chemisorption or formation of inner-sphere complexes, mostly irreversible, results from the loss of water molecules of the hydration shell and direct short-range chemical bonding, e.g. covalent bonding or hydrophobic forces [42]. Inner-sphere complexes may bond to one, two or more surface oxygens, resulting in monodentate, bidentate or multidentate configurations (Fig.

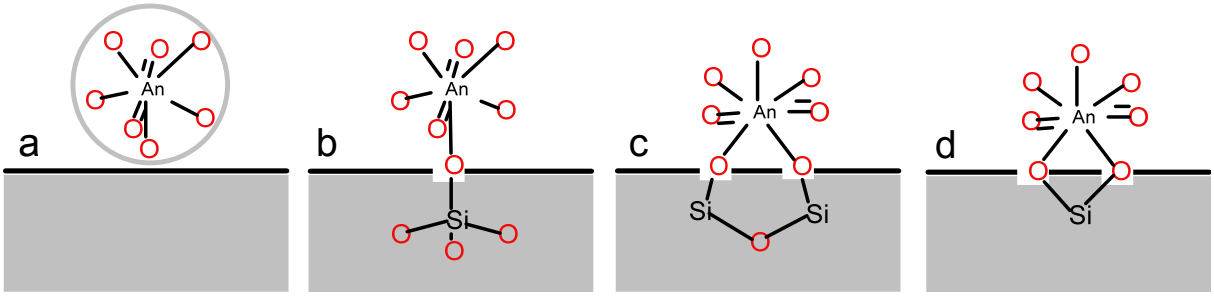

Fig. 2-2: Illustration of possible uranyl surface complexes on SiO_2: (a) outer-sphere adsorption, (b) monodentate inner-sphere adsorption, (c) bidentate inner-sphere adsorption to two silicon atoms, (d) bidentate inner-sphere adsorption to a single silicon atom. Bond angles and distances are not scaled, according to [44].

2-2b-d). Because of the different bond strengths, inner-sphere complexes are typically more strongly bound to the surface than outer-sphere complexes [43].

Batch sorption and less often diffusion experiments are carried out to determine a distribution coefficient, i.e. K_d, that is the concentration ratio between the actinide in the solid and the liquid phase [45]. In the migration assessment, K_d is used to calculate the retardation R of the contaminant through a porous media. However, K_d values strongly depend on the experimental conditions, e.g. temperature, actinide concentration, pH, presence of complexing ligands and competing elements. K_d values are often considered as equilibrium values, but, in fact, it is often difficult to ascertain the achievement of an equilibrium state. Hence, extrapolation of K_d values to environmental conditions bears some risks [46]. Sorption isotherms, e.g. Langmuir, Freundlich, and Dubinin-Radushkevich, represent the variation of the actinide concentration in the solid phase, or the variation of K_d, versus the equilibrium concentration in the aqueous phase at a constant temperature. Isotherms are fitted by mathematical methods according to some theoretical bases, but are often interpreted empirically [46].

For a more accurate quantification of sorption data, a mechanistic modeling approach involving surface complexation is required [39, 47]. Several surface complexation models (SCM) have been developed, based on geochemical principles, each with own definitions and specific parameters of the water-mineral interface [48, 49]. To simulate sorption, namely the Diffuse Layer Model, the Constant Capacitance Model and the Triple Layer Model provide capabilities for the modeling of key aspects of an observed sorption behavior [48, 49]. But in many cases, radionuclide sorption was not interpreted using SCM approaches, due to uncertainties in the thermodynamic data, lack of experimental results over a range of experimental conditions, or missing appropriate mineral specific parameters [48].

For a mechanistic understanding of the reactions occurring at the water-mineral interface and to improve modeling approaches a direct identification of molecular chemical species is crucial. This led to an increasing application of spectroscopic and microscopic techniques for the study of environmental systems [7, 43, 50]. Information on elemental and isotopic abundance, chemical form, bonding and/or speciation is provided by vibrational spectroscopy (IR, Raman), X-ray absorption spectroscopy (XANES, EXAFS), laser spectroscopy (TRLFS, LIPAS) resonance (NMR, ESR) and radiation scattering (XRD) [7, 41, 51-53]. Imaging of surfaces and further spatially resolved information can be obtained by microscopic techniques, such as electron scanning or atomic force [7]. In recent years, quantum-chemical approaches, e.g. DFT calculations, have provided additional structural information about the species and their spectroscopic properties [54-63].

Tab. 2-4 lists some of the published sorption studies performed with U(VI) and Np(V) in recent years. Although for U(VI) only a small fraction is selected, the literature of Np(V) is almost completely shown.

In case of U(VI) the sorption behavior onto numerous synthetic and natural sorbents has been investigated by batch and diffusion experiments. Furthermore the surface complexation was studied on a molecular level using spectroscopic and mictroscopic techniques. Moreover, theoretical calculations for further molecular data and modeling of sorption were preformed. In contrast, data of Np(V) sorption are seldom. Few studies report the results of batch experiments and even less investigations, only XAS, were carried out for the elucidation of sorption processes on a molecular level. New spectroscopic techniques working *in situ* at environmental conditions and at low concentrations were seldom applied to U(VI) for confirmation of the previous findings. For an mechanistic understanding they should also be adopted to the study of Np(V) surface complexation. Details of previous studies are later discussed comparatively with the results from this study.

Among the various components of geological materials, oxides and hydroxides of Fe, Al, Si, and Mn play an important role in regulating the mobility of contaminants, due to their widespread environmental presence, high sorption capacity and tendency to form coatings on mineral surfaces [108, 119]. They serve as good model systems for commonly occurring soil phases such as goethite, ferrihydrite, gibbsite, boehmite, and the octahedral sheets of clay minerals like kaolinite and micas. The exposed surface sites of these minerals are postulated to have a similar local structure and reactivity [120, 121]. Adsorption by hydroxylated aluminum and iron surface sites on these various phases is a dominant control on the fate,

Tab. 2-4: Excerpt of performed U(VI) and Np(V) sorption studies (1982-2009).

Actinide	Oxide/Mineral	Technique	Reference
U(VI)	TiO_2	Batch, Raman, XRD, ATR FT-IR, EXAFS, TRLFS, DFT	[55, 64-70]
	Iron oxy-hydroxides	Batch, ATR FT-IR, EXAFS, modeling, DFT	[58, 71-77]
	Silicon oxy-hydroxides	Batch, Raman, XRD, XAFS	[44, 55, 64, 69, 78-80]
	Aluminium oxy-hydroxides	Batch, TRLFS, XAFS, DFT	[44, 55, 56, 69, 75, 81-85]
	Kaolinite, bentonite, montmorillonite, smectite	Batch, DFT, TRLFS, EXAFS, modeling	[44, 55, 57, 78, 86-91]
	Micas (muscovite, biotite)	TRLFS	[92]
	Feldspar	Batch, modeling, XPS, AFM	[93]
	Calcite	Batch, TRLFS, EXAFS, XPS	[94]
	Apatite	Batch	[95, 96]
	Imogolite	Batch, EXAFS	[97]
Np(V)	TiO_2	Batch	[98]
	Iron oxy-hydroxides	Batch, modeling, XPS, EXAFS	[99-105]
	Silicon oxy-hydroxides	Batch, modeling	[106, 107]
	Aluminium oxy-hydroxides	Batch	[106, 108-110]
	Manganese oxy- hydroxides	Batch, XAFS	[111, 112]
	Kaolinite, bentonite, montmorillonite	Batch, modeling	[113-115]
	Micas (muscovite, biotite)	Batch	[101]
	Feldspar	Batch	[93]
	Calcite	Batch	[116]
	Apatite	Batch	[117, 118]

transport, and bioavailability of trace elements, heavy metals, and radionuclides in many environments, and plays a significant role in determining the trace element composition of the oceans [120]. In addition, these specific surfaces provide the opportunity to examine the influence of surface structure and chemical composition on reactivity.

Titanium and zinc oxides are ubiquitous in the environment, too, with an additional anthropogenic influx because of their industrial application as white pigments in construction material, cosmetics, and food. Moreover, ZnO is important for this study of Np(V) sorption since it is used for corrosion prevention in nuclear pressurized water reactors. For the investigation of sorption phenomena, TiO_2 is crucial as a trace constituent in minerals [88]. Moreover, it is often taken as a model oxide due to its stability, its low solubility over a wide pH range, and its well-known structure and surface properties [65, 98].

2.4 Migration of actinides in the environment

The performance assessment of nuclear waste disposal is one of the major issues of the nuclear fuel cycle [18]. A main concern related to the safe storage in an underground repository is the migration of radiotoxic elements in the geo- and biosphere [7, 9]. In this field, the interaction between solute, solid and gaseous environmental compartments is a crucial point. Geochemical reactions of the actinides are extremely complex, as it is schematically illustrated for Np(V) in Fig. 2-3.

For the prediction of the actinide's migration behavior, a detailed characterization of all local conditions, including the nature of site-specific minerals, temperature and pressure profiles and the conditions of the local water, in particular pH, redox potential, and ligand concentrations, is indispensable [21, 24]. Furthermore, an extended knowledge about multiple and competing chemical interactions is crucial. Processes of precipitation and dissolution of actinide bearing solids limit the upper actinide concentration in solution; complexation and redox reactions determine the distribution and the stability of the present species. The interaction of actinide species with mineral and biological phases, i.e. sorption, surface precipitation, incorporation, mineralization, diffusion and/or the formation of colloids determine if and how the migration process occurs [9, 22]. Only the mechanistic understanding of the variety of these proceses and their involving interactions results in strategies for a reliable safety assessment of nuclear waste disposals.

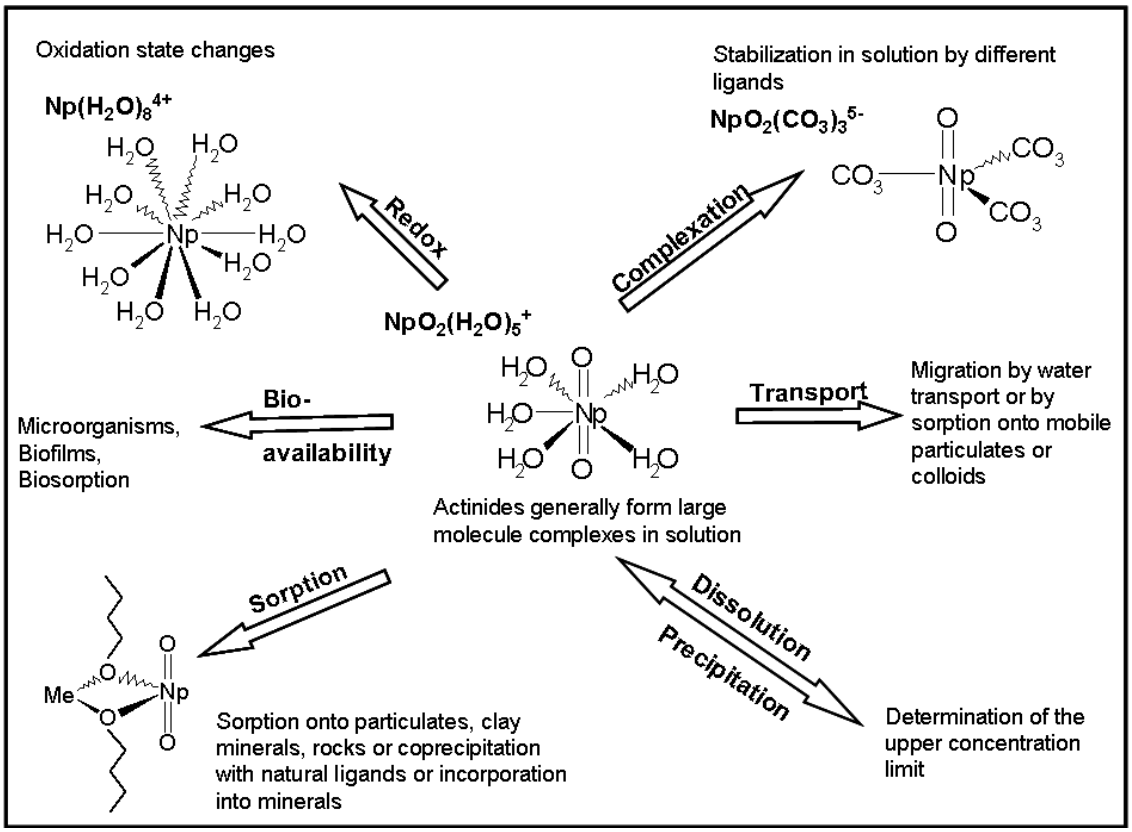

Fig. 2-3: Overview of the chemical pathways of actinides in the environment, exemplified for neptunium [22].

3. The structural information obtained by attenuated total reflection FT-IR spectroscopy

3.1 Surface analytical techniques

A detailed structural characterization of sorption, surface precipitation or even incorporation is an indispensable first step for the modeling and understanding of surface reactions. More information about surface structures on a molecular level is obtained from spectroscopic analysis, ideally by a combined approach of different spectroscopic techniques [7, 43].

Ex situ surface analytical methods, e.g. Auger and X-ray photoelectron spectroscopy (AES, XPS) are suitable to determine structural and electronic properties of certain adsorbates on clean single crystal mineral surfaces. XPS provides information on the oxidation state of the sorbed ion which may differ from the diluted species upon redox reactions, and may distinguish between different surface complexes by evaluation of changes of the binding energy for ions, such as uranyl and neptunyl [94, 103, 122, 123]. However, XPS is inefficient for most of the elements because of the small variations in the chemical environment induced by surface complexation [53]. Moreover, the measurements are performed on dried samples in a vacuum chamber. Dehydration may cause alterations or even destruction of the surface complex [124, 125]. Sorption reactions generally occur at the solid-water interface in the environment and, thus, spectroscopic techniques providing an *in situ* characterization of the molecule complexes are of special interest.

X-ray absorption spectroscopy (XAS), namely XANES and EXAFS, provides information on the nature of neighboring atoms, their coordination numbers, the distances to the central atom and the oxidation state. Thus, these methods are well suited for the study of sorption complexes, e.g. U(VI) sorption on iron (hydr)oxides, albite, and kaolinite [87, 97, 104, 112, 126-128]. However, EXAFS requires surface adsorbates with atoms that exhibit significant x-

ray absorption cross sections and is not applicable for solids composed of carbon and hydrogen atoms. Furthermore, compared to other methods, its lower detection limit hampers the application for sorption studies at low concentrations or when using sorbents with a low surface area. Because many reactions of actinides in the hydro- and geo-sphere are at interfaces surface sensitive techniques are required, such as grazing incidence XAFS (GI-XAFS) In addition, a micro-focus option is a powerful upgrade of XAS to offer spatially resolved measurements, allowing chemical state imaging (μ-XAFS), elemental mapping (μ-XRF), and identification of phases (μ-XRD) [129].

Laser fluorescence spectroscopy (LFS) is another useful technique for the *in situ* identification and characterization of sorbed molecule species on mineral phases. Time-resolved analysis (TRLFS) provides information on both lifetime and spectral signature of the adsorbed species which offers access to a number of different species and their spectral identity. The major advantages of TRLFS are its enhanced sensitivity and its combined information on concentrations and coordination. A drawback of this technique is the limited number of fluorescent species. Although U(VI) sorption complexes are investigated on gibbsite, kaolinite, albite, calcite and muscovite [82, 86, 92, 94, 128] the fluorescence properties of Np(V) are almost not studied. Moreover, the results strongly depend on the temperature of the sample and on apparatus properties. Recently, a combination of confocal laser scanning microscopy and fluorescence spectroscopy (CLSM TRLFS) has been used for the investigation of sorption processes [130].

Vibrational transitions of adsorbates measured in Raman and infrared spectroscopy occur at different energies than bulk transitions, and are sensitive to the molecular structure which makes these methods applicable for a wide range of adsorbates. A problem arising in IR spectroscopy of aqueous systems is the strong absorption of water (cf. section 3.2.3). Attenuated total reflection (ATR) elements provide conveniently short path lengths that make subtraction of strong background absorption possible [125, 131]. Reaction-induced difference spectroscopy further reduces the detection limit to the submicromolar level for the *in situ* speciation of actinide complexes in solution and on solid surfaces [27, 132], and, hence, is the technique of choice for the spectroscopic investigation of U(VI) and Np(V/VI) at the solid-liquid interface in this study.

3.2 Internal reflection spectroscopy

The principles of the ATR technique and of difference spectroscopy, as well as the methodology for *in situ* sorption experiments by coating the internal reflection element (IRE) are described in the following sections. The theory given in this chapter is adopted from selected literature [53, 125, 131, 133, 134].

3.2.1 Principles of attenuated total reflection spectroscopy

ATR, also known as internal reflection spectroscopy (IRS) bases on the formation of an evanescent electromagnetic field in a medium with a lower index of refraction (n_2) in contact with a medium of higher index of refraction (n_1) in which a propagating wave of radiation undergoes total internal reflection Fig. 3-1.

To obtain total internal reflection the angle of the incident radiation must exceed the critical angle, defined by:

$$\theta_c = \sin^{-1} n_{21}, \qquad \textbf{Eq. 3-1}$$

where $n_{21} = n_2 / n_1$ and n_1 and n_2 are the refractive indexes of the ATR crystal material and the probed medium, respectively. The amplitude of the evanescent field in the medium with the lower refraction index can be conventionally expressed as an exponential function of distance along the z axis in this medium. The decay of the electric field amplitude at the surface of this medium (E_0), to some value E at a distance (Z) from the surface is according to:

$$E = E_0 \exp\left[-\frac{2\pi}{\lambda_1}(\sin^2\theta - {n_{21}}^2)^{1/2} Z\right] = E_0 \exp(-\gamma Z), \qquad \textbf{Eq. 3-2}$$

where $\lambda_1 = \lambda_{vacuum} / n_1$ is the wavelength in the optical denser medium, θ is the internal reflection angle, and Z is the distance inside the probed medium from the surface. The penetration depth d_P of the evanescent wave from the IRE into a homogenous solution is the distance from the interface where the intensity of the electric field falls to 1 / e of its original value at the interface. According to Eq. 3-2 the penetration depth is characterized by different parameters. In a two phase system (IRE/sample) it is expressed as:

$$d_P = \frac{\lambda_1}{2\pi(\sin^2\theta - {n_{21}}^2)^{1/2}}, \qquad \textbf{Eq. 3-3}$$

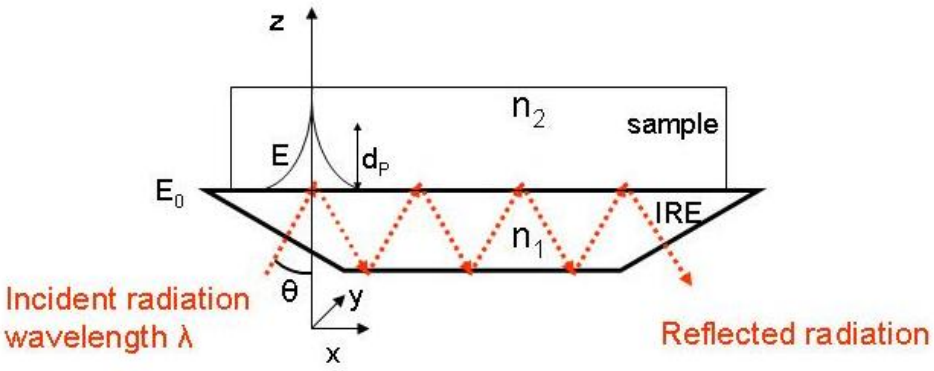

Fig. 3-1: Schematic illustration of total internal reflection with a horizontal multiple IRE, illustrating the parameters of significance: n_1 is the refractive index of the IRE; n_2 is the refractive index of the sample with $n_2 < n_1$; θ is the angle of incidence; d_P is the penetration depth. An evanescent electromagnetic field and a Cartesian axes system are also shown.

or, with υ, the frequency in wavenumbers (cm^{-1}) as:

$$d_P = \frac{10000}{2\pi\upsilon n_1(\sin^2\theta - {n_{21}}^2)^{1/2}}. \qquad \text{Eq. 3-4}$$

Although spectra resulting from ATR and transmission measurements are alike, differences are observed because of the dependence of the penetration depth on wavelength, i.e. longer wavelength radiation penetrates further into the sample, resulting in more intensive bands in the ATR spectrum. Because of the exponential decay of the intensity of the electrical field, a close contact between the sample and the surface of the IRE is essential. Typically, the value of d_P is about a few micrometers. For example, at the diamond-water interface, penetration depths from 0.8 to 2.0 µm can be calculated for the frequency range of 1800 – 750 cm^{-1} for a 45° crystal according to the refractive indexes of diamond (2.4) and water (1.33). In multiple IREs, the light is totally reflected, often several times, and the sample interacts with the evanescent wave resulting in the absorption of radiation by the sample at each point of reflection. Thus, the evanescent wave becomes attenuated and its reflectance is expressed as for N reflections as:

$$R^N = (1 - \alpha d_e)^N, \qquad \text{Eq. 3-5}$$

where α is the absorptivity of the sample. The effective thickness d_e is defined as the thickness of a film of the sample which would give the same absorbance in transmission mode as that obtained in IRS.

3.2.2 Internal reflection element materials and cell designs

Mainly two parameters are decisive for the application of *in situ* ATR FT-IR measurements of the solid-water interface: the resistance of the crystal material to solutions with acid-base characteristics (pH 4 – 10) and a low transmission threshold. In particular, when only one ATR crystal is used for measurements of different systems of solid-water interfaces, the resistance to acidic conditions is crucial regarding cleaning and potential contamination of the crystal. A low transmission threshold enables the analysis of ions with vibrational modes ≤ 800 cm^{-1} such as Np – O, Se – O, As – O. In previous *in situ* investigations of the solid-water interface, mainly ZnSe, but also AMTIR (amorphous material which transmits IR radiation, e.g. GeAsSe), Ge and diamond were used as crystal material. Other materials are less applicable, as they are soluble in water (KRS-5) or provide small transmission ranges

Tab. 3-1: Properties of ATR crystal materials [53, 125].

Material	Refractive index	Chemical resistance	Mechanical resistance	Transmission threshold / cm^{-1}
ZnSe	2.4	Etched by diluted acids and bases, eroded by zinc complexants	Easily cracked	650
AMTIR	2.5	Attacked by bases and oxidizing acids	Very brittle	750
Ge	4.0	Resistant to diluted acids and bases	Brittle	870
Diamond	2.4	Suitable to pH 1 – 14	Very hard	<200

(Si). The properties of these materials are summarized in Tab. 3-1.

According to the type of surface study, different ATR cell designs are possible, e.g. horizontal and vertical, chamber and tunnel accessories. If experiments involving adsorption to particulate matter are carried out, a horizontal trough configuration is the most appropriate.

3.2.3 Infrared spectroscopy of water

Infrared spectroscopy is one of the most sensitive physical techniques for the study of environmental processes. Nearly all geo-biochemical reactions proceed in an aqueous medium. Since water shows strong absorption bands throughout the spectral region of infrared light, the detection of vibrational modes, interfering with those of the water molecule, is impeded and interpretation of the spectra often becomes unfeasible.

The isolated water molecule shows three vibrational modes, corresponding to symmetrical and antisymmetrical stretching vibrations of the O-H bond (υ_1, υ_3), and to the bending vibration (υ_2) of the H-O-H angle [135, 136]. In contrast, the IR spectrum of liquid water is much more complex because of intermolecular interactions. The spectral ranges where the vibrational modes of light (H_2O) and heavy (D_2O) water are observed in the IR spectra are depicted in Fig. 3-2. H_2O shows a strong and very broad absorption band < 800 cm^{-1}, arising from so-called libration modes (υ_L), that represents a collective normal mode involving a network of water molecules. Further absorption at ~2130 cm^{-1} is assigned to a combination of libration and the bending vibrations (υ_2) and at ~1640 cm^{-1} is due to υ_2. The strongest band, centering at ~3400 cm^{-1} includes three components: an overtone of bending vibration ($2\upsilon_2$) and the stretching modes υ_1 and υ_3.

The isotopic shift of the vibrational modes in heavy water (D_2O) can be used to shift the frequency range of the main absorption bands of the solvent to spectral regions not interfering with vibrational modes under investigation [54, 65, 71]. The vibrational modes of D_2O are red shifted by several hundred wavenumbers, as shown in Fig. 3-2. Generally, traces from H_2O contribute to the infrared spectra resulting in vibrational modes of HDO molecules. As a

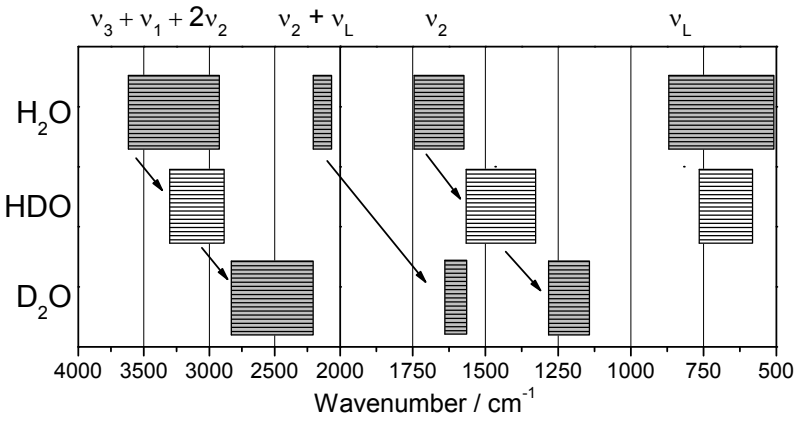

Fig. 3-2: Vibrational modes of water [135, 136].

result, υ_2 is exhibited at ~1460 cm^{-1}. Hence, using H_2O and D_2O for the performance of IR measurements, may allow an optimization of the instrumental set-up and, therefore, may enhance the spectral information. From a thermodynamic point of view, changes in the geochemical reactions according to the isotopic shift of water have not been reported, yet. In a spectroscopic study of the hydrolysis, colloid formation and solubility of Np(IV), Neck et al. found no variations of the thermodynamic constants depending on whether deuterated water was used or not [137]. In recent years several geochemical reactions, e.g. sorption, complexation, hydrolysis, and solubility have been investigated using a multiplicity of spectroscopic techniques, namely ATR FT-IR, Raman, NMR, LPAS in deuterated systems [54, 56, 65, 71, 137, 138].

3.2.4 Reaction-induced infrared difference spectroscopy

The absorbance changes observed during complexation and sorption processes of contaminants at a low concentration level are very small, i.e. they often do not exceed 0.01% of the total sample absorbance. Consequently, they can not be resolved in spectra recorded in the classical way of optical absorption spectroscopy (simple subtraction of a reference from a sample spectrum), because of precision limits for the adjustments of sample preparations and concentrations, thermal fluctuations, etc. In some cases differences can be observed by direct subtraction or by analyzing the spectra using band narrowing methods, e.g. second-derivate techniques, Fourier self-deconvolution and fine-structure enhancement [139]. However, it appears that the various methods lead to differences in the resulting spectroscopic data, thus, leaving some subjectivity for the analysis of the bands [140]. Hence, an alternative technique, called reaction-induced difference spectroscopy overcomes these difficulties and is more appropriate for most applications. The spectra of one single sample are recorded before and after a selective change of the sample (e.g. pH change, induced sorption, etc.). This strategy yields subtle vibrational difference spectra exclusively arising from the particular structural changes in the sample. Constant parts, mostly contributions from strong absorbing background comprising bulk water but also contributions from the instrumental setup are eliminated (Fig. 3-3). This implies the high demands on the stability of the components of the experiments within the time range of the reaction (up to several hours).

The single beam spectra of a carbonate containing solution before and after complexation with uranyl are exemplarily illustrated in Fig. 3-3. The difference spectrum only provides vibrational information on the formed U(VI) tricarbonate complex, with positive bands at 1507, 1382 and 893 cm^{-1}, the negative band is due to an excess of carbonate.

The “trigger” inducing the reaction should provide a minimum disturbance of the sample, but specifically and quantitatively start the reaction. A variety of reactions can be investigated using reaction-induced difference spectroscopy, e.g. complexation processes, light-driven reactions, redox-reactions [139-141]. Furthermore, the combination with time-resolved

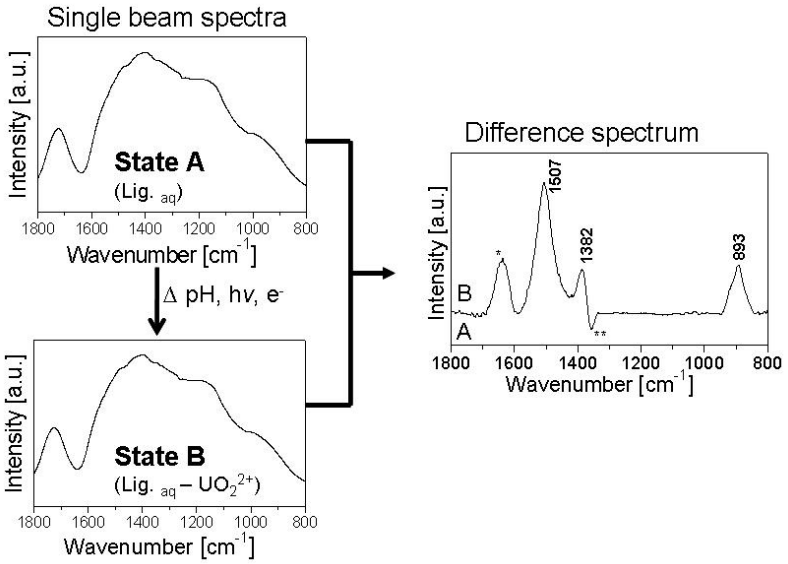

Fig. 3-3: Principle of reaction-induced infrared difference spectroscopy. The difference spectrum is calculated from two single beam spectra obtained from a unique sample before and after addition of U(VI). Constant parts from the spectra are removed (see text). Note that the amplitude of the difference spectrum is reduced by ~ 5 orders of magnitude compared to the single beam spectra.

measurements to obtain dynamic information is attractive, in particular for fast reactions from the milli- to the nanosecond time range [139, 140]. Reactions at the solid-water interface, studied in this work, are relatively slow, and the progress of surface complexation can be monitored in the subminute interval [132].

3.2.5 Interfacial spectroscopic studies of sorption processes

In recent years the *in situ* studies of surfacial processes have mainly focused on adsorption from solution directly onto the IRE, a thin film coated onto the IRE, or a finely dispersed solid making close contact with the IRE [125, 133]. The first technique can only be applied to those kinds of adsorbents that are used as reflection elements, mainly germanium, fluorite, aluminum oxide and silicon oxide [125, 134]. This limitation was overcome by investigations using a coated IRE or particulate matter in contact with the IRE.

Adherent particle films with thicknesses comparable to the penetration depth of the evanescent wave may be formed on the ATR crystal from suspensions or sols by drying small volumes, by dip coating, or by spin coating [142]. The resulting films are porous and can have a significant residual content of the solvent, e.g. water. The ATR FT-IR approach can be applied to any solid which can be formed into a particle film, remaining intact when immersed in the relevant solution. Up to date, several particulate solids have been applied, e.g. TiO_2, Al_2O_3, Fe_2O_3, FeOOH, mostly providing high specific surface areas in order to increase the likelihood of obtaining close contact and to allow the probing of a high amount of sorbed species [53, 125, 142]. Several procedures for the preparation of thin mineral films on ATR crystals are reported in the literature [124, 143, 144]. However, the characteristics of the

prepared films are less discussed in the literature. In some studies, micro Raman spectroscopy and microscopy, i.e. SEM, AFM are used to determine the distribution, the homogeneity and the thickness of the deposits on the crystal or on glass [71, 131, 143, 145]. Film thicknesses are reported to be in the 0.2 – 2.5 µm range [53, 124]. The prepared films are in many cases stable over a wide pH range [142]. Most of the measurements are performed *in situ* using flow cells, with flow rates ranging between 1 and 7 mL min^{-1} [53].

Most recent ATR FT-IR studies have dealt with the characterization of surface complexes of light oxoanions MO_n^{m-} (CO_3^{2-}, SO_4^{2-}, PO_3^{2-}, and AsO_4^{3-}) through the IR absorption by M−O stretching [54, 143-147]. For heavier oxoions, like UO_2^{2+}, NpO_2^{2+}, and NpO_2^{+}, the analysis becomes feasible by recording the double bond stretching, e.g. U=O [65, 71]. The concentrations of the dissolved species applied in solid-solution interface studies concerning environmental pollution vary between the micromolar, e.g. for radioactive tracers like uranium, to the molar range, e.g. for fertilizer particles (phosphate) or pollutants in acid mines drainage water (arsenate, sulfate) [71, 144, 145, 147]. Similar to other surface analytic methods, the sensitivity depends strongly on the surface coverage. The previously explained methodology for *in situ* sorption experiments leads to an increased volume-to-mass ratio. Consequently, high coverage can be performed even at low dissolved concentrations. Among others, the number of internal reflections, the specific surface area, the reactivity of the solid, as well as the absorptivity of the probed ion are crucial parameters for the sensitivity of the ATR measurement [53, 125].

3.3 ATR FT-IR spectroscopy at the IRC

3.3.1 Instrumental set-up

In situ ATR FT-IR spectra of aqueous solutions and sorption processes at the mineral-water interface were measured on a Bruker Vertex 80/v vacuum spectrometer equipped with a mercury cadmium telluride (MCT) detector. The spectra were averaged over 256 scans and the spectral resolution was 4 cm^{-1}. The used ATR unit DURA SamplIR II (Smiths Inc.), a horizontal diamond crystal (d = 4 mm) with nine internal reflections on the upper surface and an angle of incidence of 45°, was purged with a current of dry air (dew point < 213 K).

The detection of the absorption of diluted systems requires an adequate subtraction of the background which can satisfactorily be achieved by a thermally equilibrated acquisition system. The set up of the performed flow measurements is illustrated in Fig. 3-4.

A blank solution, i.e. reference sample, at the same conditions (pH, temperature, ionic strength) as the sample under investigation is rinsed with constant reduced flow velocity of 0.2 mL min^{-1} through a flow cell mounted on the diamond ATR crystal. The flow cell includes a volume of 0.2 ml. Thus, using a flow velocity of 0.2 mL min^{-1} the whole sample

volume is exchanged within one minute. Continuous acquisition of IR spectroscopic data monitors *in situ* the equilibration of the system. After a constant baseline is obtained, showing absorption changes less than ~10^{-4} OD in the wavenumber range of the water band at ~1640 cm^{-1} (H_2O) or at ~1200 cm^{-1} (D_2O) (cf. Fig. 3-2), the respective actinyl sample solution with adjusted concentration is led to rinse the crystal surface. Difference spectra were calculated from spectral data recorded from the reference and the sample solution solely exhibiting absorption changes caused by the actinyl(V/VI) solution. Constant parts of the spectra, in particular the strong absorbing background from the bulk water but also contributions from the ATR FT-IR accessory are eliminated. Thus, spectral features even due to minimal absorption changes (~10^{-5} OD) can be detected (cf. Fig. 3-3). Thermostability of the sample system is provided by the use of a flow cell. The measurement time ranges from a few minutes in case of aqueous solution samples to several hours for the performance of *in situ* sorption experiments.

For the FT-IR investigation of An(VI) systems, namely the speciation of U(VI) and Np(VI) in aqueous solution and the U(VI) sorption processes, normal light water was utilized as solvent, since the vibrational modes υ_3 of An(VI) occur in a satisfactory detectable wavenumber range 965 – 890 cm^{-1}. In contrast, the frequency of the Np(V) vibrational mode υ_3 interferes with water absorption at < 850 cm^{-1} (cf. Fig. 3-2). Thus, the speciation and sorption experiments had to be performed in heavy water. Due to the isotope shift of approximately 300 cm^{-1} between the absorption of D_2O and H_2O, the signal-to-noise ratio of the spectra is considerably increased allowing an accurate detection of sorbed and aqueous Np(V) species at a micromolar concentration level [54, 135].

The ionic strength is usually kept constant because of its influence on the speciation in aqueous solution and on the surface charge of the solid particles [53]. In some studies, NO_3^- and ClO_4^- are used as background electrolyte because of their lower complexing properties compared to Cl^- anions [65, 71]. Nevertheless, they show broad absorption bands at 1370 and 1100 cm^{-1}, that are the frequency ranges where vibrational bands of inorganic ligands (CO_3^{2-}) and actinyl(VI) ions are generally observed. In particular, for the low actinide's concentration levels applied in this work, strong perturbations of the signal are ineligible.

In this work, chloride was added to the solutions to maintain constant ionic strength of 0.1, since it does not absorb light in the mid-infrared region. It is often used in vibrational spectroscopic experiments and a direct comparison with reference Raman and IR data, without risking spectral differences because of the background influence becomes feasible. Furthermore, at a chloride concentration of 0.1 M, a coordination of chloride to the actinyl ions could be neglected as it was recently shown by EXAFS experiments published by Hennig et al. [148]. Such coordination to U(IV/VI) was shown to be relevant only at very high concentrations (9 M) indicating an overestimation of the chloro complexes by the calculated predictions.

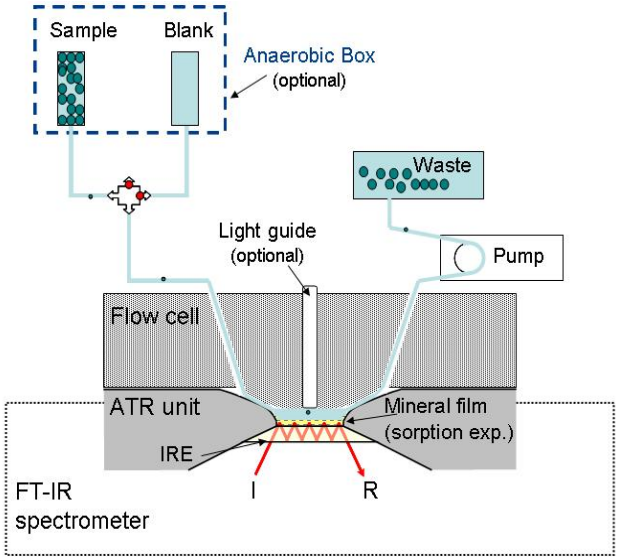

Fig. 3-4: Schematic illustration of the ATR FT-IR set-up for in situ flow experiments.

3.3.2 *In situ* ATR FT-IR spectroscopic sorption studies

In situ ATR FT-IR spectroscopic measurements of sorption processes base on the principle of reaction-induced difference spectroscopy where only spectral changes related to selectively induced changes of the investigated sample are detected. Therefore, IR single beam spectra of a mineral film (stationary phase) are continuously recorded while it is rinsed by a flushing aqueous solution for equilibration and subsequent actinide solution for induced sorption (mobile phase). Since the acquisition time of each spectrum is about 30 seconds, the progress of the sorption process can be monitored with a time resolution in the subminute time range.

The sorption experiments of this work can be described by three subprocesses, as shown in Fig. 3-5: in a first step, the mineral film is conditioned with a blank solution (0.1 M NaCl) for 60 minutes. The difference spectrum, herein after referred to as "1st conditioning" (cf. Fig. 3-5, red), is calculated from single beam spectra recorded after 30 and 60 minutes of rinsing the mineral film with blank solution. This spectrum reflects the stability of the film under the chosen conditions for a time range of 30 minutes and serves as a measure of quality for the experimental setup. In a second step, the sorption process onto the mineral film is performed generally for the following 60 minutes in case of Np(V) and 90 minutes for U(VI). Difference

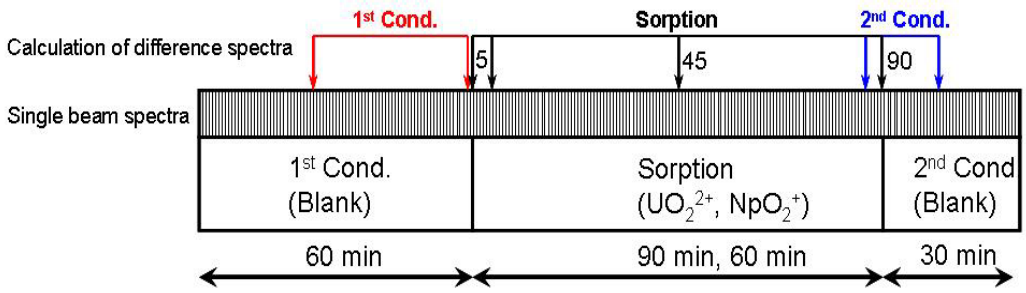

Fig. 3-5: Schematic illustration of the spectra calculation for the standard *in situ* sorption experiment.

spectra, referred to as "sorption" (cf. Fig. 3-5, black), are calculated from the last single beam spectrum obtained at the 1st conditioning and different time intervals after sorption processes have been started, e.g. for U(VI) after 5, 45, and 90 min. In a last step, the film is again flushed with the blank solution for further 30 minutes ("2nd conditioning"). The respective difference spectrum is calculated from single beam spectra recorded at the end of the sorption stage of the experiment and after ~15 min of second blank flushing (cf. Fig. 3-5, blue). This stage of the experiment can serve as a verification of the sorption processes.

The mineral films were prepared directly on the surface of the ATR diamond crystal [65, 124]. Thus, aliquots of 1 µL of a 2.5 g L^{-1} metal oxide suspension (in 1/1 water/ethanol) was pipetted onto the crystal (Ø = 4 mm; A = 12.57 mm^2) with subsequent drying under a gentle N_2 flow. This procedure was repeated several times and transmission spectra were recorded after each deposition to evaluate an optimum mineral film thickness. This procedure is exampled for γ-Al_2O_3 and kaolinite in Fig. 3-6. After more than five repetitions the absorption increase was observed to be hampered, indicating that the maximum thickness of the film concerning the measurability by the evanescent field was reached. Hence, for the sorption measurements five layers were used to coat the ATR crystal surface (red trace in Fig. 3-6) and the final deposited density was calculated to be approximately 0.1 mg cm^{-2}. The pure ethanol in the mineral suspensions was used to facilitate the formation of homogenous mineral layers on the ATR surface.

The prepared films appeared homogenous upon visual inspection. But atomic force microscopy (AFM) of a kaolinite film analogously deposited on a glass surface showed that on a micrometer scale the coating was not homogenous and conglomeration of particles occurred (Fig. 3-7). Local film heights ranged between 0 and 2 µm. The average film height was ~0.5 µm. Calculations comparing the penetration depth and the thickness of the prepared oxide layer, similarly performed to the procedure of Hug and Sulzberger, showed that the entire layer was probed by the evanescent wave [131].

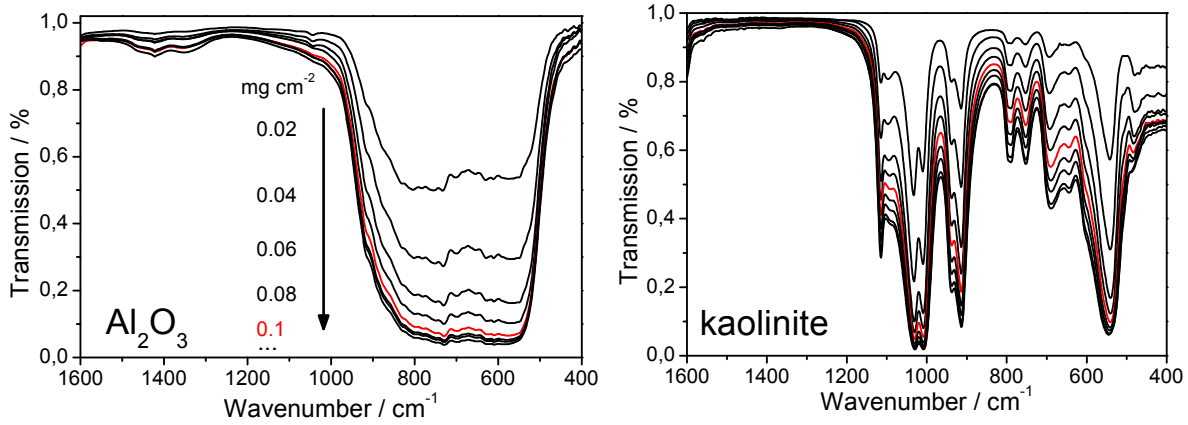

Fig. 3-6: Spectra of stepwise deposition of γ-Al_2O_3 (left) and kaolinite (right) to coat the ATR surface. Each spectrum was recorded after drying a drop of 1 µL of a 2.5 g L^{-1} suspension (addition of 0.02 mg cm^{-2}). The red spectra show the transmission of the generally produced films for sorption experiments.

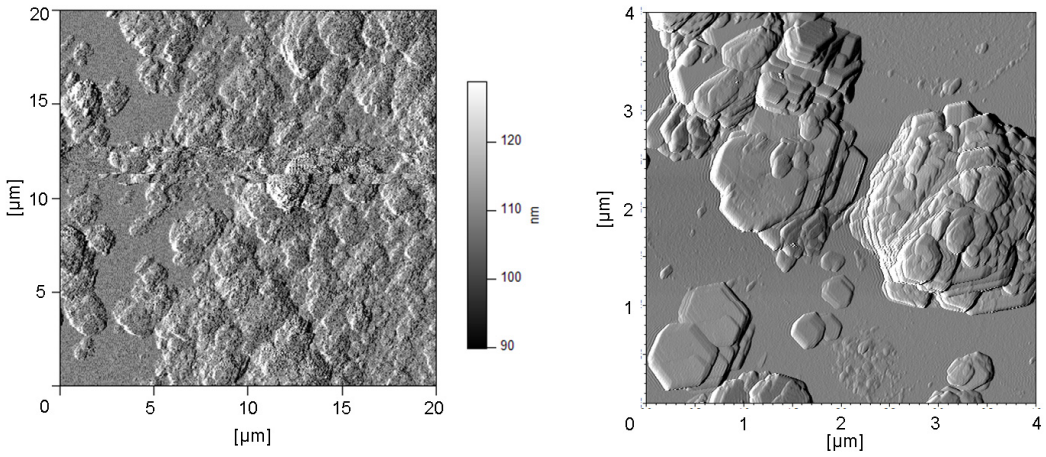

Fig. 3-7: Micrographs of a kaolinite film on a glass surface prepared analogously to the procedure applied in ATR sorption measurements.

A flow cell (total volume ~ 200 µL) was used to rinse the prepared mineral film with a blank solution for equilibration and subsequently with an actinide solution for sorption processes under dark conditions. A constant velocity of 0.1 mL min^{-1} (Np) and 0.2 mL min^{-1} (U) was maintained by a peristaltic pump (Ismatec S.A.) at room temperature.

The stability of the mineral films prepared on the ATR surface was verified by monitoring a flow experiment with a blank solution at 0.2 mL min^{-1} for 3 hours. The resulting difference spectra calculated at distinct time intervals, presented in Fig. 3-8, show no negative bands which would indicate the removal of particles from the film. A distinct baseline drift below 1000 cm^{-1} after 30 and 180 minutes is observed which can be ascribed to general instabilities in the measurement on a long time scale and is probably caused by thermal changes of the measuring system. The same trend is observed upon measuring only water, without a mineral film for a prolonged time. However, the absorption changes are very small compared to those observed during a sorption experiment.

Once the *in situ* sorption measurement was finished, the film was removed from the ATR crystal with 100 µL of 2 M HCl and analyzed by ICP-MS for U, Ti, Al, Si, respectively. The calculated ratios, e.g. U-Ti, or U-Al-Si are helpful for the interpretation of the spectral data

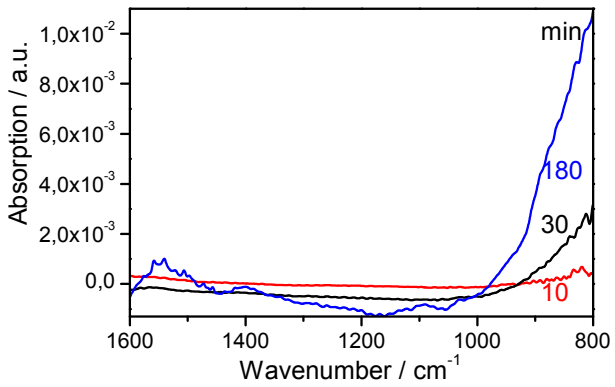

Fig. 3-8: ATR spectra of a stability measurement of an TiO_2 film conditioned with blank solution (0.1 M NaCl, pH 6).

and to ensure that U(VI) interactions occurred at the mineral interface. The presence of Np was checked by application of LSC.

The Np(V) spectroscopic measurements were performed at nitrogen atmosphere avoiding fast exchanges of D_2O by H_2O throughout all experiments. Selected U(VI) sorption measurements were also performed at nitrogen atmosphere in order to check the influence of dissolved atmospheric CO_2 on the formation of surface species. For the measurements under inert gas conditions, the samples were prepared in a glove box and transferred in a 5 L anaerob container, used for the measurements.

Furthermore, *in situ* ATR FT-IR spectroscopic experiments to study the photocatalytic reactions of U(VI) at the titanium dioxide surface were carried out. For this purpose, a special flow cell with an opening for an optical light guide (Rapp Opto Electronic) perpendicular to the ATR crystal was used (Fig. 3-4).

Exposure of metal oxide films to air can lead to carbonate surface contamination. However, washing with acidic and alkaline solutions has been found to effectively remove such surface impurities [142]. Thus, the cleaning procedure of the diamond surface between different performed experiments included washing with 1 M HCl, NaOH and ethanol, respectively, followed by rinsing with MQ water for several times and acetone as a last step.

4. Aqueous species of U(VI), Np(VI) and Np(V) and their IR spectroscopic characterization

The evaluation of sorption processes of heavy metal ions at the mineral-water interface requires information about the distribution of the metal ion species in solution and on the surface as well. Hence, for an unequivocal interpretation of spectroscopic data obtained from sorption experiments, the spectroscopic characterization of the solution species under distinct conditions is of urgent need [39].

In this chapter, the most important results from the spectroscopic verification of the currently accepted chemical set of uranyl(VI) and neptunyl(V/VI) species are presented. The data was mainly published in the articles of Müller et al. [27, 132, 149]. For the study of hydrolysis and carbonate complexation of actinyl(V/VI), a multiplicity of experiments under different conditions was performed, i.e. the concentration level was reduced from the millimolar to the micromolar range, the pH values ranged from 2 to 9 and the presence and absence of carbonate was controlled. Mainly, ATR FT-IR spectroscopy was applied, but in addition, NIR spectroscopy was used as a second method in case of Np(V/VI) speciation.

To this end, computed speciation patterns based on state-of-the-art thermodynamic models and data are compared to spectra obtained from actinyl(V/VI) solutions by applying ATR FT-IR and NIR spectroscopy. The speciations of Np(V/VI) and U(VI) in aqueous solutions at ambient atmosphere (T = 25 °C) and at an ionic strength of 0.1 M NaCl were computed using the geochemical modeling code package EQ3/6 by Wolery [150], basing on the updated NEA TDB [10-12], with minor adaptations according to the Nagra/PSI database [151].

4.1 U(VI) speciation in air

4.1.1 Calculation of micromolar U(VI) speciation

The calculation of the uranium(VI) speciation in aqueous 20 µM solution under ambient atmosphere predicts a total of nine different species appearing in the pH range from 2 to 10 (Fig. 4-1). Below pH 5 the aqueous UO_2^{2+} cation is expected to be predominant in solution whereas several species are calculated to be present simultaneously in the range between pH 5 and 6.5 (Fig. 4-1a). The dominant species are expected to be the monomers UO_2^{2+} and UO_2OH^+, the dimer $(UO_2)_2(OH)_2^{2+}$ and the trimer $(UO_2)_3(OH)_5^+$. Minor species with contributions below 10 % are given to an enlarged panel (Fig. 4-1b). At higher pH levels, the mixed hydroxo carbonate uranyl dimer $(UO_2)_2CO_3(OH)_3^-$ becomes the most relevant species and mounts up to nearly 100 % at pH 7.3 (Fig. 4-1a). A further increase of the pH leads to a disappearance of this complex and the uranyl tricarbonate complex $UO_2(CO_3)_3^{4-}$ becomes dominant. Additionally, the monomeric carbonate species $UO_2(CO_3)_2^{2-}$ is expected to mount up to a relative content of 10 % in the solution in the narrow pH range between 7.5 and 8.5 (Fig. 4-1b). The chloride content introduced into the solutions through the addition of NaCl as background electrolyte (0.1 M) yields, due to the rather weak affinity of the chloride ion when compared to the hydroxyl ion, to a maximum of 5 % UO_2Cl^+, at pH > 5 this species is

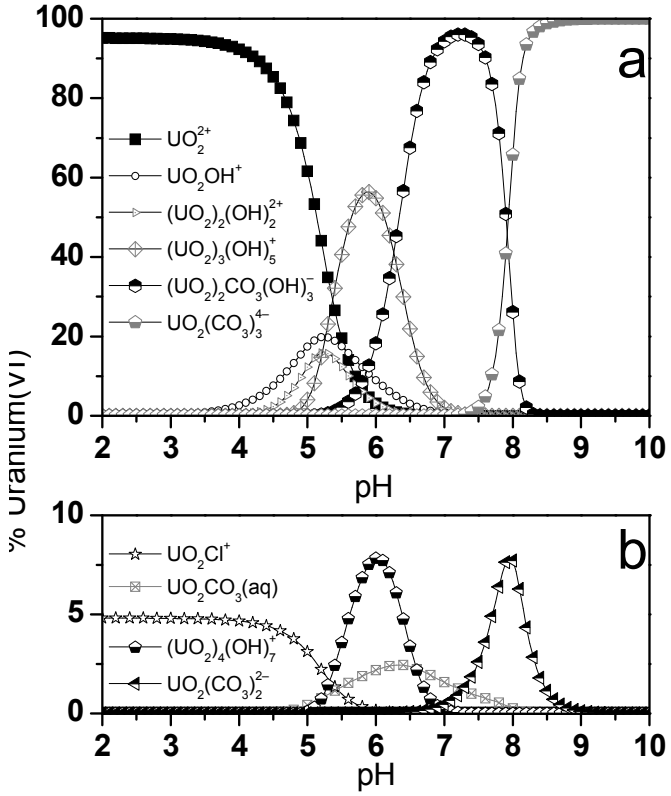

Fig. 4-1: Speciation diagram of 20 µM uranium(VI) at 0.1 M NaCl under atmospheric conditions. (a) Species exceeding 10 % of total U(VI) amount, (b) species < 10 % of total U(VI) amount (enlarged ordinate).

vanishing completely. At pH values below 5, the UO_2^{2+} is prevailing; above that, the pattern becomes more complicated but is still simpler than at millimolar uranium levels. It should also be mentioned here, that especially the region between pH 5 and pH 7 is heavily influenced by the change in the stability constant for the neutral $UO_2(OH)_2^0$, decreasing from −10.3 [152] to −12.15 [153] during the update process.

4.1.2 U(VI) speciation at pH 4

In a first step, the lowest concentration which can be investigated by the set-up of the ATR FT-IR instrumentation described in section 3.3.1 was evaluated. Therefore, spectra of aqueous solutions with different uranyl concentrations at a distinct pH value (pH 4) were recorded. This pH was selected since it constitutes the critical value where the formation of insoluble uranyl hydroxo phases in millimolar U(VI) solutions is usually observed. The concentrations span from 5 mM to 5 µM and the results are shown in Fig. 4-2. No bands were detected between 1300 and 1000 cm^{-1}, thus this region is not shown for clarity. A spectrum of the aqueous UO_2^{2+} ion is shown in Fig. 4-2a as a reference which was obtained from a 10 mM UO_2Cl_2 solution at pH 2. It shows the absorption band of the υ_3 mode of the monomeric UO_2^{2+} cation at 961 cm^{-1} which is predominantly present at the same pH value and concentration as shown by earlier Raman investigations [154]. The spectrum is in excellent agreement with spectra of the same species recorded at higher concentrations and lower pH values in recent infrared spectroscopic studies [28].

At pH 4 the spectra significantly change their shape upon reducing the uranyl concentration (Fig. 4-2b-d). The spectra of the solutions containing 5 and 0.5 mM U(VI) are characterized by two partial overlapping bands with maxima at 961 and 934 cm^{-1} (Fig. 4-2b,c) which is in good agreement with results obtained from aqueous solutions of 100 mM uranyl(VI) nitrate presented by Quilès and Burneau [28]. Decreasing the U(VI) concentration below 0.5 mM leads to a single absorption band with a maximum at 922 cm^{-1} whereas the 961 cm^{-1} band is not observed any longer (Fig. 4-2d,e). Additionally, two bands appear at 1525 and 1460 cm^{-1} in the spectra of the low concentrations. At concentrations below 5 µM U(VI), no reliable infrared spectra could be recorded due to the low signal-to-noise ratio (data not shown).

In a recent infrared spectroscopic investigation, an assignment of three uranyl(VI) species to distinct frequencies of absorption bands is given [28]. In addition to the absorption of the UO_2^{2+} cation around 960 cm^{-1}, two other species notably $(UO_2)_2(OH)_2^{2+}$ and $(UO_2)_3(OH)_5^{+}$ were identified by the υ_3 stretching mode of the UO_2^{2+} cation showing absorption maxima at 943 and 923 cm^{-1}, respectively [28]. From a Raman spectroscopic investigation, these species were also found to show absorption maxima bathochromically shifted in comparison to the UO_2^{2+} cation [155]. Although the υ_1 mode of the UO_2^{2+} cation is observed in Raman spectroscopy, its shift to lower wavenumbers of the dimer and trimer uranyl species is of the same extent as υ_3 in the infrared absorption spectra.

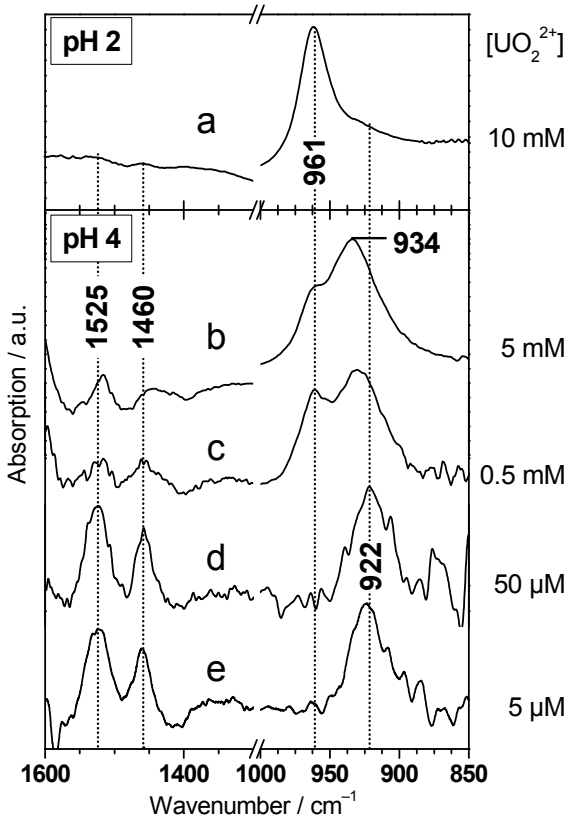

Fig. 4-2: ATR FT-IR spectra of uranyl(VI) solutions at pH 2: (a) 10 mM, and at pH 4: (b) 5 mM, (c) 0.5 mM, (d) 0.05 mM, (e) 0.005 mM. Indicated values are in cm^{-1}.

From these observations it can be assumed that the overlapping bands in the spectra of the solutions containing 5 and 0.5 mM uranyl(VI) (Fig. 4-2b,c) mainly represent the UO_2^{2+} and the $(UO_2)_2(OH)_2^{2+}$ dimer with absorption maxima at 961 and 940 cm^{-1}, respectively. Since in these spectra the peak maximum is found at 934 cm^{-1}, a small fraction of the trimer $(UO_2)_3(OH)_5^{+}$ complex possibly contributes to this vibrational band.

The single band at 922 cm^{-1} in the spectra of the lower concentrations excludes significant contributions from the monomeric UO_2^{2+} cation to the speciation (Fig. 4-2c,d). This is in contrast to the calculation of the U(VI) speciation at a micromolar level presented in Fig. 4-1 predicting the dominance of the fully hydrated UO_2^{2+} ion at this pH range. It is obvious that the speciation has changed significantly upon decreasing the U(VI) concentration to the lower micromolar range. Refering to basic principles of thermodynamic equilibrium states, these vibrational spectroscopic findings can only be explained under consideration of the formation of monomeric species.

Raman investigations and calculations of the frequency of the $\upsilon_1(UO_2)$ mode, based on empirical approaches, have shown a linear correlation between the number of OH-ligands and the decrease of the vibrational frequency of the $\upsilon_1(UO_2)$ mode with respect to the hydrated uranyl(VI) ion [155-157]. Although the validity of the correlation has not been proven unequivocally up to now, the expected frequencies of the $\upsilon_1(UO_2)$ mode in the different monomeric hydroxo complexes can be estimated [155]. Furthermore, the extent of the

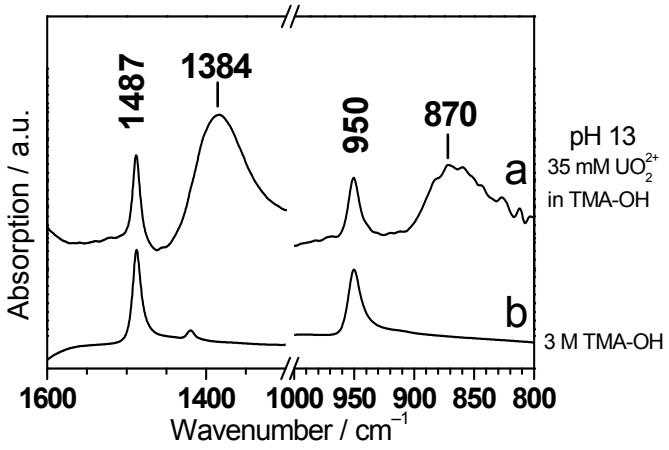

Fig. 4-3: ATR FT-IR spectra of (a) 35 mM uranyl(VI) solution in TMA-OH at pH 13, (b) 3 M TMA-OH. Indicated values are in cm^{-1}.

downshift of the frequencies with respect to the frequency of the fully hydrated UO_2^{2+} ion are suggested to be of the same size for both stretching vibrations υ_1 and υ_3 in aqueous solution, complementarily observed by Raman and infrared spectroscopy, respectively (cf. Fig. 4-16, Eq. 4-1). This has been explicitly demonstrated by investigations of the dimeric and trimeric hydroxo complexes [28]. The validity of these correlations in infrared spectroscopy is verified by the model spectrum of the $UO_2(OH)_4^{2-}$ complex shown in Fig. 4-3. The complex was prepared according to Moll et al. using tetramethylammonium hydroxide (TMA-OH) as a non-complexing agent at pH 13 [138]. Apart from significant bands at 1487 and 950 cm^{-1} which can be assigned to TMA-OH (Fig. 4-3b), additional strong bands at 1385 and 870 cm^{-1} are observed. The first band is probably due to a carbonate contamination arising from fast dissolving atmospheric carbon dioxide at pH 13 [54]. The second band is assigned to $\upsilon_3(UO_2)$, indicating a 91 cm^{-1} downshift of the frequencies compared to the UO_2^{2+} ion (Fig. 4-2a). This is in good agreement with the corresponding shifts of 88 and 84 cm^{-1} observed earlier by Raman spectroscopy [155, 158] confirming the linear correlation of the number of OH-ligands and the shift of $\upsilon_3(UO_2)$ mode in mononuclear U(VI) hydroxo species.

Consequently, the band at 922 cm^{-1} observed for the low concentrations at pH 4 is tentatively assigned to the UO_2 stretching mode of the monomeric $UO_2(OH)_2^0$ complex which was calculated to be shifted to lower wavenumbers of about 42 – 46 cm^{-1} with respect to the UO_2^{2+} ion [155]. Moreover, this assignment is in agreement with recent investigations predicting the presence of three mononuclear complexes, i.e. UO_2OH^+, $UO_2(OH)_2^0$, and $UO_2(OH)_3^-$, at U(VI) concentration levels below 10^{-5} M [(see Ref. 155 and references therein)] which fits well with the concentration range of the spectra in Fig. 4-2d,e.

The appearance of two bands at 1525 and 1460 cm^{-1} correlates with the band at 922 cm^{-1} (Fig. 4-2d,e). An assignment of these bands to distinct vibrational modes of the complex remains difficult and is tentatively given in the following section under consideration of additional experimental aspects. Possibly, these bands represent water molecules which are coordinated to the uranyl(VI) hydroxo complex.

In conclusion, the spectra of the uranyl(VI) solutions recorded at pH 4 clearly demonstrate a distinct change of the U(VI) speciation on reducing the concentration of the actinide ion from the millimolar to the micromolar range. It was shown, that low concentrations of the uranyl ion in the micromolar range can be investigated by ATR FT-IR spectroscopy providing access to vibrational data of solution throughout a wide pH range. The obtained data of micromolar U(VI) solutions provide direct evidence for the monomeric hydroxo complexes expected at low actinide concentrations.

4.1.3 U(VI) speciation in micromolar acidic solutions

The spectra of diluted uranyl(VI) solutions covering a pH range from 2 to 5.6 are shown in Fig. 4-4a-d. The concentration was 20 µM for pH values beyond 3. Due to the low absorption coefficient of the uranyl species at lower pH, the concentration was set to 100 µM to resolve the bands in the spectra (Fig. 4-4a,b). Again, between 1300 and 1000 cm^{-1} no bands were observed and, therefore, this spectral region is not shown for clarity.

In the spectrum measured at pH 2, the υ_3 mode of the UO_2 shows up as a single absorption band at 961 cm^{-1} representing the monomeric species UO_2^{2+} (Fig. 4-4a). At pH 2.5 an additional band at 923 cm^{-1} can be observed (Fig. 4-4b). In the spectra at pH values ≤ 6, it is the only band observed in this spectral region (Fig. 4-4c,d) indicating the presence of one dominant species within the pH range from ~ 3 to 6.

In homology to the results of the study of the speciation at pH 4 in the previous section, the appearance of monomeric species has to be considered within this pH range. Consequently, the band at 923 cm^{-1} likely represents the monomer $UO_2(OH)_2^0$ complex at low pH values

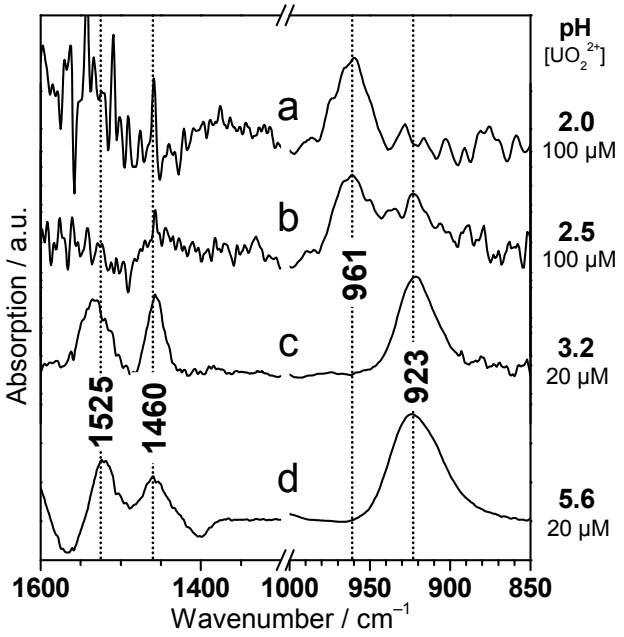

Fig. 4-4: ATR FT-IR spectra of uranyl(VI) solutions at different pH values (0.1 M NaCl). (a) 100 µM, pH 2.0, (b) 100 µM, pH 2.5, (c) 20 µM, pH 3.2, (d) 20 µM, pH 5.6. Indicated values are in cm^{-1}.

(Fig. 4-4b-d) with respect to the relative shift to lower wavenumbers of 38 cm^{-1} compared to the frequency of the $\upsilon_3(UO_2)$ mode of the fully hydrated uranyl ion (Fig. 4-2a).

Interestingly, the signal-to-noise is increased upon reducing the U(VI) concentration from 100 to 20 µM and increasing the pH from 2.5 to 3.2 (Fig. 4-4b,c). The hydroxo complex shows much higher absorption coefficient than the free uranyl complex. Similar behavior is discussed for the Np(VI) hydrolysis products in section 4.3.2.

The $UO_2(OH)_2^0$ species was characterized spectroscopically in recent studies by TRLFS [33, 159]. However, great discrepancies of the observed fluorescence lifetimes were observed which are not fully understood [160]. The origin of the deviations can be assumed to be related to different parameters of the solutions such as the selected background electrolyte or ionic strength. However, the assignments of the observed fluorescence spectra to the $UO_2(OH)_2^0$ complex are exclusively based on calculations which rely on data from thermodynamic databases. Moreover, the TRLFS spectrum of this species was not obtained directly and the lifetime has to be estimated [33]. Therefore, the peak maxima were obtained by deconvolution of the measured spectra in turn showing discrepancies to results obtained from other researchers [159]. In summary, the observed spectral changes in fluorescence spectroscopy allow a substantiated differentiation of different species formed under distinct parameters but the assignments to distinct hydroxo complexes are strictly related to the predicting calculations and the spectra do not contain intrinsic structural information about uranyl complexes. This is different for the vibrational spectra. The observed shifts of the vibrational bands can only be explained by the formation of additional species. Consequently, the assignments given here are widely independent from the thermodynamic data sets and are closely related to spectroscopically verifiable findings as it was shown for the spectrum of the $UO_2(OH)_4^{2-}$ complex.

Increasing the pH value to 5.6 leads to a slightly broadened absorption band at 923 cm^{-1} (Fig. 4-4d). Since it was shown that the absorption frequency of the trimeric $(UO_2)_3(OH)_5^+$ species is also expected at this frequency, contributions from this species can not be ruled out at higher pH levels.

In homology to the spectra of micromolar U(VI) solutions measured at pH 4 (Fig. 4-2d,e), additional bands around 1525 and 1460 cm^{-1} appear simultaneously to the band at 923 cm^{-1}. An unequivocal assignment of these bands is very difficult. Absorption bands in this spectral region are often related to antisymmetric and symmetric stretching vibrations of either carbonate ligands or carboxylic groups bound to heavy metal ions.[72, 161] Therefore, a series of experiments were performed to rule out a contamination of the aqueous U(VI) system by organic or inorganic carbon compounds and sorption processes of the actinide ions onto the ATR diamond surface.

In a first step, a contamination of the aqueous solutions by inorganic carbonate was excluded by experiments using excess of $NaH^{13}CO_3$ during the preparation of the solutions at pH 6 and subsequent titration to lower pH values. The resulting spectra showed no shifts of

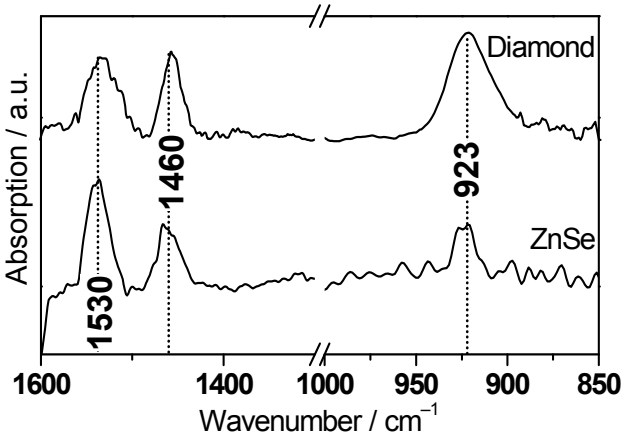

Fig. 4-5: Comparison of the FT-IR spectra of 20 µM U(VI) solutions at pH 3.2 obtained using different ATR-crystals.

the bands between 1550 and 1400 cm^{-1} related to the expected isotope effect of residual dissolved 13C-carbonate (data not shown). Therefore, the observed bands cannot be assigned to carbonate ions. Furthermore, a verification of the purity of the used MilliQ water by ICP-MS provides no evidence for contamination by organic carbon acid compounds either.

Secondly, IR experiments of micromolar U(VI) solutions were repeated using a ZnSe ATR crystal. The obtained spectra fully reproduce the results of the previous experiments obtained with the diamond ATR crystal excluding significant specific interactions of the UO_2^{2+} ion with the crystal surface (Fig. 4-5).

Furthermore, experiments were carried out to detect possible sorption processes of the uranyl(VI) ion onto a potentially oxidized diamond surface showing carboxyl groups. This was done by recording the spectral changes of aqueous uranyl solutions upon increasing the pH from 2 to 4. It is expected that protons are removed from the carboxyl groups and generate vibrational bands representing the different protonation states of the respective functional groups. Spectra of the following aqueous solutions with distinct pH values 2 and 4 were recorded and difference spectra were calculated: pure MilliQ water, 0.1 M NaCl, 0.1 mM $CaCl_2$ (0.1 M NaCl), and 0.2 mM UO_2^{2+} (0.1 M NaCl) each. All calculated difference spectra exhibit the same characteristic spectral features throughout the whole frequency range induced by the increase of the pH (Fig. 4-6). Only the spectrum of the U(VI) solution provides additional positive bands at 1530, 1455 and 923 cm^{-1} and a weak negative band around 961 cm^{-1}, representing the uranyl bands at pH 4 and 2, respectively (cf. Fig. 4-6d). A complexation of UO_2^{2+} ions to surface carboxyl groups would cause a shift of bands representing the $\upsilon_s(CO_3)$ and $\upsilon_{as}(CO_3)$ modes. Since additional bands are observed in the spectrum of the U(VI) solution the formation of a uranyl surface complex can be ruled out.

Combining these findings, it is obvious that the bands at 1525 and 1460 cm^{-1} represent intrinsic optical absorption properties of the aqueous solutions containing uranyl hydroxo species and are not due to neither formation of uranyl complexes with carbonate ligands nor sorption processes occurring at the ATR crystal surface. Furthermore, it can be excluded that

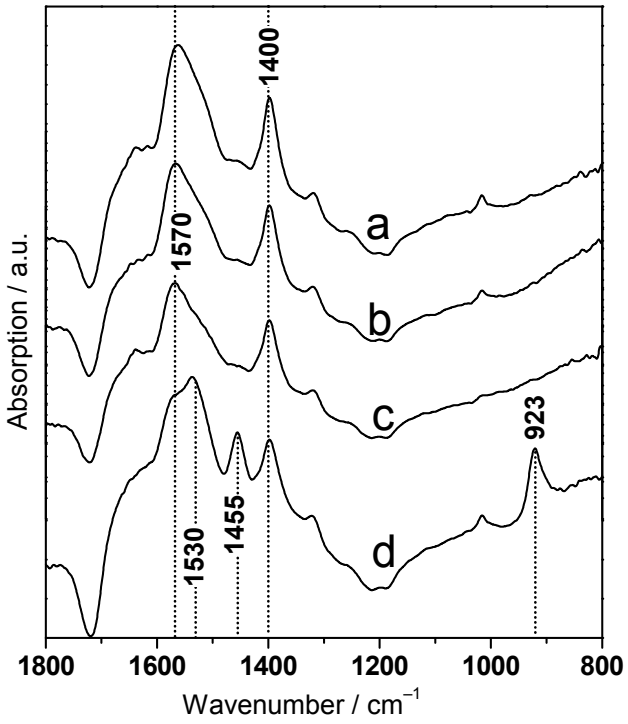

Fig. 4-6: Difference spectra calculated out of solution spectra recorded at pH 2 and 4. Negative and positive bands represent solutions at pH 2 and 4, respectively. (a) pure MilliQ water; (b) 0.1 M NaCl; (c) 0.1 mM $CaCl_2$; (d) 0.2 mM UO_2^{2+}, 0.1 M NaCl.

these bands are generally characteristic for the complexation of bivalent ions. However, an assignment to distinct vibrational modes is speculative at this state of knowledge. Possibly, these bands represent water molecules with a special coordination in the hydrate shell of the formed hydroxo complex.

In conclusion, the interpretation of the spectroscopic data of the micromolar U(VI) solutions at acidic pH values have clearly shown discrepancies between the predicted speciation and the spectral information given by infrared spectroscopy. The speciation is changed drastically at pH 2.5 – 4.5 and the presence of monomeric hydroxo species which are not predicted by the theoretical calculations, is suggested in this pH range.

4.1.4 U(VI) speciation in micromolar neutral solutions

The acquisition of infrared spectra of diluted uranyl(VI) solutions in the micromolar range with a sufficient signal-to-noise ratio makes it feasible to increase the pH without the risk of any precipitation of solid uranate phases. In the past, non-complexing reagents had to be used to prevent such precipitation in alkaline solutions [155, 158]. The spectra of aqueous 20 µM uranyl(VI) solutions spanning a pH range from 6.5 to 8.5 are shown in Fig. 4-7a-c. Again, the spectral region between 1300 and 1000 cm^{-1} is not shown for clarity, since no bands were observed.

The absorption band of the $\upsilon_3(UO_2)$ mode found at 923 cm^{-1} in the spectrum at pH 6.5 (Fig. 4-7a) shifts to lower wavenumbers upon further increasing the pH (Fig. 4-7c). At pH 7 the

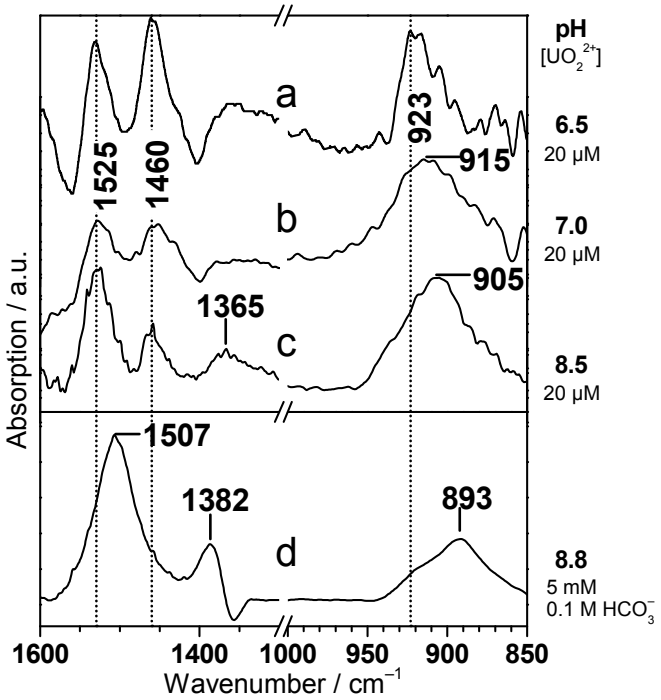

Fig. 4-7: ATR FT-IR spectra of uranyl(VI) solutions at different pH values (0.1 M NaCl). (a) 20 µM, pH 6.5, (b) 20 µM, pH 7.0, (c) 20 µM, pH 8.5, (d) 5 mM, pH 8.8, 0.1 M $NaHCO_3$. Indicated values are in cm^{-1}.

band is observed at 915 cm^{-1} (Fig. 4-7b) and at pH 8.5 the maximum is found at 905 cm^{-1} (Fig. 4-7c). In these spectra, the bands at 1525 and 1460 cm^{-1} observed already at lower pH level are still present, but an additional weak band at 1365 cm^{-1} appears in the spectrum recorded at pH 8.5. For pH values > 8.5, reliable infrared spectra from homogeneous solutions could not be obtained since the formation of uranium colloids could not be completely ruled out by photon correlation spectroscopy (PCS). For more details on the spectroscopic charateriztion of colloidal suspension of U(VI) and Np(VI) the reader is referred to section 4.2.5.

The thermodynamic calculations predict a dominance of the $UO_2(CO_3)_3^{4-}$ complex for pH values > 8 (Fig. 4-1a). Since this complex can be synthesized in aqueous solution containing excess of HCO_3^- anions, we present a model spectrum of this species obtained for a 5 mM uranyl(VI) solution in 0.1 M HCO_3^- at pH 8.8 showing all significant absorption bands in the mid infrared region (Fig. 4-7d). The absorption bands at 1507 and 1382 cm^{-1} are assigned to the doubly degenerated υ_3 mode of the free carbonate anion which splits into two bands upon binding to the uranyl(VI) cation. The band of the υ_3 mode of the uranyl(VI) is now found at 893 cm^{-1} which is in good agreement with earlier vibrational spectroscopic studies.[162]

Although an unequivocal assignment of the observed absorption bands to distinct uranyl species can not be given at this state of knowledge, there are distinct spectral features in the spectra recorded at pH > 6 which are contradictory to the results of the predicting calculation shown in Fig. 4-1.

Firstly, the dominance of the $UO_2(CO_3)_3^{4-}$ complex is predicted at a pH level > 8. However, the infrared spectrum recorded at pH 8.5 (Fig. 4-7c) shows significant deviations to the model spectrum of the $UO_2(CO_3)_3^{4-}$ complex (Fig. 4-7d) demonstrating that the $UO_2(CO_3)_3^{4-}$ complex is not the dominant species at pH 8.5 as predicted from the calculations. Other uranyl species are obviously contributing to the speciation in this pH range.

Secondly, the calculation shows a pH range (6.5 – 7.8) where the dimeric $(UO_2)_2CO_3(OH)_3^-$ species is expected to be dominant. In particular at pH 7.0, the fraction of this complex is calculated to mount up to approximately 95 %. The structure of this species was investigated by EXAFS and NMR spectroscopy suggesting a bidendate binding of the CO_3^{2-} ligand to the heavy metal ion [163]. This binding should provoke strong bands in the IR spectrum around 1500 and 1380 cm^{-1} representing the υ_{as} and υ_s mode of the CO_3^{2-} anion as they are observed in the spectrum of the $UO_2(CO_3)_3^{4-}$ complex (Fig. 4-7d). Since in this spectral region no significant bands appear at pH 7.0, the dominance of the $(UO_2)_2CO_3(OH)_3^-$ species is obviously not given at pH 7.0. However, a band at 1365 cm^{-1} is observed in the spectrum recorded at pH 8.5 which can be assigned to contribution from uranyl species containing carbonate ligands.

The shifting of the absorption band of the $\upsilon_3(UO_2)$ mode to lower wavenumbers upon increasing the pH value from 6.5 to 8.5 can be interpreted in terms of formation of polymeric and monomeric species as well. On the one hand, from Raman spectroscopic studies the two species $(UO_2)_3(OH)_7^-$ and $(UO_2)_3(OH)_8^{2-}$ were postulated (with the latter not included in the NEA database) to show a relative downshift of the $\upsilon_1(UO_2)$ mode from the frequency of the fully hydrated uranyl(VI) ion of about 48 and 58 cm^{-1}, respectively [155]. Assuming a homology between the relative shifts of the $\upsilon_3(UO_2)$ and the $\upsilon_1(UO_2)$ modes, these two species may contribute significantly to the speciation of the uranyl(VI) system in this pH range. On the other hand, from the correlation of the number of OH-ligands and the shift of $\upsilon_3(UO_2)$ mode in mononuclear U(VI) hydroxo species the formation of further monomeric species such as $UO_2(OH)_3^-$ can also be derived (cf. section 4.3.2 and [154]). For this species, the frequency of the $\upsilon_3(UO_2)$ mode is calculated to be red-shifted about 66 cm^{-1} relative to the absorption frequency of the fully hydrated UO_2^{2+} ion and should be found around 895 cm^{-1} in the infrared spectra. Therefore, this species can only contribute to the spectrum recorded at pH 8.5 to a significant extent since at a pH level below 8 the uranyl absorption band appears at considerable higher wavenumbers (Fig. 4-7a,b).

In this section the first infrared spectroscopic analysis of uranyl solutions at high pH values without the addition of non-complexing media such as TMA-OH are provided using the ATR technique. The spectra of micromolar uranyl solutions at pH $\geq$ 7 strongly suggest the formation of a uranyl species containing a carbonate ligand in ambient atmosphere. The spectrum at pH 8.5 clearly demonstrates that the uranyl tricarbonate complex does not govern the speciation above pH 8 as supposed by the thermodynamic modeling (Fig. 4-1a and Fig. 4-7c).

Consequently, the calculations based on current thermodynamic data bases insufficiently reflect the true U(VI) speciation. This might be due to an incorrect set of chemical entities related to the uranyl hydroxo species and / or uncertainties in the complex stability constants exceeding the currently accepted values.

There are rarely independent proofs of evidence for well-defined hydroxo complexes of U(VI) by spectroscopic or computational methods. As already mentioned above, the species sets which were selected for the NEA database were mainly derived from potentiometric and to a smaller extent from X-ray spectroscopic techniques both limited to millimolar concentrations. In contrast, in this study U(VI) solutions in the micromolar range (200 – 5 μM) were investigated which may explain the discrepancies between the spectroscopic findings and calculated predictions. Possibly, the presence of polynuclear hydroxo species which were disregarded during the updating process of the NEA database, have to be taken into account in future times in particular for higher pH levels.

The uncertainty of thermodynamic parameters is intrinsically linked to an estimation of the experimental errors which cannot be given easily [10]. Furthermore, since all uncertainties of the stability constants of uranyl complexes were treated as being independent from each other, the quantification of the errors on speciation pattern results in too broad uncertainty bands [164]. In fact, with respect to the simultaneous fitting of several reactions to one set of experimental data, there is a significant correlation of these parameters. Some of them exhibit a negative correlation, thus shrinking the uncertainty band widths. In contrast, in the updated NEA database, the deviations of log K values for some uranyl species are larger than the originally assigned uncertainties in the first issue of the NEA database. This indicates that some of the uncertainties have not been well supported and that further corrections of some stability constants are conceivable.

Since this study provides evidence for significant change of the U(VI) speciation upon decreasing the concentration from the milli- to the micromolar concentration range (cf. Fig. 4-2), an critical extrapolation of the thermodynamic data to micromolar concentrations has to be challenged in future times.

Further vibrational spectroscopic investigations of the speciation of actinide cations under distinct environmental parameters have now become feasible. For instance, the verification of speciations of actinide ions (U(VI), Np(V/VI)) including inorganic ligands such as carbonate or under inert gas atmosphere are the topics presented later (cf. sections 4.2, 4.3, 4.4). A more detailed knowledge of the presence of certain actinide species under distinct parameters will lead to a deeper understanding of the chemistry of the actinides in the environment. However, for the infrared spectroscopic investigation of U(VI) surface complexation, the spectra of 20 μM U(VI) obtained in the pH range 2 – 8.5 are indispensable references of the species present under the same conditions in aqueous solution.

4.2 Np(VI) speciation in air

The spectroscopic study of the U(VI) speciation at a considerably reduced concentration level shows new pathes for the verification and characterization of species predicted by the current accepted thermodynamic data. In a next step, the seldom studied Np(VI) is chosen for spectroscopic experiments. Unfortunately, only very few reference data is available for this redox species and its formed complexes in aqueous solution. To overcome this difficulty, on the one hand, NIR spectroscopy is used as a further technique, on the other hand, U(VI) which provids a similar structure serves as a model in the ATR FT-IR spectroscopic part.

4.2.1 Calculation of Np(VI) speciation in comparison to U(VI)

The modeling of a 500 µM Np(VI) solution at ionic strength of 0.1 predicts five species in the pH range from 2 to 6 (Fig. 4-8a,b). The species exceeding 2% of the total Np amount are shown in (Fig. 4-8a, the remaining are shown to an enlarged scale in (Fig. 4-8b. The cation NpO_2^{2+} is calculated to dominate in acidic solution below pH 4.5, whereas the neptunyl chloride complex NpO_2Cl^+ increases to 10%. The mixed dimeric hydroxo carbonate complex $(NpO_2)_2CO_3(OH)_3^-$ turns out to be the most relevant species in solution at pH > 4.5. Monomer and dimer hydroxo complexes, i.e. NpO_2OH^+ and $(NpO_2)_2(OH)_2^{2+}$, contribute to the Np(VI) speciation between pH 3 and 5 only to a very small amount (< 2%).

The speciation pattern of aqueous U(VI) at a concentration of 500 µM in the pH range from 2 to 6 is shown in (Fig. 4-8c,d. Again, the major species, exceeding 7.5%, are shown in (Fig. 4-8c, the remaining species are shown to an enlarged scale in (Fig. 4-8d. The cation UO_2^{2+} predominates at pH ≤ 4.7. In contrast to the Np(VI) system, U(VI) forms several hydrolysis

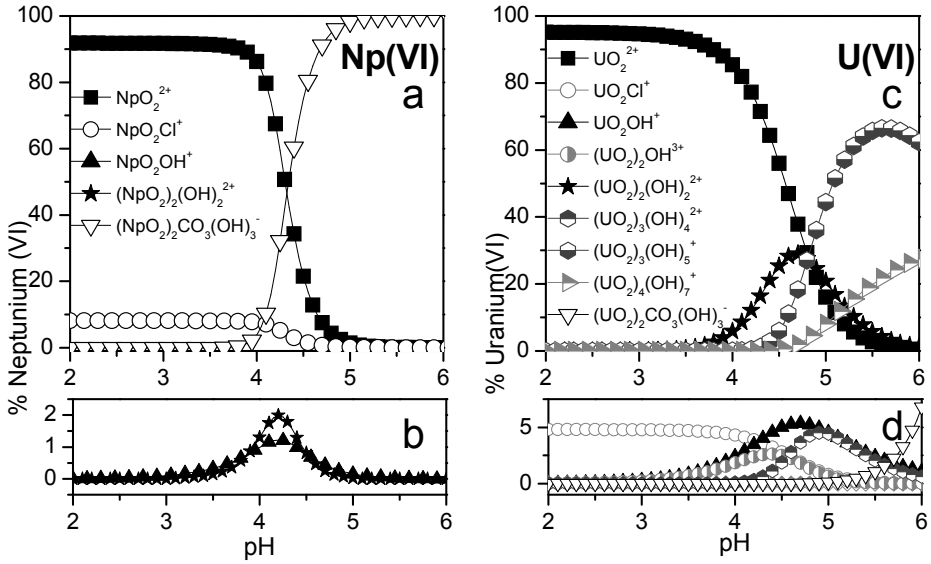

Fig. 4-8: Speciation diagram of 500 µM Np(VI) and U(VI) in aqueous solution at 0.1 M NaCl at ambient atmosphere. (a) Np(VI) species exceeding 2% of total Np(VI) amount, (b) Np(VI) species < 2% of total Np(VI) amount (enlarged ordinate) c) U(VI) species exceeding 7.5% of total U(VI) amount, (b) U(VI) species < 7.5% of total U(VI) amount (enlarged ordinate).

complexes, in particular the dimer $(UO_2)_2(OH)_2^{2+}$, and the trimer $(UO_2)_3(OH)_5^{+}$ govern the U(VI) speciation in the pH range 4 – 6. According to the presently accepted thermodynamic data, the dimeric U(VI) mixed hydroxo carbonate complex $(UO_2)_2CO_3(OH)_3^{-}$ becomes dominant only at pH > 6.

From these modeling efforts, it becomes evident that the speciation patterns of the two actinyl(VI) cations discussed here differ significantly. With respect to the rather similar molecular structures and effective charge distribution of both ions, this result is quite unexpected. However, one has to consider that the experimental database available to establish a set of chemical species and derive respective thermodynamic parameters is more restricted and less reliable in the case of Np(VI) when compared to U(VI). This was clearly demonstrated by the cumulative view on the related NEA TDB volumes presented in section 2.3 [10-12]. Thus, the probability that the currently accepted set of Np(VI) hydrolysis products and carbonate complexes is incomplete and/or combined with inaccurate reaction constants is not negligible.

4.2.2 NIR spectroscopy of Np(VI) solutions in the acidic pH range

The NIR spectra of a 500 µM Np(VI) solution at varied pH conditions at ambient atmosphere and an ionic strength of 0.1 M were obtained as described in section 6.2.7 and are shown in Fig. 4-9. The absorption band of the NpO_2^{2+} species is observed at 1222 nm [165, 166] in the NIR spectra obtained at pH ≤ 4.0 (Fig. 4-9c, lower traces). Upon increasing the pH, the absorption band maximum is shifted to 1218 nm at pH 4.5 and to 1204 nm at pH 5.3 (Fig. 4-9c, upper traces). Simultaneously to the observed shift of the absorption maximum, a weak shoulder arises around 1175 nm at pH values ≥ 4.5 showing increasing intensity with increasing pH.

Since the hexavalent neptunium is potentially reduced to the more stable $Np^{V}O_2^{+}$ ion in ambient atmosphere, the spectral absorption range of the $Np^{V}O_2^{+}$ ion (λmax = 979.5 nm) was monitored during the NIR measurements of Np(VI). The results are presented in Fig. 4-9b showing the intensity increase of the absorption band at 979.5 nm. It was found that the final amount of Np(V) does not exceed 30% of total Np concentration after six hours of measurement time. Due to strong extinction differences of the bands at 979.5 nm (395 L Mol^{-1} cm^{-1}) and 1222 nm (45 L Mol^{-1} cm^{-1}) for Np(V) and Np(VI), respectively [167], it is reasonable to show absorption changes of few wavelengths upon pH increase separately and enlarged for Np(VI) in Fig. 4-9c. However, because of the great spectral distance of the absorption bands of both neptunyl ions, an interference of Np(V) species in the spectra of the Np(VI) solution shown in Fig. 4-9a can be ruled out. In ATR FT-IR experiments, the impact of redox reactions is not significant, since preparations and measurements were carried out within 1 hour.

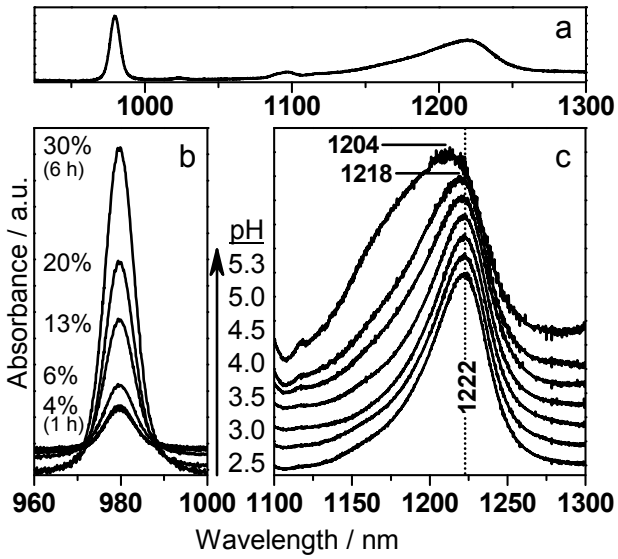

Fig. 4-9: NIR spectra of 500 µM neptunyl(VI) solutions (0.1 M NaCl) recorded at different pH values. (a) Overview NIR spectrum at pH 5. (b) Detailed view at the absorption of the Np(V) ion The spectra reflect the reduction of Np(VI) to Np(V) during NIR measurement time (~ 6 h). The relative amount of originated Np(V) is indicated. (c) Absorption of the Np(VI) ion at different pH values: 2.5, 3.0, 3.5, 4.0, 4.5, 5.0, and 5.3 (from below to top). Indicated values are in nm.

From the NIR spectra recorded at low pH values ≤ 4, the predominance of the NpO_2^{2+} species is verified since no significant spectral alterations are observed. At pH > 4, a change in the Np(VI) speciation can be derived by the appearance of a shoulder around 1175 nm and the observed shift of the maximum to shorter wavelengths. The small displacement of 4 nm between pH 4 and 5.3 may be due to an overlapping of absorption bands representing one or more additional species. With respect to the results of the calculated aqueous speciation of Np(VI) several species might contribute to the spectrum in the pH range > 4 (cf. Fig. 4-8a,b). The species which is predicted to become predominant in the mildly acidic pH range is the dimeric $(NpO_2)_2CO_3(OH)_3^-$. Hence, the spectral alterations in the NIR spectra at $4 < pH \leq 5.3$ should mainly be due to this species. However, no structural information can be gained from the spectrophotometric measurement at least. Thus, vibrational spectroscopy, i.e. ATR FT-IR, is applied to the same solution system, firstly to prove the mentioned observations, and secondly to get structural information about the formed hydrolysis and carbonate complexed species.

4.2.3 Isostructural complexes of Np and U

Infrared studies of the aqueous actinyl ion speciation in the submillimolar concentration range generally reach the detection limit of conventional instrumental setups. For this reason, the spectra are expected to show a relative low signal-to-noise ratio which might impede an accurate evaluation of the data. Furthermore, the characteristic absorption bands of the hydrolysis products representing the υ_3 mode are expected to appear at longer wavelengths compared to those of the free monomer species. The extent of this shifting potentially

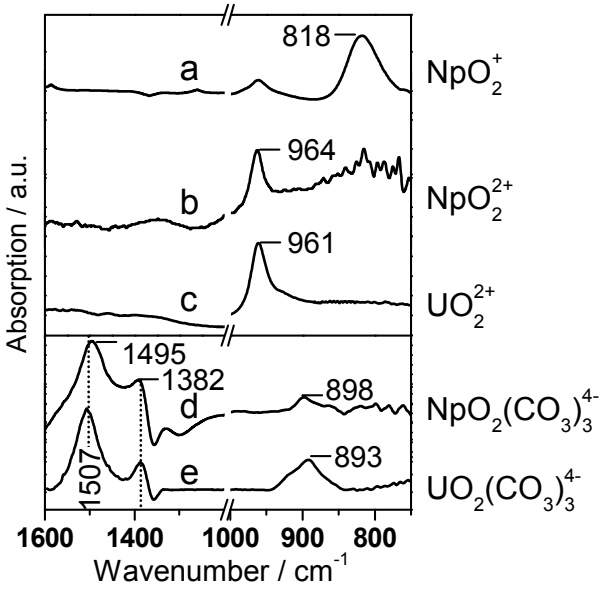

Fig. 4-10: ATR FT-IR spectra of the actinyl monomers (a) 100 mM Np(V), (b) 5 mM Np(VI) and (c) 5 mM U(VI) at pH 1.5 and of actinyl(VI) tricarbonate complexes (d) 1 mM Np(VI), (e) 5 mM U(VI) in 0.1 M $NaHCO_3$, 0.1 M NaCl, pH 8.8. Indicated values are in cm^{-1}.

provides additional information about the formed species [28, 168]. Consequently, on one hand, a detailed knowledge of the spectra of the monomeric non-complexed actinyl ions will be helpful to discriminate between spectral features which can be ascribed to residual absorptions of these ions and randomly appearing noise. On the other hand, these spectra allow an accurate determination of the extent of the frequency shift of the υ_3 mode upon formation of hydrolysis species which was found to provide valuable information for spectra interpretation.

Therefore, we present the spectra of the monomeric hexavalent actinyl ions, NpO_2^{2+} and UO_2^{2+}, recorded at low pH (1.5) and at millimolar concentrations (Fig. 4-10, lower traces). For comparison, the spectrum of the most stable neptunium species, i.e. the pentavalent species NpO_2^+, recorded under the same conditions is also shown (Fig. 4-10, upper trace). All spectra show the absorption bands of the antisymmetric stretching vibration modes (υ_3) at 818, 964 and 961 cm^{-1} for the NpO_2^+, NpO_2^{2+} and UO_2^{2+} ion, respectively, as they were previously reported [28, 169, 170].

Firstly, the spectra allow an unequivocal spectral distinction between the pentavalent and hexavalent state of neptunium because of the different frequencies of their absorption maxima (~ 150 cm^{-1}). Complex formation of the actinyl ions in aqueous solutions, i.e. hydrolysis products and carbonate complexes from dissolved atmospheric carbon dioxide, is expected to generate band shifts to lower wavenumbers up to a maximum extent of 100 cm^{-1}. From the better known U(VI) system, such shifts were reported to be from ~100 to ~70 cm^{-1} for hydroxo ($UO_2(OH)_4^{2-}$) and carbonate ligands ($UO_2(CO_3)_3^{4-}$), respectively [27, 65]. Thus, when studying Np(VI) species in aqueous solution, interferences of bands from Np(V) species can be ruled out.

Secondly, the υ_3 modes of the hexavalent aqua ions of uranium and neptunium show very similar absorption frequencies at 961 and 964 cm^{-1}, respectively. These frequencies are in good agreement with the data obtained by authors using a dispersive IR spectrometer. Besides U(VI) and Np(VI), Jones et al. investigated also Pu(VI) and reported the υ_3 mode occurring at 962 cm^{-1} [19] The deviation between the υ_3 frequencies is within 10 cm^{-1} [19]. This is in good agreement with results from density functional theory calculations using a scalar four-component relativistic method. From this approach, the corresponding wavenumbers were computed to 971, 977, and 970 cm^{-1} for U(VI), Np(VI) and Pu(VI), respectively [171]. Due to the actinide contraction, the An-O_{ax} bond distances are slightly shortened from UO_2^{2+} over NpO_2^{2+} to PuO_2^{2+} which shall result in an increased frequency of the υ_3 mode. On the other hand, in going from U(VI) to Np(VI) and to Pu(VI), there are increasing numbers of unpaired electron(s) which go(es) mainly into non-bonding 5fδ and 5fϕ orbitals [63]. In the higher actinides, more electrons are localized on the metal atom and, therefore, the polarization of the actinide-oxygen bond is reduced resulting in a decreasing frequency of the υ_3 mode. Finally, these two effects mainly compensate each other and the frequency of the υ_3 mode remains almost constant in the AnO_2^{2+} series.

With respect of the same $D_{\infty h}$ symmetry and a similar binding force constant derived from the similar frequency of the υ_3 mode of both hexavalent ions UO_2^{2+} and NpO_2^{2+}, similar spectral shifts of this mode can be expected when isostructural complexes may occur in solution. A verification of this effect is exemplarily shown for the tricarbonate complex as a model of both hexavalent ions (Fig. 4-10d,e). The vibrational mode υ_3 of the actinyl(VI) unit AnO_2 and symmetric and asymmetric vibrational modes of the complexed carbonate occur at very similar wavenumbers, at 898, 1495 and 1382 cm^{-1} for Np(VI) and at 893, 1507 and 1382 cm^{-1} in case of U(VI).

In consequence, the hydrolysis of the U(VI) system which was extensively investigated by spectroscopic approaches in the past, can serve as a reference system for ATR FT-IR investigations of Np(VI) complexes in diluted aqueous solutions [28, 61]. Therefore, the infrared experiments were performed with both actinyl systems to obtain spectra which can be comparatively interpreted.

4.2.4 Np(VI) and U(VI) speciation in aqueous solutions in the acidic pH range

The ATR FT-IR spectra obtained for 500 µM Np(VI) solutions at different pH values are shown in Fig. 4-11a. In the region between 1300 and 1000 cm^{-1}, only one band was observed which is due to residual perchlorate from the Np(VI) stock solution providing no relevant information. Therefore, this spectral region is not shown for clarity.

The absorption band of the υ_3 mode of the neptunyl ion is observed at 964 cm^{-1} at pH 3 (Fig. 4-11a upper trace). Upon increasing the pH to 4 and 4.6 a new band at 931 cm^{-1} is observed whereas the intensity of the band at 964 cm^{-1} is considerably reduced (Fig. 4-11a

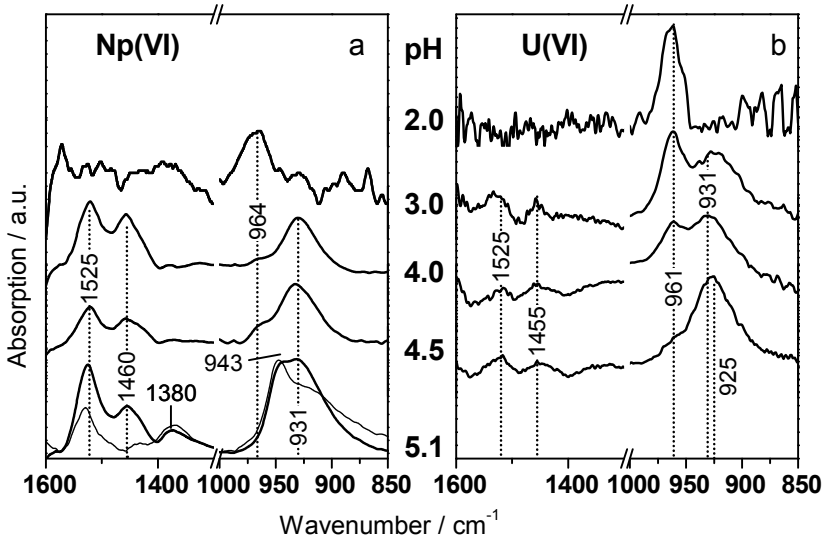

Fig. 4-11: ATR FT-IR spectra of 500 µM oxic neptunyl(VI) and uranyl(VI) solutions at varied pH (0.1 M NaCl). (a) Spectra of Np(VI) solutions at pH 3.0, 4.0, 4.5, and 5.1 (from top to bottom). (b) Spectra of U(VI) solutions at pH 2.0, 3.0, 4.0, and 4.5 (from top to bottom). Indicated values are in cm^{-1}.

middle traces). At pH 5.1 two overlapping bands at 943 and 931 cm^{-1} are observed (Fig. 4-11a lower trace). Additional spectral features are observed in the region between 1600 and 1300 cm^{-1}. Starting from pH 4.0, two bands are detected at 1525 and 1460 cm^{-1}, the latter showing a reduced relative intensity at higher pH (Fig. 4-11a). Above pH 5.1, an additional band grows up at 1380 cm^{-1} (Fig. 4-11a lower trace).

For comparison, the obtained spectra of 500 µM U(VI) at varied pH conditions are presented in Fig. 4-11b in the manner described above. At pH 2, a single band at 961 cm^{-1} is observed (Fig. 4-11b upper trace). Its intensity decreases upon increasing pH and an additional band with absorption maximum at 931 cm^{-1} appears in the spectra at pH ≥ 3 (Fig. 4-11b middle traces). This band is shifted to 925 cm^{-1} in the spectrum recorded at pH value 4.5 (Fig. 4-11b lower trace). In analogy to the spectra of the Np(VI) solutions, additional bands at 1525 and 1455 cm^{-1} are observed at pH values ≥ 3.

In the spectrum of the Np(VI) solution recorded at pH 3, the band at 964 cm^{-1} is assigned to the free ion NpO_2^{2+}, indicating the predominance of this species at pH ≤ 3 and at least its contribution to the speciation up to pH 4.5 (Fig. 4-11a). In analogy, the absorption band at 961 cm^{-1} in Fig. 4-11b is due to the free uranyl species UO_2^{2+}, strongly participating in the U(VI) speciation at pH ≤ 4.5. The obtained spectral information agrees with the predictions from the thermodynamic data (cf. Fig. 4-8). According to previous findings, the spectra of the uncomplexed species NpO_2^{2+} and UO_2^{2+} show obviously a reduced signal-to-noise ratio compared to the complexed species formed at higher pH level [27]. A lower absorption coefficient of the free actinyl (VI) species compared to their hydrolysis species seems to be generally characteristic.

The modeled U(VI) speciation predicts distinct formation of hydrolysis species, i.e. monomeric, dimeric and trimeric species range between pH 4 and 6. Quilès and Burneau

reported IR bands at 943 and 923 cm^{-1} in 0.1 M U(VI) solutions at pH 3.2 and 4.1 and assigned them to $(UO_2)_2(OH)_2^{2+}$ and $(UO_2)_3(OH)_5^{+}$, respectively.[28] Thus, the U(VI) band at 931 cm^{-1} observed in this work at pH 3 and 4 (Fig. 4-11b, middle traces) may show both species present in the 500 µM U(VI) solution in the pH range between 3 and 4. Upon further increasing the pH, the monomeric UO_2^{2+} species is hardly observed and the fraction of the trimeric hydroxo species is obviously slightly increased resulting in a small shift of the absorption band from 931 to 925 cm^{-1} at pH 4.5 (Fig. 4-11b, lower trace).

From our recent work of the aqueous speciation of U(VI) at the low micromolar concentration level, another interpretation of the bands observed at pH ≥ 3 has to be taken into account. A band at 923 cm^{-1} was observed at pH ≥ 2.5 in a 20 µM solution and was assigned to a monomeric hydroxo complex. [27]. From principle thermodynamic aspects, the formation of monomeric species is more reasonable than polymeric complexes at low micromolar concentrations. However, the 500 µM concentration level used in this work might represent the concentration range of the transition from polymeric to monomeric species. Thus, contributions of a monomer uranyl hydroxo complex in the 500 µM U(VI) solution may result in the band with absorption maximum at 925 cm^{-1}. Nevertheless, the infrared spectra shown in Fig. 4-11b provide evidence of the formation of hydrolysis products already at lower pH conditions than predicted by the thermodynamic data (cf. Fig. 4-8b). This is in agreement with previous results [27, 28].

In opposition, the thermodynamic data of Np(VI) do not predict hydrolysis products contributing to the speciation to a significant extent. From the NEA database, the presence of a monomeric (NpO_2OH^{+}) and a dimeric species ($(NpO_2)_2(OH)_2^{2+}$) can be suggested with a relative amount of less than 2% which is not expected to be detectable by a conventional spectroscopic technique (cf. Fig. 4-8a). The IR spectra present contradictory results as shown in Fig. 4-11a: at pH 4 the spectrum of the Np(VI) solution shows a strong shift of the υ_3 band to lower frequency of 33 cm^{-1}. This must be due to a drastic change in the Np(VI) speciation. A species with absorption maximum at 931 cm^{-1} (Fig. 4-11a) is probably formed by hydrolysis reactions at pH 4 and exists up to pH 5.1.

In contrast to the spectra of the U(VI) solutions recorded between pH 3 and 4, no significant absorption occurs around 940 cm^{-1} for the neptunyl(VI) system which makes the formation of a dimeric hydrolysis product of Np(VI) unlikely. Therefore, the band at 931 cm^{-1} is tentatively assigned to a monomeric hydroxo species. Furthermore, this assumption is supported by the ATR FT-IR spectra presenting a speciation change at a fixed actinide to hydroxide ratio in Fig. 4-12a-c. Upon reducing the Np(VI) concentration from 5 mM to 0.5 mM at pH 4, the two bands at 964 and 931 cm^{-1} show decreasing and increasing intensities, respectively. These spectra demonstrate that, beside the NpO_2^{2+} ion, one additional major species dominates the speciation depending on the Np(VI) concentration. Because of the decreasing concentration, this species has to be monomeric. Polymeric species can be

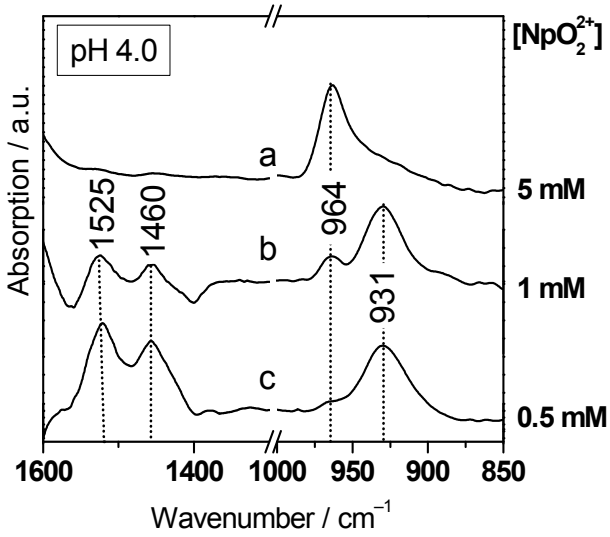

Fig. 4-12: ATR FT-IR spectra of neptunyl(VI) solutions at pH 4: (a) 5 mM, (b) 1 mM, (c) 0.5 mM. Indicated values are in cm^{-1}.

ruled out at this pH level. Because of precipitation, millimolar concentrations can not be investigated at higher pH without addition of non-complexing ligands, e.g. TMA-OH.

Further insight can be obtained from previous Raman spectroscopic investigations on neptunium(VI) speciation. Although the υ_1 mode of the NpO_2^{2+} cation is observed in the Raman spectra, its shift to lower wavenumbers upon hydrolysis reactions is expected to be of the same extent as for the υ_3 mode observed by infrared spectroscopy [28]. The symmetric stretching vibration (υ_1) of NpO_2^{2+} appears at 854 cm^{-1} in the Raman spectrum [169]. In an investigation of 0.1 M Np(VI) solutions in the pH range from 1.7 to 3.7, a broadening of this band was observed at pH 3.3 which was due to the presence of two bands at 854 cm^{-1} and a band, shifted about 20 cm^{-1} to lower wavenumbers, at 834 cm^{-1} as it was demonstrated by deconvolution techniques [169]. The shifted band was assigned to the formation of Np(VI) hydroxo complexes. According to the results of vibrational spectroscopic investigations of the hydrolysis reaction of U(VI), a bathochromic shift of 20 cm^{-1} of the actinyl stretching mode can be assigned to a dimeric hydroxo species [28]. Additionally, modeling of a 0.1 M Np(VI) solution based on the NEA data predicts the formation of the dimer $(NpO_2)_2(OH)_2^{2+}$ at pH 3.5 – 4.2 (data not shown) which might explain the observed spectral component at 834 cm^{-1} observed in the Raman spectra of Madic et al. [169]. However, direct comparison of the respective Raman spectra and the IR spectra presented here is difficult because of the concentration level reduced by a factor of 200.

At pH ≥ 4.5 the thermodynamic data of Np(VI) in 500 µM solutions predict the formation of a dimeric neptunyl mixed carbonate hydroxo complex (cf. Fig. 4-8). The respective IR spectrum obtained at pH 5.1 exhibits an additional band at 943 cm^{-1} (Fig. 4-11a, lower trace). In homology to the observed spectral changes discussed above, a shift of 21 cm^{-1} compared to the free neptunyl species strongly suggests the presence of a dimeric complex [27, 28]. In addition, the appearance of a band at 1380 cm^{-1} correlates with the band at 943 cm^{-1} in the

spectrum recorded at pH 5.1. From the previous IR spectroscopic investigation of U(VI) in submicromolar solutions, it is assumed that the band at 1380 cm^{-1} can be ascribed to the symmetric stretching vibration of carbonate ligands complexed with a U(VI) species, e.g. $UO_2(CO_3)_3^{4-}$ [27]. The corresponding antisymmetric stretching mode of the carbonate ligand is observed at 1525 cm^{-1} which, in fact, shows considerably increased relative intensity in the respective spectrum (Fig. 4-11a, lower trace). Since the pH 5.1 spectrum obviously represents contributions from two different Np(VI) species, the spectrum of the monomeric species predominating at pH 4 was subtracted. The resulting spectrum shows bands at 1529, 1370 and 946 cm^{-1} with a shoulder around 930 cm^{-1} representing residual contributions from the monomeric hydroxo species due to incomplete subtraction (Fig. 4-11a, lower thin trace). The residual absorption can be eliminated by increasing the subtraction factor leading to spectral artifacts in the spectral range > 1400 cm^{-1}. Consequently, the bands at 1375 and 1525 cm^{-1} can be assigned to the symmetric and antisymmetric stretching vibration of coordinated carbonate ligands, respectively. According to the previously performed study of carbonate coordination to U(VI), the splitting of these vibrational modes strongly suggests bidentate binding of the carbonate to the neptunyl(VI) ion (cf. Fig. 4-10d,e and [27]). Thus, the dominant neptunyl species at pH > 4.5 most probably is a carbonate containing species, e.g., $(NpO_2)_2CO_3(OH)_3^-$ as suggested by the thermodynamic data (cf. Fig. 4-8).

The bands at 1525 and ~ 1460 cm^{-1} appear in the spectra of both U(VI) and Np(VI) solutions when the first hydrolysis species is formed, i.e. at pH 3 for U(VI) and pH 4 for Np(VI) indicating the formation of similar hydroxo complexes. However, an unequivocal assignment of these bands is difficult. One may assume that these bands are generated by a contamination with organic or inorganic ligands or by sorption processes on the used ATR crystal as well. But, this was excluded by a series of experiments in our previous study on the U(VI) speciation at low micromolar concentration level providing evidence for these spectral features as intrinsic optical absorption properties of the aqueous uranyl solutions [27]. The bands possibly represent water molecules with a special coordination in the hydrate shells of the formed hydroxo complexes.

In summary, it has been shown that the combined approach of NIR and ATR FT-IR spectroscopy is appropriate to study the Np(VI) speciation in micromolar aqueous solutions. From NIR spectroscopy, information about changes in the aqueous Np(VI) speciation are obtained by slight changes of the absorption band around 1220 nm with increasing pH. The identification of different neptunyl(VI) species in solution is accomplished by ATR FT-IR spectroscopy. For the first time, the results allow the verification of current thermodynamic data by spectroscopic findings providing structural information of the aqueous Np(VI) species present at a micromolar concentration level up to pH 5.3 under distinct conditions.

The FT-IR spectra clearly demonstrate the presence of three different aqueous Np(VI) species in the acidic pH range up to pH 5.1 in ambient atmosphere. The fully hydrated

neptunyl ion dominates the Np(VI) speciation below pH 3. The dimeric hydroxo carbonate complex, $(NpO_2)_2CO_3(OH)_3^-$, is the most relevant species at pH > 4.5. These results are in good agreement with the thermodynamic data from the NEA database. In the pH range 3 − 5, discrepancies between the obtained spectral information and the predicted speciation based on thermodynamic data become obvious. The ATR FT-IR spectra provide evidence for the formation of an additional hydroxo complex, most likely a monomeric hydroxo complex. In contrast, current thermodynamic data exclude the presence of hydrolysis species of a relevant amount. The origin of the contradictory results might be due to the following aspects. The vast majority of the data in the NEA database are taken from non-structural elucidating experiments, e.g., potentiometry which were not yet verified by spectroscopic techniques providing independent structural information. Furthermore, contributions of monomeric and polymeric species to the speciation strongly depends on the neptunyl(VI) concentration. In previous spectroscopic studies the concentrations of the investigated solutions were higher by several orders of magnitudes restricting the formation of monomeric hydroxo species.

4.2.5 Colloidal species of Np(VI) and U(VI)

In the assessment of the actinide migration behavior the solubility and, thus, the formation of colloidal phases plays a crucial role. There are transport-facilitating and transport-impeding effects caused by colloids [172, 173]. Consequently, the investigation of the U(VI) and Np(V/VI) speciation in aqueous solution and upon sorption processes requires the monitoring of the formation of insoluble solids. Interestingly, the vast majority of the spectroscopic work concerning the aqueous U(VI) speciation published during the last decade fail to provide detailed information about formation of colloids in the examined solutions. This aspect rises further questions about the interpretation of the published data.

Photon correlation spectroscopy (PCS) is a useful tool for checking precipitation in solution, since it is able to detect colloids with diameters down to 1 nm depending on the concentration. However, in order to rule out a possible formation of colloids in highly diluted solutions of U(VI) and Np(V/VI), PCS analysis alone might be not sufficient. Therefore, a series of experiments using ultracentrifugation in combination with PCS, ICP-MS and ATR FT-IR spectroscopy were exemplarily applied to micromolar U(VI) solutions.

In a first step, a considerably high concentrated U(VI) solution (10 mM, pH 7.0) was investigated to provoke the formation of a precipitate which was distinctly confirmed by PCS analysis. In the respective IR spectrum a significant band at 938 cm^{-1} representing the antisymmetric stretching vibration of the UO_2^{2+} ion is observed (Fig. 4-13a). In contrast to the absorption bands of completely dissolved hydroxo and carbonate U(VI) species in the micromolar concentration range at pH ≥ 7, the sharp band at 938 cm^{-1} clearly indicates the presence of a precipitate and can serve as a marker band for the formation of colloidal species in the IR spectra. This is confirmed by the spectrum obtained from 50 µM U(VI) solution at

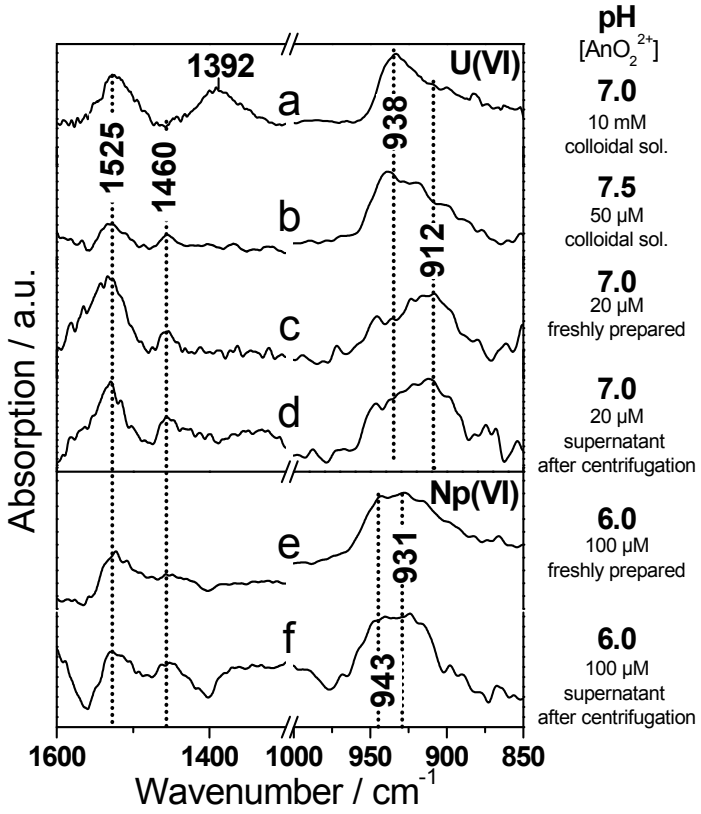

Fig. 4-13: ATR FT-IR spectra of aqueous U(VI) and Np(VI) solutions (0.1 M NaCl, ambient atmosphere): U(VI) solutions containing colloids as shown by PCS: (a) 10 mM, pH 7.0, and (b) 50 µM U(VI) pH 7.5,. Freshly prepared solutions of 20 µM U(VI); pH 7.0 before (c) and after ultracentrifugation (117,000 g, 1 hour) (d) and 100 µM Np(VI); pH 6.0, before (e) and after ultracentrifugation (117,000 g, 1 hour) (f).

pH 7.5 (Fig. 4-13b) which was shown to contain colloidal species by PCS. Since the ATR FT-IR spectra in Fig. 4-13 do not show a band at 938 cm^{-1} the presence of colloids in the investigated solutions can be neglected. In a second step, ultracentrifugation for 1 hour at a maximum RCF of 117,000 g was applied after the preparation of a solution containing 20 µM U(VI) at pH 7.0. PCS, ICP-MS and ATR FT-IR measurements were applied to the supernatant and the remaining solution at the bottom of the centrifugation tube. The results from PCS evidence the absence of precipitates, moreover, the U(VI) concentrations determined by ICP-MS were the same before and after ultracentrifugation. Additionally, the obtained ATR FT-IR spectra are in excellent agreement and do not show the colloids indicating band at 938 cm^{-1} (Fig. 4-13c,d).

A similar procedure was applied to diluted 100 µM Np(VI) solutions at pH 6. Again, no differences were observed before and after centrifugation (Fig. 4-13e,f). The marker band in the IR spectrum of Np(VI) colloids was observed at 937 cm^{-1} [149]. The application of nanofiltration for the separation of colloids seems questionable since traces of glycerol from the membranes used were found to provoke disturbing bands in the infrared spectra.

In summary, from this spectroscopic findings it is deduced that ATR FT-IR represents a sensitive technique for the detection of actinyl(VI) colloids, since spectra of precipitates and

of solutions containing both dissolved and colloidal species show characteristic spectral features. The monitoring and the description of colloid formation is a crucial aspect for the investigation of actinide stability constants and their interpretation. In particular, previous studies and constant contributing to current databases should be evaluated critically concerning the formation of solid phases.

4.3 Np(VI) and U(VI) speciation in the absence of atmospheric carbonate

Previously, the speciation of the hexavalent ions of neptunium and uranium has been investigated under ambient conditions. When working at ambient atmosphere, the speciation becomes more complex, since the carbonate concentration varies in dependence of pH and a set of several different carbonate complexes are formed with Np(VI) and U(VI). Nevertheless, the study was performed at ambient atmosphere, since it is relevant for environmental applications as the partial pressure of CO_2 generally ranges between 10^{-3} and 10^{-2} in subsurface waters. However, in order to simplify the systems at neutral pH conditions and to confirm the spectroscopic findings at low pH, *in situ* ATR FT-IR speciation studies have been performed for micromolar Np(VI) and U(VI) solutions at inert gas atmosphere (N_2).

In gloveboxes at N_2 atmosphere, the presence of CO_2 and O_2 is significantly reduced ($\leq$ 0.1 ppm). For redoxsensitive compounds this may indicate the transformation to other oxidation states. In this work the reduction of Np(VI) to Np(V) was carefully monitored using NIR spectroscopy according to the experiments performed in air (cf. section 4.2.2)

4.3.1 Calculation of Np(VI) and U(VI) speciation at N_2

The speciation of micromolar Np(VI) and U(VI) in aqueous solutions at inert gas atmosphere, excluding dissolved atmospheric carbon dioxide were computed and the major contributing species ($\geq$ 10%) are shown in Fig. 4-14. The modeling prognoses two dominating Np(VI) and U(VI) species in the pH range 3 – 7, namely the monomer AnO_2^{2+} (An = U, Np) at pH < 5.5 and the hydroxo trimer $(AnO_2)_3(OH)_5^+$ at pH > 5.5. Additionally, the contribution of the dimer complex $(AnO_2)_2(OH)_2^{2+}$ to a relative amount of around 20% at pH 4.5 – 6 is predicted for both actinyl(VI) cations. However, for the better investigated U(VI) system further species are included in the NEA TDB, namely the (1,1) complex mounting up to 20% at pH 4.5 – 6 and the (4,7) complex increasing up to 20% at pH 7. As mentioned previously (cf. section 2.3), the thermodynamic data is much more rudimentary for Np(VI) than for U(VI), only one reference, i.e. the work by Cassol et al. from 1974 was taken into account for the NEA review of Np(VI) hydrolysis in 2001, and the NEA TDB was not enriched by new

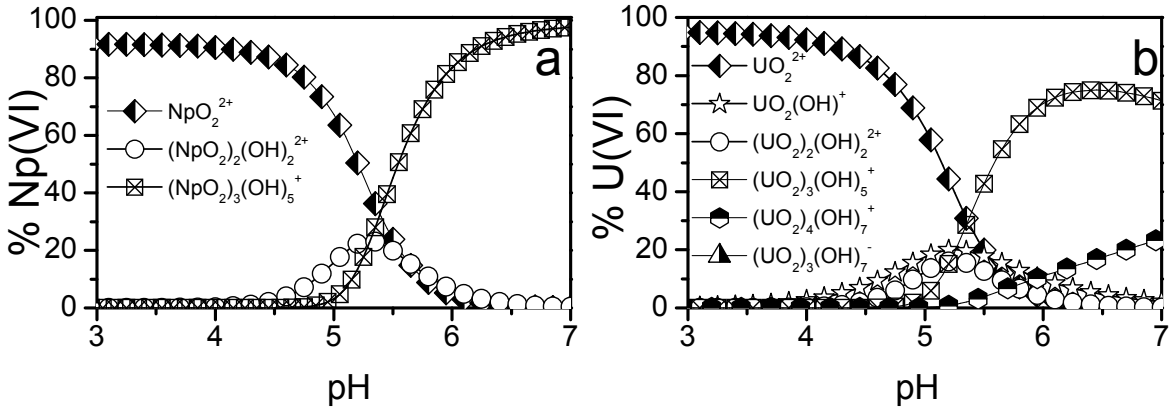

Fig. 4-14: Speciation diagrams of anoxic neptunyl(VI) and uranyl(VI) in aqueous solution at 0.1 M NaCl under nitrogen atmosphere. (a) 100 µM Np(VI), (b) 20 µM U(VI) Species < 10% of total actinyl(VI) amount are eliminated from the graph for clarity.

data during the update process in 2003 [11, 12, 37]. That may explain the unexpected much easier set of hydroxo complexes in the speciation of Np(VI).

4.3.2 The species of micromolar Np(VI) and U(VI) solutions in the acidic pH at N_2

The spectra of micromolar Np(VI) and U(VI) solutions in the pH range 4 – 6 are comparatively shown in Fig. 4-15 and a bathochromic shift of the actinyl stretching mode $\upsilon_3(AnO_2)$ is clearly observed for both cations upon increasing pH. In the Np(VI) spectrum at pH 4, one band at 928 cm^{-1} with a shoulder at 964 cm^{-1} is observed. At pH 5, the shoulder becomes reduced in intensity and completely disappears at pH 6. Between pH 5 and 6 the band representing υ_3 is shifted by 20 cm^{-1}, from 928 to 908 cm^{-1} (Fig. 4-15a). Such a shift clearly indicates strong changes in the speciation in the mentioned pH range. The resulting band shows a large bandwidth, suggesting the presence of more than one species. Possibly, the band at 928 cm^{-1} is still contributing to a smaller extent. Whereas the limit for distinct detection of Np(VI) hydrolysis species was found to be at 100 µM, the signal-to-noise ratio of the spectra of U(VI) allowed the reduction of the U(VI) concentration even to 20 µM. At pH 4, one band centering at 922 cm^{-1} is observed. Upon increasing the pH, the band becomes broad and its maximum is shifted to 910 cm^{-1} (Fig. 4-15b). Comparing the extent of the shift of $\upsilon_3(AnO_2)$ in the Np(VI) and U(VI) solutions, the formation of similar hydroxo complexes in the pH range from 4 to 6 can be deduced. This is supported by the occurrence of further bands at 1525 and ~1460 cm^{-1} in the pH series of both cations.

In comparison to the ATR FT-IR spectra of An(VI) hydrolysis species obtained at ambient atmosphere (cf. sections 4.1 and 4.2), the similarity of several spectral features are distinct. Firstly, the same monomeric hydrolysis complexes dominate the speciation in micromolar solutions at pH 4, for Np(VI) with absorption at ~930 cm^{-1} and for U(VI) with absorption at ~925 cm^{-1} (cf. Fig. 4-15 and Fig. 4-11). The related bands at higher frequency, namely at 1525 and ~1460 cm^{-1}, have also been detected previously and can be interpreted to characteristics of these first hydrolysis product of U(VI) and Np(VI) at a micromolar

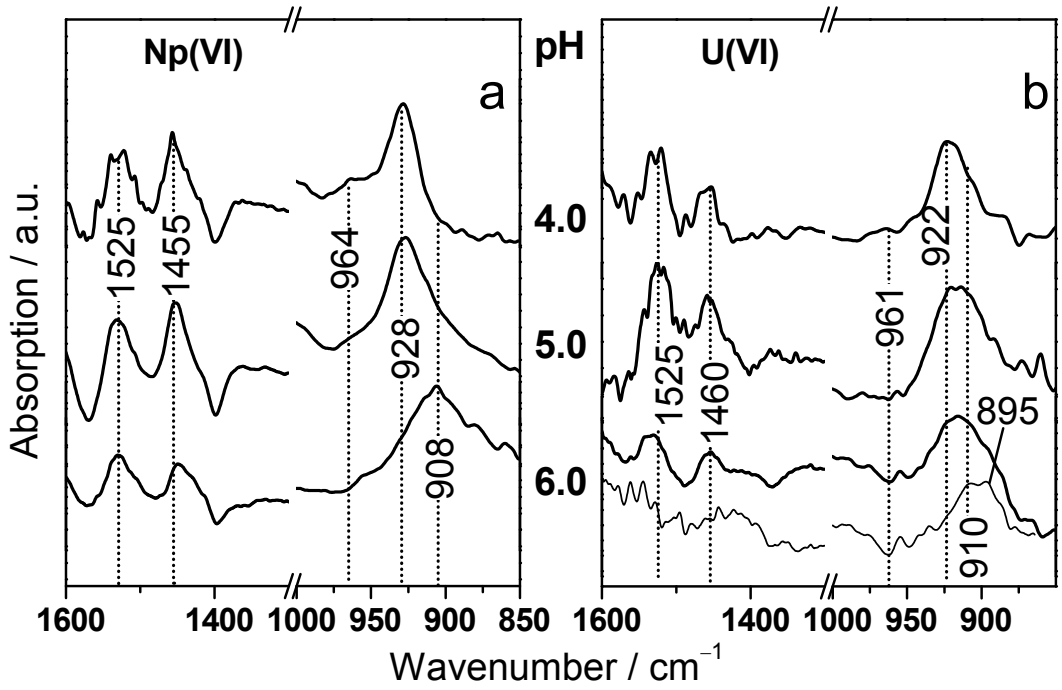

Fig. 4-15: ATR FT-IR spectra of anoxic Np(VI) and U(VI) solutions at varied pH (0.1 M NaCl). (a) Spectra of (a) ca. 100 µM Np(VI) and (b) 20 µM U(VI) solutions at pH 4.0, 5.0, and 6.0 (from top to bottom). The thin line in the lower trace represents a spectrum corrected by subtraction. For details, see the text. Indicated values are in cm^{-1}.

concentration level. Secondly, the spectra of 20 µM U(VI) solutions do not change drastically up to pH 5 depending on the atmospheric conditions. Hence, the speciation of micromolar U(VI) at pH ≤ 6 is not influenced by dissolved atmospheric CO_2 and the bands at 1525 and ~1460 cm^{-1} do not correspond to carbonate. The Np(VI) spectra obtained at pH > 4 and ambient atmosphere evidence changes in the speciation depending on the presence of carbonate. In air, the formation of binuclear carbonate complexes with absorption maxima at 943 cm^{-1} for $\upsilon_3(NpO_2)$ and 1380 cm^{-1} for $\upsilon_3(CO_3)$ can be deduced from the spectra. In contrast, at N_2 atmosphere, these bands are absent and further hydrolysis complexes contribute to the speciation under the mentioned conditions (cf. Fig. 4-11 and Fig. 4-15).

The spectra of 20 µM U(VI) solutions at ambient atmosphere at pH ~6 show broad bands slightly shifted to lower wavenumbers, most probably contributing to a mixture of hydroxo complexes. IR spectral evidence for carbonate complexation was only found at pH 8.5, due to the appearance of the band at 1365 cm^{-1} for $\upsilon_3(CO_3)$ [27]. At N_2 atmosphere, the spectrum obtained at pH 6 exhibits also a broad band again indicating the presence of several different hydroxide complexes. Upon subtraction of the spectrum obtained at pH 4 from the pH 6 spectrum, it was tried to separate spectral information. The resulting spectrum shows a red-shifted absorption band with maximum at 910 and a distinct shoulder at 895 cm^{-1}. The shoulder at 922 cm^{-1} could be eliminated (Fig. 4-15b, thin line). Hence, it can be suggested that at least two species with absorption at 895 and 922 cm^{-1} contribute to the U(VI) speciation at pH 6.

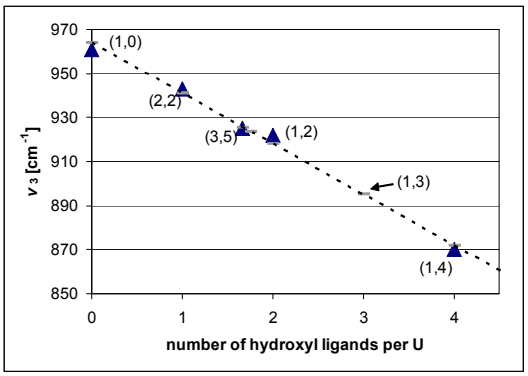

Complex	$\bar{n}$	$\upsilon_3(UO_2)$	Reference	$\upsilon_3(UO_2)$ Eq. 4-1
UO_2^{2+}	0	961	[27, 28]	964
$UO_2(OH)^+$	1			**941**
$UO_2(OH)_2^0$	2	922	[27]	918
$UO_2(OH)_3^-$	3			**895**
$UO_2(OH)_4^{2-}$	4	870	[27]	872
$(UO_2)_2(OH)_2^{2+}$	1	943	[27, 28]	941
$(UO_2)_3(OH)_5^+$	1.7	925	[27, 28]	926

Fig. 4-16: Linear correlation between the number of hydroxide ligands coordinated to each uranium atom ($\bar{n}$) and the asymmetric vibrational frequency $\upsilon_3(UO_2)$ of uranyl hydrolysis products (R^2=0.998).

The currently accepted thermodynamic data predicts the formation of the trimer hydroxo complex $(UO_2)_3(OH)_5^+$ and of the tetranuclear hydroxo complex $(UO_2)_4(OH)_7^+$ between pH 5.5 and 9 (Fig. 4-14). Previously, the trimer was identified in millimolar solutions by $\upsilon_3(UO_2)$ occurring at 923 cm^{-1} in the IR spectrum [28]. However, the formation of this polymeric species to a dominating level may occur only at higher concentrations (> 0.3 mM) [155]. In contrast, at a micromolar concentration level the formation of monomeric hydroxo species is conceivable.

In accordance to Nguyen-Trung [155] and Lefèvre [65], a linear correlation between the asymmetric vibrational frequency $\upsilon_3(UO_2)$ and the average number of hydroxide ligands coordinated to each uranium atom has been applied using literature data and the data obtained in this study (Fig. 4-16, Eq. 4-1).

$$\upsilon_3 = -22.96 \times \bar{n} + 964 \qquad \textbf{Eq. 4-1}$$

$$\upsilon_1 = -22 \times \bar{n} + 870 \ [155] \qquad \textbf{Eq. 4-2}$$

The obtained correlation equation for the asymmetric stretching mode $\upsilon_3(UO_2)$ is in excellent agreement to the one for the Raman-active symmetric stretching mode $\upsilon_1(UO_2)$, reported by Nguyen-Trung [155] (cf. Eq. 4-1and Eq. 4-2). The slope of both equations is around ~22, the factors 964 and 870 represent the vibrational modes υ_3+$\upsilon_1(UO_2)$ of the free UO_2^{2+} ion.

From the correlation equation (Eq. 4-1), values of $\upsilon_3(UO_2)$ were calculated for the uranyl monomers with one and three hydroxo groups, occurring at 941 and 895 cm^{-1}, respectively. These values support the interpretation of the spectrum obtained at pH 6 and its deconvolution to a mixture of two monomeric species at minimum. However, the presence of a small amount of polymeric species can not be completely ruled out.

In summary, from the spectral data of the aqueous speciation of micromolar Np(VI) and U(VI) at inert gas atmosphere, it is suggested that structural similar monomeric hydroxo complexes are formed. The spectra series up to pH 5 confirm the findings from previously

performed measurements at ambient atmosphere, showing the same band maxima and relative intensities, characteristic for monomeric hydroxo species, e.g. $AnO_2(OH)_2^0$.

At pH 6, the atmospheric carbonate in ambient solutions increases, and Np(VI) forms mixed hydroxo carbonate complexes, U(VI) hydrolyzes to additional species. At N_2 atmosphere, excluding atmospheric carbonate, hydrolysis reactions may occur with both actinyl(VI) cations. In fact, the spectrum of Np(VI) completely differs compared to normal atmosphere, indicating the absence of carbonate. In contrast, the U(VI) spectrum at pH 6 is very similar to ambient conditions, confirming the predominance of hydrolysis reactions at weak acidic pH at ambient and inert gas atmosphere. From the similar spectra of U(VI) and Np(VI) at pH 6, the formation of similar hydroxo complexes is deduced. This is in agreement with the thermodynamic data. However, the shift of $\upsilon_3(AnO_2)$ fits better to a stronger contribution of additional monomeric species, e.g. $AnO_2(OH)_3^-$, than to the predominance of polymeric complexes.

4.4 Np(V) speciation in the absence of atmospheric carbonate

Among the various neptunium oxidation states, the pentavalent form, i.e. the neptunyl(V) ion NpO_2^+, dominates the speciation within a wide range of environmental conditions in aqueous solution [6]. Thus, for the risk assessment on a long term, reliable data of Np(V) speciation in aqueous solution and its speciation at the water-mineral interface are crucial contributions to allow an improved modeling of Np migration in the environment. Similar to U(VI), structural information on the distribution of the aqueous Np(V) species is required for the interpretation of surface complexation spectroscopic data. Hence, the speciation of Np(V) was investigated under identical conditions as the sorption studies performed afterwards.

4.4.1 Calculation of Np(V) speciation at N_2

A speciation pattern of a 50 µM Np(V) solution under inert gas atmosphere in the pH range from 2 to 11.5 is shown in Fig. 4-17. Compared to U(VI) and Np(VI), the speciation of Np(V) in aqueous solution is much simpler. The calculation clearly shows that the fully hydrated neptunyl(V) ion, that is NpO_2^+, is the predominant species in the pH range from 2 to 10. (Fig. 4-17a) A strong contribution of the chloride complex NpO_2Cl (aq) which might result from the use of NaCl as background electrolyte is ruled out at an ionic strength of 0.1 M. Two hydrolysis products, i.e. NpO_2OH (aq) and $NpO_2(OH)_2^-$, are predicted at pH ≥ 10 by the thermodynamic data. However, their contribution to the speciation is expected to sum up only to a very small extent (< 5%) up to pH 10.

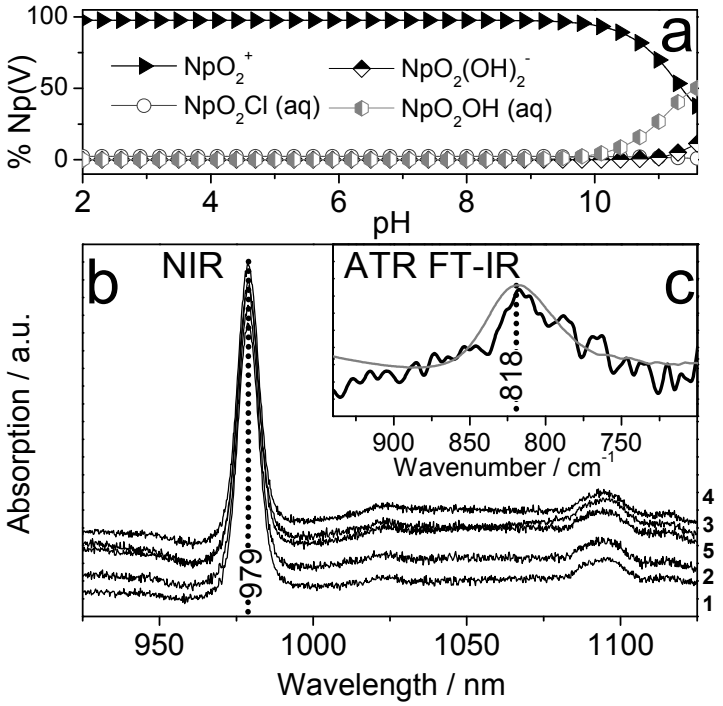

Fig. 4-17: (a) Speciation diagram of 50 µM Np(V) in aqueous solution at 0.1 M NaCl under nitrogen atmosphere, excluding atmospheric CO_3^{2-}. (a) NIR spectra of 50 µM Np(V) in aqueous solution (D_2O, 0.1 M NaCl, N_2 at different pH values 2.5 (1), 3.0 (2), 5.6 (3), 6.5 (4), and 7.7 (5). (c) ATR FT-IR spectra of NpO_2^+ at 50 µM Np(V) at pH 6 (D_2O, 0.1 M NaCl, N_2, black) and at 100 mM Np(V) at pH 1.5 (H_2O, gray). Indicated values are in nm and cm^{-1}, respectively.

4.4.2 Np(V) speciation in micromolar solutions at N_2

The NpO_2^+ ion shows two characteristic absorption bands in the near-infrared region: a strong peak at 979 nm with a molar extinction coefficient of 395 L Mol^{-1} cm^{-1} and a broad peak at 1090 nm [166, 167, 174]. Thus, the Np(V) speciation in aqueous solution can be verified easily by using direct absorption spectrophotometry even at a low neptunyl(V) concentration of 50 µM. The NIR spectra, shown in Fig. 4-17b, were obtained in the pH range between 2.5 and 7.7 as described in section 6.2.7. The spectra present no significant changes neither of the maxima of the absorption peaks nor of the relative absorbance intensities upon increasing pH throughout the investigated range. Thus, the predominance of the fully hydrated species NpO_2^+ predicted by the thermodynamic data is confirmed in the pH range from 2.5 to 7.7.

In the ATR FT-IR spectrum of an aqueous Np(V) solution the asymmetric stretching vibration (υ_3) of NpO_2^+ is observed at 818 cm^{-1} (Fig. 4-17c). This is in agreement with the results of Jones and Penneman, who investigated very high concentrated actinide solutions using a dispersive IR spectrometer in the 1950´s [19]. In diluted aqueous systems, this band is overlapped by the strong water absorption at ~800 cm^{-1}. The lowest concentration of Np(V) in acidic solution (pH 2) detectable with the instrumental set-up at the IRC was found to be 50 mM. Such a concentration level is hardly relevant in an ecological context. Thus, ATR FT-

IR spectroscopic measurements have been performed in heavy water [65]. Because of the isotopic shift of the D_2O absorption band, the detection limit for the NpO_2^+ ion can be reduced by three orders of magnitude to concentrations appropriate for environmental processes. However, this spectrum shows a relatively low signal-to-noise ratio and might not serve as a adequate reference for the aqueous Np(V) species. Therefore, a spectrum of a 0.1 M aqueous Np(V) solution at pH 1.5 was added (Fig. 4-17, grey trace). This spectrum shows a high signal-to-noise ratio and no frequency shift with respect to the considerably higher concentration and decreased pH value. Both spectra provide further evidence for the unique presence of NpO_2^+ in the 50 µM solution at pH 6.

In summary, the predominance of the fully hydrated NpO_2^+ in Np(V) aqueous solutions at a micromolar concentration level and up to pH 7.7 is deduced from NIR and ATR FT-IR spectroscopic measurements.

4.5 Conclusions and Outlook

The aqueous speciation of pentavalent and hexavalent cations of uranium and neptunium has been investigated on a molecular level using NIR spectroscopy and, in particular by ATR FT-IR spectroscopy. The obtained spectral information is compared to results from modeling updated NEA data.

The Np(V) spectroscopic findings substantiate the predicted speciation of modeled thermodynamic data. In contrast, the species distribution of the hexavalent actinyl cations is more complex. Whereas the millimolar U(VI) and Np(VI) speciations fit well to the NEA data, discrepancies are apparent in the submillimolar and micromolar ranges. In fact, the species sets which were selected for the NEA TDB were mainly derived from potentiometry in the millimolar concentration range, where the formation of polymeric species is likely. In contrast, at a micromolar level, as used in this FT-IR work, monomeric species are more favored from a thermodynamic point of view. Hence, a critical extrapolation of the thermodynamic data to micromolar concentrations has to be challenged in future times.

Using the experiences from U(VI) and Np(V/VI) speciation, further vibrational spectroscopic investigations of the speciation of actinide cations under distinct environmental parameters have now become feasible. For instance, the speciations of actinide ions (U(VI), Np(V/VI)) in the presence of inorganic and organic ligands, e.g. carbonate, phosphate can be verified. A more detailed knowledge of the presence of certain actinide species under distinct parameters will lead to a deeper understanding of the chemistry of the actinides in the environment.

Additionally, for the infrared spectroscopic investigation of U(VI) and Np(V) surface complexation, the obtained spectroscopic information on the aqueous speciation is indispensable as a reference.

5. Species of U(VI) and Np(V) on mineral oxide surfaces and their *in situ* spectroscopic characterization

5.1 Introducing remarks on U(VI) sorption onto mineral surfaces

The sorption of U(VI) on a multiplicity of naturally occurring and artificial substrates was intensively studied in the last decades, using macroscopic batch and column experiments, spectroscopic and microscopic analysis, and modeling. For an overview, a literature survey is given in Tab. 2-4.

In air ($p(CO_2) \approx 37.5$ Pa), uranium sorption onto mineral surfaces generally is at a maximum at near neutral pH and decreases sharply toward more acidic or more alkaline conditions [55, 69, 73, 83, 88, 95, 97]. U(VI) adsorption is limited at acidic pH conditions by electrostatic repulsion between positively charged uranyl and the protonated oxide surfaces, and at alkaline pH conditions, between negatively charged U(VI) carbonate complexes and the hydroxylated surface which forms above the zero point of charge (PZC) [84]. At near neutral conditions, deprotonation of oxides surface hydroxyl groups provides additional adsorption sites, and several uranyl hydroxo species dominate the speciation. These changes increase the chemical and electrostatic affinity between cation and surface. They are accompanied by stronger inner-shell surface adsorption and possibly by the formation of aqueous as well as sorbed polynuclear complexes, including surface precipitates [44, 83] (c.f section 2.4).

Vibrational spectroscopy is a tool to distinguish between the different sorption processes (c.f chapter 3). Previous investigations have shown the sensitivity of the UO_2 symmetric and asymmetric stretching modes (υ_1 and υ_3) to changes in coordination environment (cf. chapter 4 or [27, 64, 65, 71, 149, 175]). Complexation of UO_2^{2+} weakens the O=U=O bonds, increasing bond lengths and causing shifts to lower frequency of $\upsilon(UO_2)$, with the extent of this shift related to the stability of the uranyl ligand interaction. This sensitivity allows the use

of these modes as markers for molecularly specific information on surface coordination of surfacial bound UO_2^{2+} [176].

The reactivity at the solid-water interface is controlled by the surface structure, composition, purity and bonding together with solution conditions, namely, speciation, pH, concentration, ionic strength [43]. Thus, a variation of these conditions may allow a complex interpretation of the spectroscopic data resulting in a more complete understanding of the occurring reactions at the interface. Using reaction induced difference spectroscopy the mineral as a stable stationary phase coated on the ATR crystal is monitored in contact with a mobile phase, i.e. the sorptive solution (cf. section 3.2). By a stepwise variation of the parameters of the mobile phase, changes on the mineral are induced. The resulting spectra can be interpreted unequivocally concerning the changed parameter.

In this study, the sorption mechanism of U(VI) on different oxide surfaces, namely TiO_2, α-, γ-Al_2O_3, and SiO_2 were studied on a molecular level by application of *in situ* ATR FT-IR spectroscopy. The investigated mineral oxides have been chosen for several reasons: (1) they act as model oxides for more complex mineral systems; (2) they are ubiquitary in the environment, because of natural occurrences or industrial purposes and contribute to many soils and soil components; (3) their surface properties have been extensively studied; (4) they present high sorption capacities of heavy metal ions; (5) they are inert [108, 119]. For the elucidation of the occurring reactions, the U(VI) sorption on TiO_2 and γ-Al_2O_3 was systematically investigated by variation of sorbent and solution properties at different time ranges.

Additionally, the sorption of U(VI) onto the more complex alumosilicates, i.e. kaolinite, biotite and muscovite, has been evaluated on a molecular level. Kaolinite is applied as a model for 1:1 layer-structured silicate minerals, representative for clay minerals; in contrast, the micas present 2:1 layer-structured silicate minerals and are characteristic constituents of granite.

5.2 U(VI) sorption on titanium dioxide

For the ATR FT-IR spectroscopic investigation of the U(VI) sorption onto TiO_2 a standard protocol was performed, using the conditions listed in Tab. 5-1. The measurement and the analysis of the resulting IR spectra were done as described in section 3.3. The U(VI) speciation in aqueous solutions has been investigated intensively in the sections 4.1 and 4.2 and acts as reference for the study of sorption processes. The free UO_2^{2+} ion is present in very acidic solutions and shows one absorption band at 961 cm^{-1}, corresponding to the antisymmetric stretching vibrational mode υ_3. In micromolar U(VI) solutions at pH 5, the formation of a monomeric hydroxo U(VI) species was suggested by analysis of the ATR FT-IR spectrum, providing the υ_3 band at 922 cm^{-1} [27].

Tab. 5-1: Standard conditions and their variation ranges for *in situ* ATR FT-IR experiments of U(VI) sorption on TiO_2.

Mobile phase	U(VI) concentration	20 µM (5 – 50 µM)
	Ionic strength (NaCl)	0.1 M
	pH	5.0 (3 – 7)
	Solvent	H_2O (D_2O)
Stationary phase	Deposited TiO_2	0.1 mg cm^{-2}
		5 layers (each 1 µL of a 2.5 g L^{-1} suspension)
		Various TiO_2 samples (cf. Tab. 5-2)
Performance	1st conditioning (Blank)	60 min
	Sorption (U(VI))	90 min
	2nd conditioning (Blank)	30 min
	Atmosphere	Normal (also inert gas)
	Temperature	Room temperature (i.e. 20 – 23°C)
	Flow velocity	0.2 mL min^{-1} (0.053 – 1)

5.2.1 Monitoring the U(VI) sorption process onto TiO_2

The course of an *in situ* sorption experiment is reflected by the spectra shown in Fig. 5-1. The spectrum referred to as "1st conditioning" reflects the equilibrium state of the TiO_2 film after flushing it with a blank solution for 60 minutes. No significant absorption changes are observed in the spectral region from 1600 to 800 cm^{-1} within a time period of 60 minutes. Since in this spectral region, in particular below 900 cm^{-1}, absorption of TiO_2 can be expected, the absence of bands in this spectrum indicates a sufficient stability of the mineral film on the ATR crystal's surface under the chosen conditions. Similar stabilities have also been confirmed for the oxide layers of alumina, silica and the alumosilicate samples.

The ATR FT-IR difference spectra calculated between the 1st conditioning and after 5, 10, 20, 40, 60 and 90 minutes of the induction of U(VI) sorption are shown in Fig. 5-1 (upper traces). These spectra exhibit absorption bands in the spectral ranges 1550 – 1350 and 1100 – 880 cm^{-1}. The intensities of the bands increase during the time of sorption reflecting accumulation of U(VI) on the mineral's surface. The assignment of these bands to distinct vibrational modes may clarify the mechanisms occurring at the U(VI) solution – TiO_2 interface.

The absorption band at ~900 cm^{-1} is assigned to the antisymmetric stretching vibration υ_3 of the uranyl(VI) species sorbed on TiO_2. In comparison to the free U(VI) species, UO_2^{2+}, the $\upsilon_3(UO_2)$ mode of the surface species is red-shifted about ~60 cm^{-1}. This frequency shift is due to a reduction of the U=O force constant as a result of complexation with TiO_2 units of the mineral phase in the equatorial plane or of interactions with the axial oxygen atoms. Such a strong shift to lower frequencies can only be explained by a formation of an inner-sphere surface complex. A coordination of the actinyl ion by electrostatic attraction would not modify the absorption frequency to such an extent [71]. Recently, U(VI) inner-sphere sorption on hematite and titanium dioxide has been investigated using ATR FT-IR spectroscopy. Lefèvre et al detected one peak at 906 cm^{-1} attributed to $\upsilon_3(UO_2)$ for U(VI) sorption onto

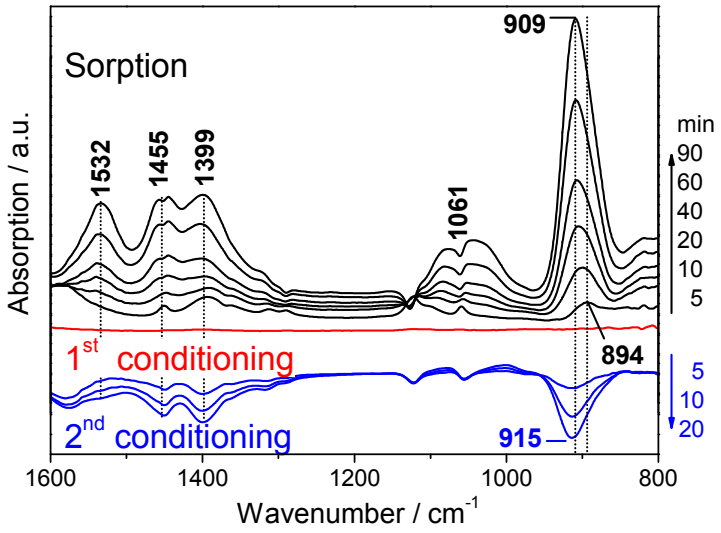

Fig. 5-1: ***In situ*** **time-resolved ATR FT-IR spectra of U(VI) sorption on TiO_2 (S6). The spectra of the sorption process are recorded at different times after induction as given. The conditioning stages represent the equilibration of the TiO_2 film by flushing a blank solution before (1^{st}) and after (2^{nd}) the induced sorption process. Indicated values are in cm^{-1}.**

hematite [71]. For titanium dioxide a band centering at 915 cm^{-1} was deconvoluted into two peaks at 905 and 920 cm^{-1} [65]. Although the band maxima may slightly differ which will be discussed later, these findings support the assignment to uranyl(VI) inner-sphere complexation onto TiO_2.

The IR spectral features at 1550 – 1350 and at 1150 – 1000 cm^{-1} can not be assigned unequivocally up to now. Their assignment to interactions of the background electrolyte, i.e. NaCl or of water with the TiO_2 can be ruled out, since the blank spectra obtained during the first conditioning stage give no evidence for any complexation. Possible explanations will be discussed later.

The progress of U(VI) sorption on the TiO_2 surface can be monitored online by the time-dependent increase of the absorption band at ~900 cm^{-1}. After around 90 minutes only slight intensity increase was observed, indicating almost steady state conditions under the performed conditions. Interestingly, the band of the sorbed U(VI) species shows different frequency maxima and half-band widths throughout the time interval of induced U(VI) sorption. At a low surface loading up to 10 minutes of contact time a broad band with maximum at 894 cm^{-1} is observed. Upon continued U(VI) accumulation the band is hypsochromically shifted to 909 cm^{-1}. Such spectral appearance may evidence the formation of different types of surface complexation. Upon variation of well defined parameters in the experimental set-up of the time-resolved measurements, e.g. U(VI) concentration, flow rate, pH value, such phenomena might be clarified.

After 90 minutes of sorption, a "2^{nd} conditioning" of the TiO_2 film with blank solution was performed for the next 30 minutes. The respective difference spectra exhibit a distinct negative band at 915 cm^{-1} (Fig. 5-1, blue trace). Since this band is again assigned to the $\upsilon_3(UO_2)$ mode it represents the removal of a U(VI) species from the mineral film. The

presence of several kinds of sorption complexes might be reasonable. It can be suggested that this species may slightly adhere in the pores of the oxide film and is weakly bound to the titanol groups. Since aqueous monomeric species present in micromolar solutions provide the $\upsilon_3(UO_2)$ mode at similar frequencies (~922 cm^{-1}), it is also assumable, that the 915 cm^{-1} band represents a solution species, not bound to the TiO_2 surface, but complexed with potential, ligands, such as phosphate or organics, dissolved from the mineral into the aqueous phase. The aspect of surface impurities and their possible impact on the sorption will be discussed in section 5.2.4 together with washing procedures applied to the TiO_2 samples.

5.2.2 Identification of different U(VI) surface species on TiO_2

The sorption mechanisms occurring at the water-mineral interface strongly depend on the contact time of the pollutant with the soil and the formation of different species is conceivable involving thermodynamically stable phases and a series of metastable steps along the way [7]. However, the formation of different species is evidenced by the IR spectra arising from the online monitoring (Fig. 5-1).

To evaluate the transformation of surface species as a function of surface coverage, a long-time experiment for 360 minutes of induced sorption and at reduced flow rate (0.053 mL min^{-1}) was performed under standard conditions (cf. Fig. 5-1). The difference spectra, shown in Fig. 5-2 (left), were calculated stepwise in time intervals of 60 minutes, i.e. they do not refer to the first conditioning step. But, the spectra represent what kind of reaction occurs in different time intervals of induced sorption, e.g. 0 – 60, 60 – 120 minutes.

Obviously the 898 cm^{-1} species dominates the U(VI) surface speciation at low surface coverage within the first 60 minutes. At an advanced sorption stage, ≥ 240 minutes, a species with maximum at 915 cm^{-1} becomes predominant. A simple spectra addition represented in Fig. 5-2 (right), using the data after 60 (red trace) and 240 min (green trace), results in a

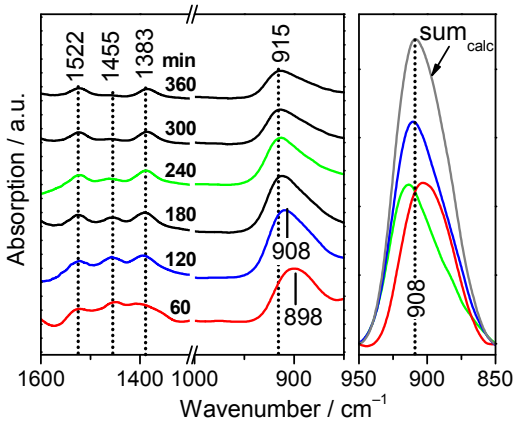

Fig. 5-2: Elucidation of U(VI) surface species on TiO_2. Left: Long-time sorption experiment (20 µM initial U(VI), 0.1 M NaCl, pH 5, S6, flow rate 0.053 mL min^{-1}). Right: Comparison of single species spectra and calculated spectra (the red, blue, and green spectra are experimental data, the grey spectrum is the calculated sum of the red and the green spectra). Indicated values are in cm^{-1}.

calculated band with maximum at 908 cm^{-1} (grey trace). A comparison of this addition spectrum and the one obtained after 120 minutes (blue trace) clearly evidence, that the band at 908 cm^{-1} represents a mixture of two species, one at low and one at high surface coverage.

Similarly, from TRLFS measurements performed by Vandenborre et al. the presence of two U(VI) complexes on the surface of rutile was concluded: one arising from the sorption of UO_2^{2+} on two bridging oxygen atoms, while the other one is favored as the sorption rate increases, involving the reaction of UO_2^{2+} onto one bridging and one top oxygen atoms [67].

Furthermore, Den Auwer et al. performed XAS measurements on U(VI) sorbed on mono- and polycrystalline TiO_2 samples. Both grazing incidence EXAFS on the (110) plane and isotropic EXAFS on polycrystalline TiO_2 reveal comparable sorption behavior, namely as a bidentate complex. Grazing incidence EXAFS on the (001) plane suggests the formation of an outer-sphere uranium complex [66].

Moreover, the formation of different U(VI) species depending on the surface coverage or higher initial U(VI) concentrations is reported for several surfaces, e.g. albite [128], alumina and silica [44] and montmorillonite [90].

To gain further structural information on the surface molecule complexes, sorption experiments have been performed with previously saturated TiO_2 (Fig. 5-3). In a first step, a prepared standard TiO_2 film was flushed with standard U(VI) solution overnight, the spectrum calculated from the data at the end of the "1st sorption" stage represents bands at 915, 1522 and 1383 cm^{-1} (Fig. 5-3, lower trace). The spectrum agrees with the spectra obtained in the long-time experiment, indicating the presence of the U(VI) surface species at high coverage (Fig. 5-3, upper traces).

In a second step, an additional conditioning was performed ("2nd cond."). The resulting spectrum is inversely to the sorption spectrum with negative bands at 915, 1522 and 1383 cm^{-1}. A comparison with the spectrum of the 1st sorption clearly indicates that the same surface species is removed from the TiO_2 during simple flushing a blank solution under the same conditions.

In a third step, a 2nd sorption stage was induced with the 20 µM uranyl(VI) solution which was already used for the 1st sorption stage. No differences between the sorption spectra obtained at the end of the 1st and during the 2nd stage can be detected, indicating that the same U(VI) surface species was attached to the TiO_2 which was previously removed by the blank solution.

In a last step, a 3rd conditioning with the blank solution was carried out. Again, no changes of the spectral characteristics of both conditioning spectra are observed, indicating full reversibility of the occurring reactions. Obviously, the spectra in Fig. 5-3 present the same U(VI) surface species interacting with TiO_2 previously saturated with U(VI). Such easy desorption evidence a weak, more electrostatic surface complexation probably occurring in the pores of the oxide film. Hence, the band of $\upsilon_3(UO_2)$ with maximum at 915 cm^{-1} is assigned to U(VI) outer-sphere surface complexes on the TiO_2. In contrast, the species with

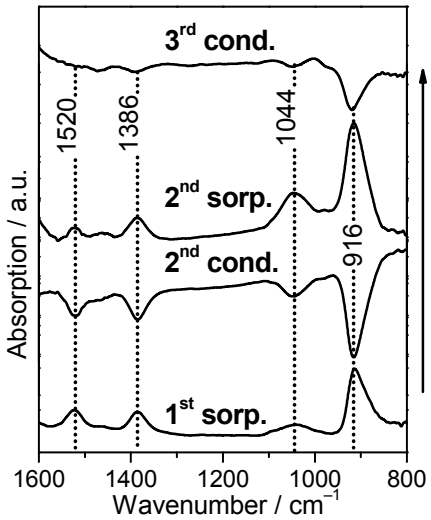

Fig. 5-3: Saturation of U(VI) on TiO_2 (20 µM initial U(VI), 0.1 M NaCl, pH 5, S6). From bottom to top: The 1st sorption step was performed at 53 µL min^{-1} for 18 h to saturate the TiO_2 with U(VI), the spectrum represents absorption changes between 360 and 300 min of induced sorption (cf. Fig. 5-2). The 2nd conditioning was performed for 60 min, the 2nd sorption for 90 min, and the 3rd conditioning for further 30 min. The last steps were done at 0.2 mL min^{-1}. Indicated values are in cm^{-1}.

absorption maximum at 890 cm^{-1} is not removed easily from the surface using the blank solution, and hence, is assigned to an inner-sphere U(VI) surface complex.

Further *in situ* sorption experiments have been performed for substantiation and characterization of the different identified U(VI) surface species on TiO_2. In a systematic study, the influence of the TiO_2 crystallographic form, and purity, and of sorptive parameters, e.g. pH, U(VI) concentration, flow rate was investigated.

5.2.3 Influence of TiO_2 crystallographic form

TiO_2 polymorphs occur as the tetragonal forms anatase and rutile and as orthorhombic brookite. The minerals possess octahedral coordinated structures (TiO_2^{6-}) differing by the distortion of each octahedron and by the assembly patterns of the octahedral chains. Anatase is built up from octahedra linked by their vertices, whereas in rutile, the edges are connected. Brookite shows bonded vertices and edges. (Fig. 5-4). Thermodynamic calculations based on calorimetric data predict that rutile is the most stable phase at all temperatures and pressures up to 60 kbar. However, the transformation enthalpy of anatase to rutile is very low [177, 178]. The surface chemistry of TiO_2 minerals is dominated by OH groups derived from the interaction of H_2O with surface planes of ions [178]. The development of negative and positive charges on surfaces is strongly influenced by pH, nature and concentration of present cations and anions. The point of zero charge values are 5.3 and 6.2 for rutile and anatase [178]. In recent spectroscopic investigations of U(VI) sorption onto TiO_2 mainly single crystal rutile has been used [66, 67]. However, the sorption mechanisms of U(VI) on anatase and rutile have not been comparatively studied up to now.

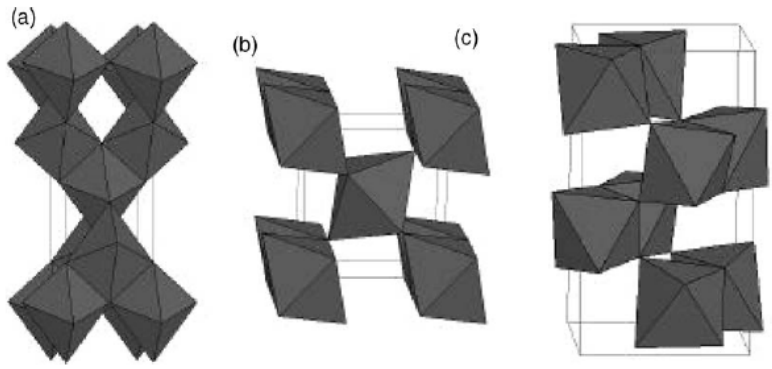

Fig. 5-4: Crystal structures of TiO_2 polymorphs: (a) anatase, (b) rutile, (c) brookite. [177]

A set of highly purified and well characterized TiO_2 phases, differing in their origins, in the ratio of the most stable polymorphs, i.e. anatase and rutile, in specific surface area and in particle size distribution was investigated (Tab. 5-2). Within the studied samples S4 and S5 are pure rutile and S6 is pure anatase. Generally, the samples with predominant anatase contribution (S1, S2, S6, S7) show higher BET surface areas compared to the rutile samples (S3 – S5). The sample S5 was synthesized by the use of S3 according to Hippel et al. [179]. The particle size ranges from the nm to μm scale, in particular the TiO_2 samples with high BET surface areas provide very small particle sizes.

All TiO_2 samples listed in Tab. 5-2 have been applied to standard *in situ* U(VI) sorption experiments (Tab. 5-1) by ATR FT-IR spectroscopy. The respective spectra obtained after 90 minutes of induced sorption are presented in Fig. 5-5. Generally, from the higher signal-to-noise ratio in the spectra obtained from S1, S2, and S6 a higher U(VI) surface loading can be derived. This observation correlated with the results from the BET measurement (Tab. 5-2), as a higher specific surface area provides an increased number of surface binding sites per mass unit [181].

A comparison of the spectral data shows only minor changes between the applied TiO_2 samples (Fig. 5-5, left). The band of the stretching vibrational mode $\upsilon_3(UO_2)$ is slightly shifted between 909 and 917 cm^{-1}. However, in all spectra the band shows an asymmetrical shape with a shoulder at lower frequencies, indicating the formation of more than one U(VI) surface species, but not correlating with the crystallographic form, the particle size, and the specific surface area.

In a previous ATR FT-IR spectroscopic study, Lefèvre et al. investigated the U(VI) sorption on TiO_2 sample S1 applying a different protocol [65]. For qualitative comparison, this sample was investigated with the standard protocol described in section 3.3.2 and the band of $\upsilon_3(UO_2)$ mode was found to be fully reproduced (cf. [65] and Fig. 5-5 upper trace).

Furthermore, each spectrum provides strong overlapping absorption bands in the range 1000 – 1200 cm^{-1}. A correlation between the relative intensities of these bands and the band of $\upsilon_3(UO_2)$ and overall the sorption capability of each solid is observed. In case of low sorption, e.g. at samples providing a low BET value, both bands are of similar intensity,

Tab. 5-2: Characteristics of the used TiO_2 samples.

Sample / Partner	Purity in %[a]	Origin	Composition	BET in $m^2\ g^{-1}$	Particle size
S1 ENSCP	99.9	Alfa Aesar No. 40458	Mixture of 80-90% anatase and rutile	223[c]	14% < 6 nm 38% 6 – 20 nm 34% 20 – 80 nm 14% > 80 nm [65]
S2 ANSTO	high	Degussa P-25 Nippon Aerosil Co, Ltd, supplied by Degussa Australia Pty Ltd Melbourne No. 4166120498	Mixture of 86% anatase and 14% rutile	50[a] / 56.4[b]	av. particle size 21 nm[b]
S3 ENSCP	99.5	Cerac Inc., Milwaukee, WI, USA	Mixture of 90% rutile and 10% anatase	5[a] / 5.20[b]	90% < 2.50 µm[b]
S4 ENSCP	>99.7	Tronox Pigments GmbH (Krefeld), via Kerr McGee Pigments (USA); No. TR-HP-2	100% rutile	7[a] / 5.88[b]	av. particle size 0.4 µm [180]
S5 FZD		S3 calcinated (6 h at 1000° as in [179])	100% rutile	2.19[b]	Not determined
S6 ANSTO	99.99	MTI Corporation Richmond, CA, USA; No. NP-TiO2-A-10	100% anatase	234[b] / 305[d]	5 – 10 nm[a]
S7 ANSTO	99.8	Aldrich No. 232033	Mixture of 91% anatase and 9% rutile	9.18[b]	Not determined

[a] specification by the manufacturer; [b] determined at FZD; [c] determined at ENSCP; [d] determined at ANSTO.

whereas high sorption is characterized by an intense U(VI) peak and almost no absorption bands at 1000 – 1200 cm^{-1}.

This correlation is supported by the U-Ti ratios presented in Fig. 5-5 (right), directly determined from the TiO_2 film after each standard experiment by ICP-MS analyis. As suggested from the high signal-to-noise ratios and the high intensities of the band concerning $\upsilon_3(UO_2)$, the samples S1, S2 and S6 show high U(VI) retention (≥ 160 mg U / 1 g TiO_2). In contrast, the samples S3, S4, S5, S7 with low intensities relative to the absorption bands in the range 1000 – 1200 cm^{-1} present low U(VI) bonding capacity (< 90 mg U / 1 g TiO_2). However, these values of U-TiO_2 values must be carefully evaluated. Since the coated amount of TiO_2 is very low and may vary for different experiments, even for the same protocol, also the concentration of U(VI) bound on the TiO_2 is different. Nonetheless, the ratios clearly show whether U(VI) sorption occurred or not. Further on, they may distinguish between high and low sorption, confirming the spectral information obtained by comparison of the signal-to-noise ratios (Fig. 5-5).

Up to now, an assignment of the absorption bands at ~1100 cm^{-1} to distinct vibrational modes is not possible. However, because of their high reproducibility in TiO_2 samples of different origin, they might represent TiO_2-surface processes correlating with chemical and physical properties of the sorbed cation. Additionally, bands at 1527, 1456, and 1390 cm^{-1} are detected in different intensities in each spectrum; in particular they are conspicuous in spectra representing high signal-to-noise ratios.

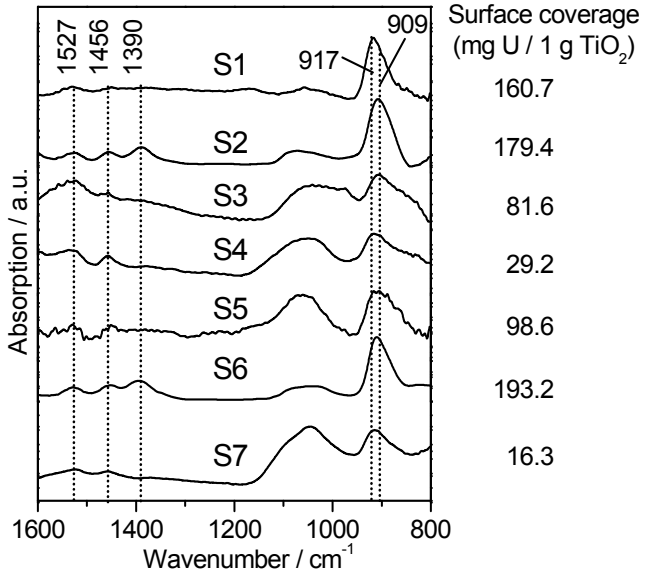

Fig. 5-5: ATR FT-IR spectra of U(VI) sorption onto different TiO_2 samples (20 µM initial U(VI), 0.1 M NaCl, pH 5) (left) and U-Ti ratios of removed TiO_2 film from the ATR crystal subsequent to sorption experiment determined by ICP-MS (right).

As a result of previously performed experiments and this spectroscopic comparison of different TiO_2 samples, S6 has been chosen as a reference material. Due to its high specific surface area and its small particle size, the U(VI) sorption has been evaluated to be on a high level. In the ATR FT-IR spectroscopic sorption experiments S6 allows a homogenous film preparation, an elevated signal-to-noise ratio and a high reproducibility of the spectral data. Furthermore, unique for S6, all U(VI) sorption species were identified separately in disrtinct time ranges.

5.2.4 Influence of TiO_2 purity

Because of the different origins and manufacturing of the TiO_2 samples, the chemical composition might cause minor spectral changes. Hence, a TiO_2 microwave digestion and subsequent analysis of minor constituents were performed. The results from ICP-MS analysis evidence major contamination for S6, in particular for Mg, Si, Zn, Nb, and Ta (Tab. 5-3). Two other samples show also elevated concentrations for Zr and Nb (S4, S7). Although the weight percentage of impurities is very low, <0.1%, their distribution in the solid may directly influence the surface reactivity. According to Lefèvre et al., several possibilities of solid contamination can be assumed: (1) the impurities are in the bulk of the solid and their impact is negligible, (2) they are present as a foreign phase, e.g. Na_2SO_4 and washing can purify the solid, or (3) they form surface complexes with high impact on the surface reactivity. In the last case, a purification of the solid is difficult to achieve [181].

In a collaborative study with the Australian Nuclear Science and Technology Organisation (ANSTO) the effect of washing the TiO_2 on U(VI) sorption was investigated, aiming at the removal of possible anionic and cationic contaminants from the oxide surface. In the literature

several treatments have been applied to TiO_2 including washing with acid, base and purified water in numerous washing-boiling decantation cycles [182-184]. Within this collaboration two strategies were proven, slight and extensive washings were performed using weak (0.1 M) and strong (5 M) acid (HCl) and base (NaOH). Again, digestion and ICP-MS analysis were carried out to control the effect of the washings (Tab. 5-3).

The concentrations of Na, Si, and Zn were partially reduced by the washing procedures, indicating their presence as surface complexes or impurity foreign phases. Comparing the success of both washing procedures, no significant changes are observed. Since no evolution of the concentrations of most of the impurities has been observed, they are probably bound to the inner structure, i.e. to the bulk solid and not on the surface of the TiO_2. In consequence, they are not removed by the mentioned procedures, but are determined in the decomposition by ICP-MS.

In contrast to the determination of impurities by analytical techniques, as ICP-MS, changes in the IR spectra allow precise conclusions concerning the impact of impurities on the surface reactivity. Standard *in situ* sorption studies of U(VI) were conducted with TiO_2 obtained after each washing step to monitor the progress of the procedure and to assign possible spectroscopic changes to removed contaminants. Fig. 5-6a shows the obtained spectra for the slight washing of the sample S6. No significant changes in the location of band maxima and in the relative intensities were observed upon slight washing. Furthermore, the intensity of TiO_2 washing, whether using strong (5 M) or weak (0.1 M) agents does not influence signifi cantly the sorption process of U(VI), as shown for S2 in Fig. 5-6b. Thus, the impurities, e.g. Na, Si, reduced upon washing, have no impact on the U(VI) surface speciation on TiO_2.

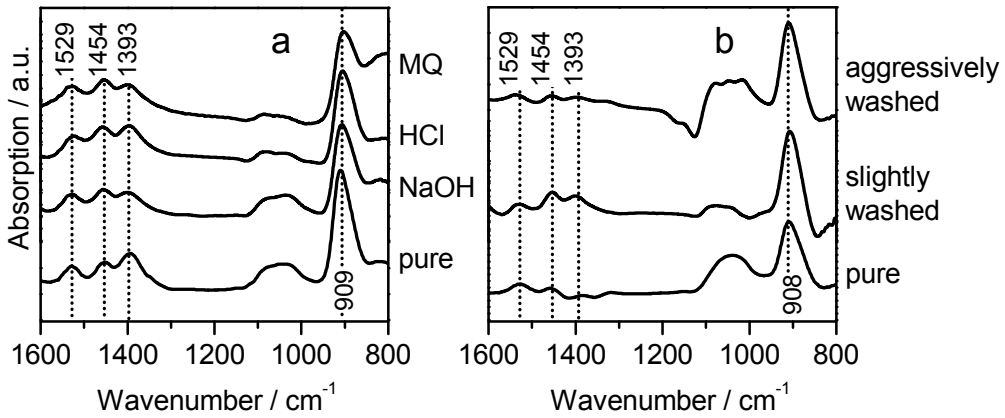

Fig. 5-6: ATR FT-IR spectra of the impact of TiO_2 washing on U(VI) sorption (20 µM initial U(VI), 0.1 M NaCl, pH 5, 90 min of induced sorption). (a) S6, sorption performed of the pure sample and after each washing step (from bottom to top). (b) S2, Comparison of the effect of two different washing protocols. Indicated values are in cm^{-1}.

Tab. 5-3: Minor constituents of the TiO_2 samples before and after the cleaning procedure derived from ICP-MS analysis. Impurities < 5 µg g^{-1} are not shown.

	S1	S2			S3	S4	S5		S6		S7		
[µg g^{-1}]	(pure)	(pure)	(0.1 M)	(5 M)	(pure)	(pure)	(pure)	(0.1 M)	(pure)	(0.1 M)	(pure)	(0.1 M)	(5 M)
Na		-	8.1	8.4	94.7	16.3	102.8	15.5	113.7	39.5	28.3	16.2	8.43
Mg	14.3	72.3	56.1	43.2	85.2	71.6	65.6	60.7	143.0	124.1	63.3	53.0	48.2
Al		5.9	13.1	-	40.1	67.1	90.2	48.3	13.1	19.4	37.6	5.9	-
Si		279.5	208.8	212.0	278.1	169	798.0	418.0	734.0	472.4	645.5	314.0	289.0
K		-	19.3	16.9	53.8	36.4	17.4	15.5	21.9	20.2	15.7	16.4	14.2
Fe		-	-	-		18.4	26.5	21.0	15.2	9.9	21.2	-	-
Zn	21,7	-	-	-	5.1		6.2	5.2	573.1	136.2	-	-	-
Zr		-	-	-	42.8	199.5	44.9	42.1	26.2	25.4	119.7	124.9	272.0
Nb		-	-	-	118.6	99.8	134.5	135.9	978.0	978.4	76.1	78.2	72.9
Sn		-	-	-	5.8		9.9	9.1	19.2	19.2	-	-	-
Ba		-	-	-	34.3		38.3	-	-	-	-	-	-
Ta		-	-	-	7.7	7.6	10.4	9.7	88.7	84.9	6.9	7.7	7.7
W		-	-	-			-	-	35.9	35.2	-	-	-
Pb	7.64	-	-	-			-	-	39.8	35.9	-	-	-

Additionally, the spectra evidence that the absorption bands observed in the U(VI) sorption spectra between 1200 and 1000 cm^{-1} are not due to removable impurities at the TiO_2 surface.

In summary, the investigation of TiO_2 purity and the application of several washing strategies indicated no differences in the U(VI) sorption behavior between acid and base washings even at increased concentrations. Nevertheless, for the elucidation of molecular sorption processes washing is generally recommended to check possible surface contamination, influencing the reactions at the solid-water interface.

5.2.5 Influence of the U(VI) solution properties on the sorption onto TiO_2

In a first step, standard *in situ* sorption experiments were performed at different flow rates, ranging between 0.053 and 1 mL min^{-1}. Distinct shifts of the band of $\upsilon_3(UO_2)$ are observed in the spectra obtained after 90 minutes of induced sorption (Fig. 5-7). At flow rates > 0.053 mL min^{-1}, only the formation of the 908 cm^{-1} species is detected (Fig. 5-7, upper traces). These results substantiate, that only at a low U(VI) coverage on TiO_2 the species at 895 cm^{-1} dominates the surface speciation and is probably overlapped and/or transformed to the species with absorption maximum at 908 cm^{-1}.

In a second step, the influence of U(VI) concentration in the range from 5 to 50 µM at fixed pH 5 was studied and the spectra obtained after 90 minutes of induced sorption are shown in Fig. 5-8a-c. At an initial U(VI) concentration of 5 µM, and consequently only sparsely covered surface, the $\upsilon_3(UO_2)$ is exhibited as a broad absorption band at 890 cm^{-1} (Fig. 5-8a). Upon increasing the U(VI) concentration in the sorptive solution, this band becomes hypsochromically shifted to 908 cm^{-1} at 20 µM and 50 µM (Fig. 5-8b,c). These results support the findings that the type of complex depends strongly on the U(VI) saturation level on TiO_2.

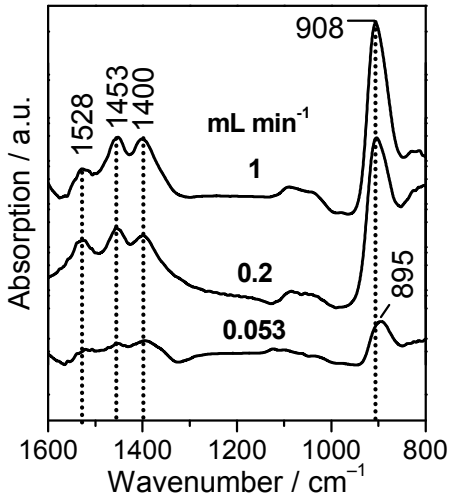

Fig. 5-7: Variation of the flow rate (20 µM initial U(VI), 0.1 M NaCl, pH 5, S6, 90 min of induced sorption). Indicated values are in cm^{-1}.

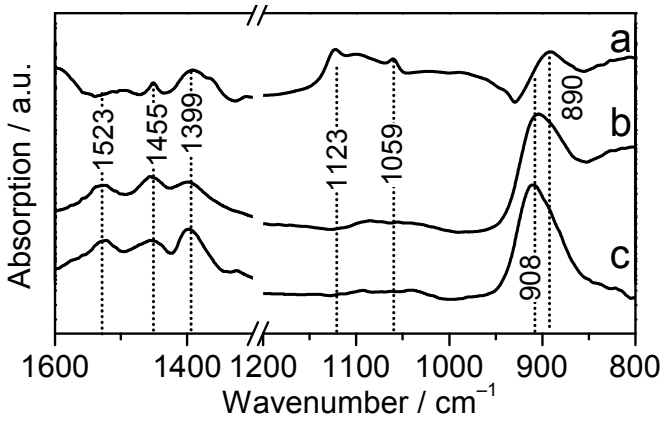

Fig. 5-8: ATR FT-IR spectra of U(VI) sorption onto TiO_2 (S6). Influence of U(VI) concentration at pH 5: (a) 5 µM; (b) 20 µM; (c) 50 µM. (0.1 M NaCl, 90 min, air). Indicated values are in cm^{-1}.

In a third step, ATR FT-IR spectra are collected at differing pH conditions ranging from 3 to 7, but at a fixed uranyl(VI) concentration of 20 µM (Fig. 5-9). At pH 3, a less intense band representing $\upsilon_3(UO_2)$ is observed at 890 cm^{-1} (Fig. 5-9a). Upon increasing pH to 4, this band is shifted to 900 cm^{-1} (Fig. 5-9b). At pH 5, the respective band is hypsochromically shifted to 908 cm^{-1} and appears much more intensive relative to the bands at ~1100 cm^{-1} (Fig. 5-9c). Upon increasing pH to 7, no further spectra changes are observed (Fig. 5-9d). In the pH range from 3 to 7 the spectroscopic data evidence increasing U(VI) uptake of TiO_2 which agrees with results from macroscopic batch experiments and previous vibrational spectroscopic studies [65, 68, 69].

The spectroscopic data arising from the pH series are comparable to those from the concentration series. At pH 3 sorption is inhibited and the surface is less covered by U(VI) than at higher pH. Similar to the spectrum obtained at 5 µM at pH 5, only a small band of $\upsilon_3(UO_2)$ at 890 cm^{-1} is characteristic for sorption at 20 µM at pH 3 (cf. Fig. 5-8a and Fig. 5-9a). At higher concentration (20 – 50 µM) and at increased pH (5 – 7) the sorption of U(VI) is enhanced and the TiO_2 surface becomes more covered, resulting in a shift of $\upsilon_3(UO_2)$ to

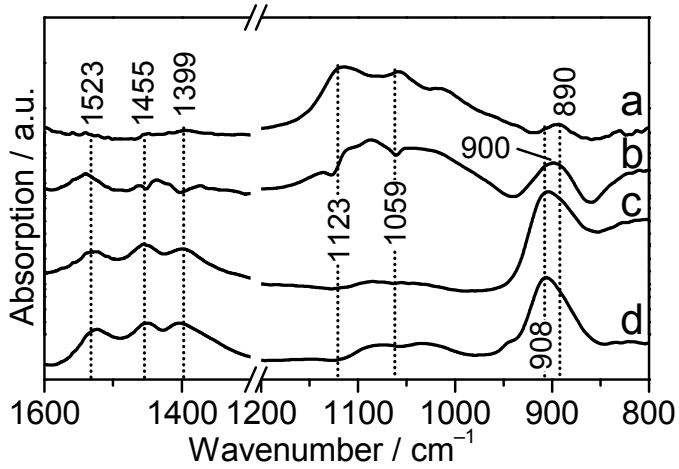

Fig. 5-9: ATR FT-IR spectra of U(VI) sorption onto TiO_2 (S6). Influence of pH conditions at 20 µM U(VI): (a) pH 3; (b) pH 4; (c) pH 5; (d) pH 7. (0.1 M NaCl, 90 min, air). Indicated values are in cm^{-1}.

908 cm^{-1}. This assumption is supported by the U/TiO_2 ratios measured by ICP-MS analysis from the removed films, less than 100 mg U / g TiO_2 for sorption at pH ≤ 4 and 5 µM initial U(VI) concentration and ratios higher than 150 mg U / g TiO_2 for sorption at increased pH and initial U(VI) concentration, respectively.

Carbonate species are abundant in soils and soil solutions and are known to adsorb on the mineral surfaces. In turn, the adsorbed carbonate affects surface chemical properties such as surface charge and protonation and the sorption of other ions [146, 185]. Hence, a standard *in situ* sorption experiment at inert gas atmosphere has been conducted.

The comparison with the spectrum obtained under the same conditions at normal atmosphere shows no distinct differences in the position of the relevant IR absorption bands (cf. Fig. 5-10). However, the relative intensities are varied. The 1040 cm^{-1} band is considerably increased relative to $\upsilon_3(UO_2)$. In contrast the bands at 1523 and 1455 are slightly decreased and the band at 1399 cm^{-1} is absent. Since these bands may indicate symmetric and asymmetric vibrational modes of carbonate ligands, their reduced contribution to the spectrum at nitrogen atmosphere may indicate a low influence of atmospheric carbonate on U(VI) sorption.

The small changes can also be due to changed sorption kinetics, most probably, U(VI) sorption is more slowly at N_2 compared to normal atmosphere. However, the comparison of the data sets illustrates a low sensitivity of U(VI) sorption on changes of the partial pressure at pH 5, even if the formation of a ternary complex can not be ruled out at this state of knowledge.

The IEP of the TiO_2 (S1) was found to occur at pH 5.2 [65] and the negative charged surface may facilitate outer-sphere sorption processes of positive hydrolysis products of UO_2^{2+}, namely $UO_2(OH)^+$, $(UO_2)_2(OH)_2^{2+}$, $(UO_2)_3(OH)_5^+$. However, ATR FT-IR analysis of micromolar U(VI) solutions evidenced that monomeric U(VI) hydroxyl species are more favorable than polynuclear species at low concentration levels of 20 µM (cf. section 4.1 and [27]). The ATR FT-IR spectra of 20 µM U(VI) solutions in the pH range from 3.2 to 6.5

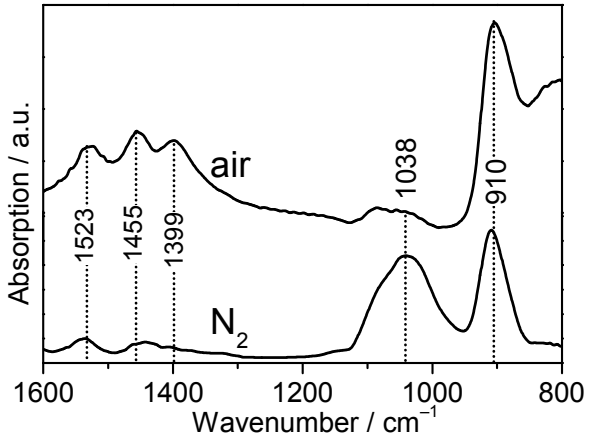

Fig. 5-10: ATR FT-IR spectra of U(VI) sorption onto TiO_2 (S6). Influence of CO_2 absence (20 µM initial U(VI), 0.1 M NaCl, pH 5, 90 min). Indicated values are in cm^{-1}.

shows absorption of $\upsilon_3(UO_2)$ at 923 cm^{-1} [27]. Hence, according to the currently accepted thermodynamic data and considering the spectroscopic findings, the neutral monomeric species $UO_2(OH)_2^0$ is important in the aqueous U(VI) speciation too, but would probably be insensitive to IEP changes of TiO_2. However, in the weak acidic pH range the speciation of U(VI) is complex, i.e. several hydrolysis species may simultaneously contribute. Hence, a complex U(VI) surface speciation, showing various sorption levels and configurations, depending on pH and / or initial concentration is conceivable.

In a previous ATR FT-IR study of U(VI) sorption on TiO_2, using the sample S1, Lefèvre et al. performed a pH series in the range from pH 4.1 to 7 using a circulating flow system [65]. The $\upsilon_3(UO_2)$ is increased in intensity upon increasing pH conditions, that is in accordance to the observations of this study. Further on, deconvolution of the absorption band of $\upsilon_3(UO_2)$ evidenced the presence of two peaks at 905 and 920 cm^{-1} with almost constant contribution ratios along the measured pH range. The peaks were assigned to one type of surface complex, a trimer linked by two uranyl ions to the TiO_2 surface.

The spectra obtained in this study show bands at ~895 and 917 cm^{-1}, partly overlapping with the maximum at 908 cm^{-1}. One explanation for these differences can be the higher concentration level (100 µM) in the study of Lefèvre et al. From previously performed ATR FT-IR spectroscopic studies of U(VI) speciation in aqueous solution, it is known, that polymerization of hydrolysis products may occur in the submillimolar range, whereas in the micromolar range, monomeric species are predominant (cf. section 4.1. and [27]).

Another explanation for the mentioned differences could be the instrumental set-up, e.g. ZnSe vs. diamond crystal differing in its physical-chemical properties and dimensions, the circulation system, the use of different solvents etc. resulting in different solid-liquid ratios, flow velocities and U(VI) saturation states. Regarding these differences and for comparison of the results obtained by two instrumental FT-IR setups additional experiments were performed using the S1 sample and D_2O at pH 4 in a collaborational work with the Ecole Nationale Supérieure de Chimie de Paris (ENSCP). The results are presented in Fig. 5-11. Since the spectra exhibit strong absorption bands at 1200 and 1450 cm^{-1}, due to the use of D_2O (cf. Fig. 3-2), this region is not shown for clarity. The spectra are compared to the spectrum of U(VI) sorption onto S1 at standard conditions, showing $\upsilon_3(UO_2)$ at 917 cm^{-1} (cf. Fig. 5-5).

In a first step, the solid-liquid ratio was increased from 0.1 mg cm^{-2} to 0.4 mg cm^{-2}. At both conditions an unchanged band of $\upsilon_3(UO_2)$ at 912 cm^{-1} is observed. The small shift from 917 cm^{-1} to 912 cm^{-1} can be explained by the use of D_2O.

In a second step, the U(VI) concentration was varied between 1 µM and 20 µM at pH 4, in order to rule out a parallel detection of an aqueous species, additional to the surface species. Comparing the $\upsilon_3(UO_2)$ bands, no shifts as a function of U(VI) concentration are observed. Since the detection limit of U(VI) species in aqueous solution at pH 4 is higher than 5 µM (cf. section 4.1.2 and [27]), the contribution of spectral characteristics arising from diluted species can be excluded here. However, all spectra show absorption at ~ 1050 cm^{-1} in differing

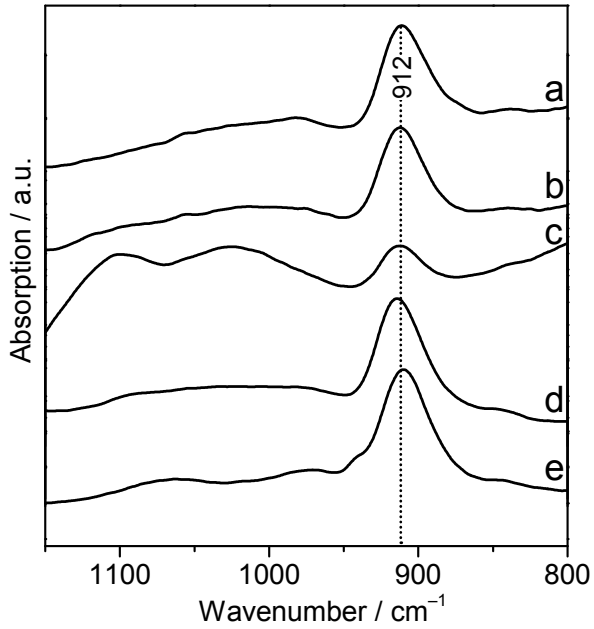

Fig. 5-11: ATR FT-IR spectra of U(VI) sorption onto TiO_2 (S1) in D_2O. Influence of solid-liquid ratio at 5 µM U(VI), pH 4: (a) 0.1 mg cm^{-2}; (b) 0.4 mg cm^{-2}. Influence of U(VI) concentration at 0.1 mg cm^{-2} and pH 4: (c) 5µM; (d) 20 µM. Influence of pH: (e) 20 µM pH 7 (0.1 M NaCl, 90 min). Indicated values are in cm^{-1}.

intensities as a function of U(VI) concentration. At the lowest concentration of 1 µM they are more distinct than at higher concentration. Hence, their appearance might be insensitive whether H_2O or D_2O is used.

In a last step, the pH was increased from 4 to 7 at 20 µM U(VI). Again, no differences are observed for $\upsilon_3(UO_2)$. These results are in accordance to those published for S1 by Lefèvre et al. [65], indicating the formation of one U(VI) surface complex. Since the U(VI) concentration level in this study is very low, down to 1 µM, a polymeric species is unlike to be formed already at the beginning of induced sorption.

However, upon comparison to the TiO_2 sample S6, spectral differences have been observed concerning the series of U(VI) concentration and pH (cf. Fig. 5-11a-e). The only difference from S1 and S6, is a small amount of rutile (10 – 20%), and the contribution of major particles in S1. The impact of the predominant crystallographic form was ruled out previously (cf. Fig. 5-5) and the particle contribution in the nm scale might be not that important. However, the U(VI) saturation level of both samples at different time steps might be different and could cause different spectral data.

In summary, the sorption of U(VI) from micromolar solutions onto TiO_2 was investigated intensely *in situ* by application of ATR FT-IR spectroscopy. The strategic study considered the impact of modifications in the purity and crystallographic form of TiO_2, namely anatase and rutile, variations in the aqueous U(VI) system, e.g. pH and U(VI) concentration and changes of the reaction time at the U(VI)-TiO_2 interface. The spectroscopic findings substantiate the formation of U(VI) surface complexes on TiO_2 under the chosen conditions. As a function of accumulated U(VI) concentration on the TiO_2 surface different complexes

are suggested: one inner-sphere complex and additionally, one outer-sphere complex at U(VI) saturated or at least at highly covered surfaces. Sorption parameters, such as concentration, pH and contact time significantly influence the U(VI) uptake and hence, determine the type of complexation. The crystallographic form plays a minor role, although surface specific parameters, such as surface area, porosity and changes in PZC are important.

5.3 Photocatalytic effects during the U(VI) sorption on TiO_2

In addition to the ATR FT-IR spectroscopic study, the U(VI) sorption onto TiO_2 can be studied by other surface sensitive methods. Due to the excellent fluorescence properties of U(VI) the application of TRLFS measurements is capable. Using laser irradiation for the excitation of U(VI) fluorescence may change the U(VI)-TiO_2 sorption sytem. Hence, within this work, the influence of light on the sorption was investigated using ATR FT-IR spectroscopy and preliminary TRLFS experiments were carried out.

Uranium(VI), is known to be the most stable oxidation state of uranium in oxygenated waters (cf. Pourbaix diagram in Fig. 2-1). Thermodynamic unstable U(IV) complexes might be formed in oxygenated waters by photoreduction of U(VI) supplied by solar radiation. Although U(VI) photoinduced reduction is reported to occur in acidic solutions, it is prevented at neutral conditions because of structural arrangements resulting from hydrolysis reactions. However, sorbed U(VI) species at the water-mineral interface on particles with semiconducting properties, e.g. TiO_2 have shown different redox behavior than solution species [160, 186, 187] since photocatalytic reactions mainly occur in the interface [188].

TiO_2 is the material mostly applied for the investigation of photocatalysis, due to its exceptional optical and electronic properties, chemical stability and low cost. The mixed sample of 80% antase and 20% rutile Degussa P-25 (S2, Tab. 5-2) was investigated for U(VI) photoreduction using laser fluorescence spectroscopy [160, 186]. For these measurements the laser irradiation is used twice, to provide the energy necessary for photogeneration of charge carriers and to monitor the photoinduced changes of the oxidation states. Eliet and Bidoglio monitored the kinetics of the change from U(VI) to U(IV) in the pH range 4.5 – 7 using the decay of the fluorescence intensity upon time and suggest that only U(VI) adsorbed species are photoreduced by TiO_2 [186]. Furthermore, the reduction was found to be enhanced by U(VI) complexation with humic acids [160].

ATR FT-IR spectroscopy which was applied to monitor photoreactions of oxalic acid, has not been applied for U(VI), yet. Although the photoproduct U(IV) as a non-polyatomic molecule U^{4+} can not be identified by FTIR, the disappearance of the initial U(VI) may be monitored similar to TRLFS experiments. Therefore, within this study the effects of UV-visible light on the sorption processes of U(VI) onto TiO_2 were investigated by application of *in situ* ATR FT-IR spectroscopy, using a flow cell with integrated fiber optics. Changes of the

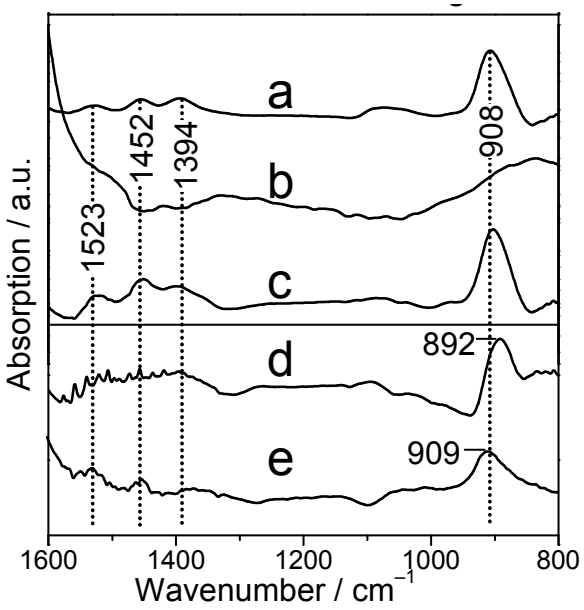

Fig. 5-12: Influence of UV light radiation on U(VI) sorption onto TiO_2 (20 µM initial U(VI), 0.1 M NaCl, pH 5, 30 min). (a) S2 (0.1 M washed), dark, (b) S2 (0.1 M washed) at Hg vapor light, (c) S2 (0.1 M washed) Hg vapor light and 580 nm filter, (d) S6 at Hg vapor light, (c) S4 at Hg vapor light. Indicated values are in cm^{-1}.

excitation wavelength and the TiO_2 phase, namely anatase (S6), rutile (S4), and a mixture of both (S2), were considered (Tab. 5-2).

The *in situ* experiments were performed using the standard conditions listed in Tab. 5-1 and the results are shown in Fig. 5-12. For illumination a mercury vapor lamp was used with excitation in the range 226 – 761 nm.

From the obtained spectra using the P-25 sample (S2) a distinct influence of UV light on the sorption can be derived since the U(VI) marker at 908 cm^{-1} band is not observed in case of illumination (Fig. 5-12a,b).

The TiO_2 semiconductor has a band gap of about 3.1 eV, corresponding to a wavelength of 390 nm. Thus, only irradiation < 390 nm provides the TiO_2 particles with the energy necessary to cross the band gap and create reactive charge carriers [186, 187]. This is clearly demonstrated upon comparing the spectral changes in Fig. 5-12a-c. Using an optical filter passing light only >580 nm (c) results in the same IR features as obtained at dark conditions (a) using the closed flow cell from the standard sorption measurements.

Photocatalytic activity at the water-TiO_2 interface depends on several parameters, including crystallinity, impurity, surface area and density of surface hydroxyl groups, but also on the crystallographic form, i.e. anatase or rutile. Anatase is photocatalytically more active than rutile [188-190]. But interestingly, the activity level of P-25 (S2) was reported to exceed that of pure anatase in several reaction systems, probably resulting from photo-induced interfacial electron transfer from anatase to rutile [190]. In Fig. 5-12 the different photocatalytic activities are demonstrated for U(VI) species sorbed on P-25, S2 (b), pure anatase, S6 (d) and pure rutile, S4 (e). Although the spectrum of S2 (Fig. 5-12b) does not provide any spectral

feature of U(VI), the spectra of the pure forms show characteristic bands of the vibrational $\upsilon_3(UO_2)$ mode.

The spectrum obtained of the pure anatase sample, S6, at illuminated conditions shows a band concerning $\upsilon_3(UO_2)$ at 892 cm^{-1}. Although this band is characteristic at an early stage of U(VI) sorption on this sample (< 20 minutes at standard conditions), the absence of the 908 cm^{-1} band, generally appearing at ~ 20 minutes is an obvious spectral difference comparing the data obtained at dark conditions (Fig. 5-1) and at illumination (Fig. 5-12d). However, even after 90 minutes of induced sorption and illumination the band of $\upsilon_3(UO_2)$ remains at 892 cm^{-1}. In the sorption studies, the 892 cm^{-1} band was assigned to a stronger sorbed species occurring at the very beginning of the sorption complex, when all binding sides are available. In contrast, the species with absorption at 917 cm^{-1} was found to be characteristic at higher U(VI) coverage. From the experiments at illumination, it seems that the accumulation of U(VI) at the TiO_2 surface is inhibited. It is assumable, that the beginning of U(VI) sorption is similar to dark conditions. Due to the excitation of TiO_2, the sorbed U(VI) becomes reduced to U(IV) species which may subsequently be restructured at the surface. Upon further U(VI) input to the system, the binding sites favored for the hexavalent species become occupied again. This would indicate that sorption of U(VI) onto the pure anatase sample occurs faster than reduction of the sorbed species, in contrast U(VI) reduction on the Degussa P-25 sample proceeds in similar time ranges as U(VI) sorption. The pure rutile sample, S4, does not show any differences compared to the spectrum obtained at dark conditions (Fig. 5-5); probably this sample does not show photocatalytic properties.

For comparison, laser-induced fluorescence measurements have been performed for U(VI) sorption onto P-25 (S2). In Fig. 5-13 the emission spectra of U(VI) sorbed onto TiO_2 obtained after excitation at different time intervals are presented. The excitation of 266 nm, generally used for U(VI) measurements [191], also provides the TiO_2 particles with sufficient energy to cross the band cap and create charge carriers. Obviously, the concentration of U(VI) in the TiO_2 suspension is reduced upon ongoing illumination. The decay curve, calculated from the area under the emission peak, is shown on the right graph in Fig. 5-13. After 65 minutes of excitation at 266 nm, U(VI) was not detectable anymore. In a following step, the same solution was excited using a wavelength of 410 nm in order to receive a signal from the possible intermediate photoproduct U(V) [192]. But unfortunately, no U(V) could be found. A next step should be the analysis of this sample concerning U(IV). Tetravalent uranium in solution, namely U^{4+} is excited at 245 nm and the emission spectrum exhibits several bands [193, 194], but very few data is published as reference for U(IV) solid compounds.

In conclusion, the impact of illumination on the surface reactions at the TiO_2-U(VI) interface was studied, using different crystallographic forms, namely anatase, rutile and a mixture of both, Degussa P-25 which is known for its high photocatalytic activity level. The ATR FT-IR sorption measurements were performed *in situ*, using a flow cell with integrated

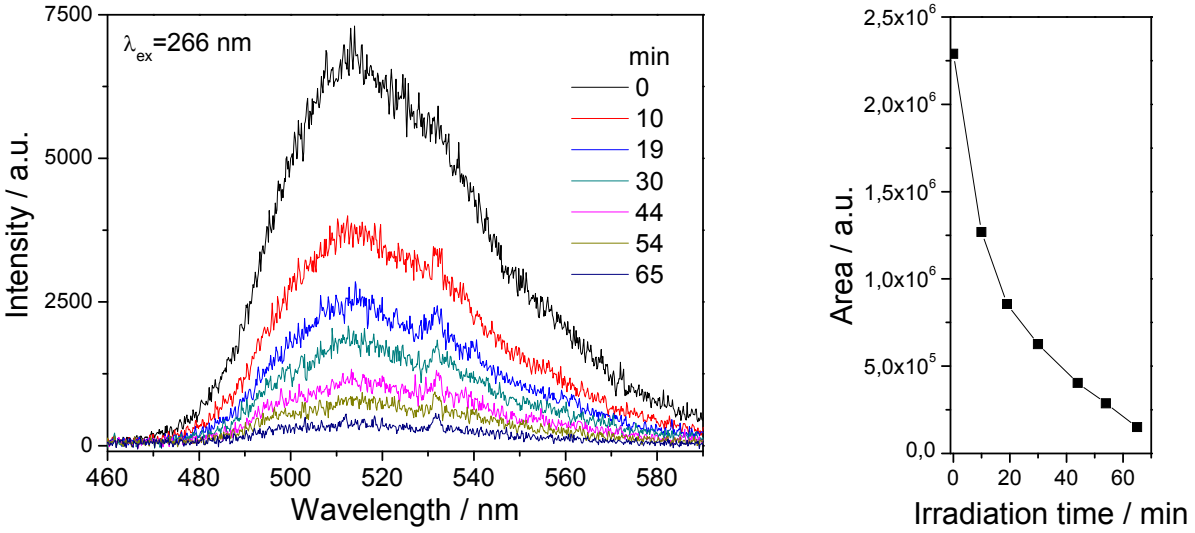

Fig. 5-13: Laser-induced fluorescence measurement of U(VI) photoreduction. (100 ppm S2 (0.1 M washed), 0.1 mM initial U(VI), 0.1 M $NaClO_4$, pH 7, N_2 atmosphere, 3 d contact time, then 2x washing with 0.1 M $NaClO_4$, pH 7) Emission spectra after different times of excitation (left) and fitted area under the emission peak (460 – 590 nm) in dependence of different times of excitation (right).

fiber optics. The photoinduced reduction of U(VI) to U(IV) is indirectly observed by the absence or changes of the band of $\upsilon_3(UO_2)$ of sorbed U(VI). For the Degussa P-25 sample, complete reduction is observed, in contrast to the pure phases: the rutile sample does not show photocatalytic properties. For the anatase sample, a reduction has partially been observed. It is suggested that sorption occurs much faster than the photocatalytic degradation. Presumably, the activity of the anatase system can be increased by convenient variation of reaction parameters, i.e. temperature, photonic flux, etc. The performed spectroscopic measurements show that the elucidation of reaction mechanisms of redoxsensitive actinides can be investigated by ATR FT-IR and TRLF spectroscopy. Furthermore, such comprehensive data sets may help to optimize further spectroscopic experiments and facilitate the interpretation of the obtained data. For example, the performed ATR FT-IR spectroscopic analysis of U(VI) sorption onto TiO_2 at dark and illuminated conditions clearly indicate that in TRLFS measurements U(VI) can not be excited by the generally used wavelength at 266 nm, because of the photocatalytic properties of TiO_2, but probably by excitation at ≥ 405 nm.

5.4 U(VI) sorption onto oxides of aluminium and silica

Since only few vibrational spectroscopic data of sorption complexes of hexavalent actinyl ions, namely U(VI), are reported in literature [65, 71, 72, 176, 195] and, thus, less reference data providing structural information are available, a detailed interpretation of the presented sorption spectra of U(VI) onto TiO_2 at a molecular level remains difficult. Therefore, additional sorption experiments have been performed with further metal oxides as sorbents for comparison, acting as models for the elucidation of molecular processes on more complex

mineral surfaces. A set of pure and well characterized oxides of aluminum and silicon, namely, trigonal γ-Al_2O_3 and tetrahedral SiO_2, differing in their crystal structure, in specific surface area and in particle size distribution was investigated.

Both, aluminates and silicates contribute to the formation of clay minerals. Hence, they play an important role in regulating the mobility of contaminants, due to their widespread environmental presence and their contribution in rock and soil formation, and their tendency to form coatings on mineral surfaces [9]. Additionally, as major contributors to clay and granite rock minerals, oxides of alumina and silicon play an important role in the long-term assessment of final repositories of nuclear waste. Since clay minerals present advantageous geochemical characteristics, e.g. low permeability and high retention capability essential for the use as host rock and as backfill material [196]. Although pure aluminum oxide/hydroxides rarely exist in nature, they can be used as model systems to elucidate sorption reaction mechanisms of actinyl cations on natural alumosilicate mineral surfaces which also provide surface aluminol sites.

By quantum quemical approaches the U(VI) retention on clay is calculated to occur via the sorption onto Al- and Si-edge sites of the clay, whereas the Al-sites are more reactive compared to the Si sites. [55, 57]. Furthermore, in recent experimental studies, U(VI) was found to sorb via inner-sphere complexation in bidentate configuration onto kaolinite [86, 87].

The various alumina and aluminum hydroxide phases have different crystal structures. Here, the term alumina is used to refer to the anhydrous aluminum oxides of the chemical formula Al_2O_3, including the most stable form corundum (α) and a number of transition aluminas (γ, χ, κ, δ, φ and η). The aluminum hydroxides include the trihydroxides ($Al(OH)_3$) gibbsite (γ) and bayerite (α), and monohydroxides (AlOOH) boehmite (γ) and diaspore (α) [197]. The structure of γ-Al_2O_3 is of spinel type with oxygen in approximately face centered cubic packing, fairly well ordered, in contrast to the tetrahedral Al lattice which is strongly disordered [198]. The surface chemistry of Al_2O_3 becomes even more complex when thermodynamic solubility data are inspected. Neither γ-Al_2O_3, nor α-Al_2O_3 are stable in aqueous solution. Either bayerite, [199, 200] or gibbsite or mixtures of various $Al(OH)_3$ phases form at the oxide-water interface [200-202]. It is, thus, reasonable to assume that the actual sorption reaction does not occur at any bulk terminated Al_2O_3 crystal surface structure but at secondary Al-hydroxide phases. $Al(OH)_3$ is structurally defined as an approximately hexagonal close packed hydroxyl lattice with aluminium atoms in two-thirds of the available octahedral holes. The basic structure can be described as a "sandwich" of aluminium atoms between a double layer of hydroxyl groups. Within the sandwich the $Al(OH)_6$ octahedra are joined along edges while sheets of hydroxyl groups in adjacent sandwiches are held together by hydrogen bonding [197, 198].

Tab. 5-4: Characteristics of the used oxide samples.

Sample	Purity in %[a]	Origin	BET in $m^2 g^{-1}$	Particle size
SiO_2	99.98	Merck No. 115111	505[a]	90% 15 – 40 µm[b]
γ-Al_2O_3	99.5	Alfa Aesar No. 44931	37[a]	40 – 50 nm[b]
α-Al_2O_3	99.99	Alfa Aesar No. 39814	10.9[a]	0.9-2.2. µm[b]
Gibbsite (γ-$Al(OH)_3.xH_2O$)	p.a.	Merck No. 101093	1.08[a]	95% <45 µm[b] [82]
ZnO*	Not specified	Aldrich No. 544906	11[a]	Av. Particle size 71 nm[b]

*ZnO was only applied to *in situ* experiments of Np(V) sorption (cf. section 5.8) [a] determined at FZD; [b] specification by the manufacturer.

In this study, silica gel was used as model for silica, since it represents enhanced sorption capacities compared to quartz, due to its very high specific surface area. The fundamental unit of all silicate structures is the SiO_4 tetrahedron, consisting of four O^{2-} ions at the apices of a regular tetrahedron coordinated to one Si^{4+} at the center. The individual tetrahedra are linked together by shared corners, i.e. only by O^{2-} ions to form more complex structures and several different arrangements occur, partly accounting for the large number of silicate minerals. The tetrahedra can be arranged as a single or double, in rings, single or double chains, sheets or three-dimensional frameworks [119].

Some characteristics of the used oxides and hydroxides are listed in Tab. 5-4. In preliminary FT-IR experiments, the preparation of thin films was tested and the stability of the obtained film under flow conditions for at least 3 hours were confirmed.

The ATR FT-IR spectra obtained from standard *in situ* experiments after 90 minutes of induced U(VI) sorption (cf. Tab. 5-5) onto γ-Al_2O_3 and SiO_2 are shown in Fig. 5-14. Different spectral characteristics are observed in the range 1600 – 800 cm^{-1}.

The U(VI) related vibrational mode varies depending on the oxide, a single band of $\upsilon_3(UO_2)$ occurs at 913 cm^{-1} for SiO_2 (Fig. 5-14, lower trace). For γ-Al_2O_3 a split band is observed and local maxima were determined to be at 947, 927 and 912 cm^{-1} using second-derivate analysis (Fig. 5-14, upper trace). Interestingly, such high frequencies, as in case of Al_2O_3, have not been found for U(VI) surface species at surfaces of ferrihydrite [203] and TiO_2 (cf. section 5.2), or in the literature [54, 65, 71]. This clearly indicates the formation of different types of surface complexes.

Additionally, in the spectrum of γ-Al_2O_3 strong absorption bands appear between 1150 and 1000 cm^{-1}. Concerning SiO_2 a huge peak centering at 1022 cm^{-1} is observed because of SiO stretching [119]. These bands are similar to those observed for TiO_2, and might be assigned similarily to interactions of the cations, and hence, reorganization processes at the surface.

Moreover, in case of γ-Al_2O_3 absorption bands at higher frequency (1350 – 1600 cm^{-1}), similar to the TiO_2 – U(VI) system, but with distinctly increased intensities are detected. In

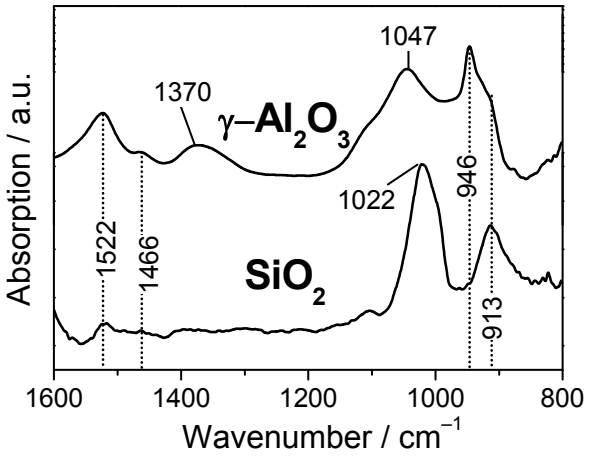

Fig. 5-14: ***In situ*** **ATR FT-IR spectra of U(VI) sorption on γ-Al_2O_3 and SiO_2 (20 µM initial U(VI), 0.1 M NaCl, pH 6, 90 min). Indicated values are in cm^{-1}.**

particular, the bands at 1522 and 1370 cm^{-1} might be due to stretching vibrational modes of carbonate ligands, hence, suggesting the formation of ternary surface complexes.

In conclusion, the spectra of U(VI) sorption onto SiO_2 and γ-Al_2O_3 fit well to the spectroscopic findings of U(VI) sorbed at the TiO_2 surface. The red shift of $\upsilon_3(UO_2)$ with an extent of 43 cm^{-1} compared to the free UO_2^{2+} cation strongly supports the formation of an inner-sphere surface complex of U(VI).

Furthermore, from these data, the coordination type, i.e. monodentate and bidentate, can be elucidated. In a bidentate complex the electrostatic characteristics of the mineral phase should generate a kind of fingerprint on the stretching frequency of the heavy metal ion. A comparison of $\upsilon_3(UO_2)$ of U(VI) sorption onto titania, silica and alumina results in shifted absorption maxima ranging from 890 to ~915 cm^{-1}. Hence, bidentate configuration is suggested for the U(VI) inner-sphere sorption complex and is in accordance to previously reported spectroscopic findings [44, 67, 78, 79, 128].

In contrast, the obtained ATR FT-IR spectrum of U(VI) surface species on γ-Al_2O_3 exhibits several interesting spectroscopic features, e.g. overlapping bands of $\upsilon_3(UO_2)$ and bands

Tab. 5-5: Standard conditions for *in situ* ATR FT-IR experiments of U(VI) sorption on the used oxide samples. The variation ranges for the investigation of γ-Al_2O_3 are presented in parentheses.

Mobile phase	U(VI) concentration	20 µM
	Ionic strength (NaCl)	0.1 M (0.01 – 1 M)
	pH	6.0 (4 – 7)
	Solvent	H_2O
Stationary phase	Deposited Al_2O_3, and SiO_2	0.1 mg cm^{-2}
		5 layers (each 1 µL of a 2.5 g L^{-1} suspension)
		α and γ Al_2O_3 phases, aged and freshly prepared
		different gibbsite samples
Performance	1st conditioning (Blank)	60 min
	Sorption (U(VI))	90 min
	2nd conditioning (Blank)	30 min
	Atmosphere	Normal (also inert gas)
	Temperature	Room temperature (i.e. 20 – 23°C)
	Flow velocity	0.2 mL min^{-1} (0.053 – 0.2 mL min^{-1})

possibly corresponding to carbonate ligands. Therefore, further systematic *in situ* sorption experiments have been performed using this system, in order to clarify which U(VI) surface reactions are responsible for the observed spectral characteristics. The sorption process was monitored in the minute range and the influence of sorptive properties; e.g. pH, ionic strength, and the absence of atmospheric carbonate were studied. Furthermore, the U(VI) surface speciation was studied on different aged γ-Al_2O_3 samples and on gibbsite $Al(OH)_3$ to exemplify a hydrated form of alumina. The conditions are listed in Tab. 5-5 and the variation of the experimental parameters is given in parentheses.

5.4.1 Monitoring the U(VI) sorption process onto γ-Al_2O_3

The course of a sorption standard experiment (cf. Tab. 5-5) is shown in Fig. 5-15. As previously mentioned, no positive or negative bands have been observed during the 1st conditioning, confirming the stability of the prepared alumina film on the diamond crystal (Fig. 5-15, red trace).

The U(VI) sorption spectra are presented in dependence of induced uranyl(VI) – alumina contact time (Fig. 5-15, black traces). In the first few minutes ($\leq$ 4 min) a band at 912 cm^{-1} is observed for the vibrational mode $\upsilon_3(UO_2)$. Upon increased U(VI) accumulation on the surface, this band is hypsochromically shifted firstly to 927 cm^{-1}, resulting in a band at 946 cm^{-1} with narrow width and shouldering to lower wavenumbers.

Similar to the spectral data obtained from other sorbent materials, bands at higher frequency occur additionally to $\upsilon_3(UO_2)$ upon sorption, namely at 1522, 1466 and between 1100 and 1000 cm^{-1}. One additional band is detected at 1352 cm^{-1} which shifts hypsochromically to 1374 cm^{-1} upon time. The relocation of this band is similar to the shift of $\upsilon_3(UO_2)$ and seems to be correlated with the appearance of the 946 cm^{-1} band.

From these spectra, a differing surface complexation behavior can be deduced upon increasing U(VI) surface coverage on γ-Al_2O_3. The first U(VI) sorption band at 912 cm^{-1} appears at similar wavenumbers compared to the bands observed for TiO_2 and SiO_2 (cf. Fig. 5-1 and Fig. 5-15). Similar shifts of $\upsilon_3(UO_2)$ onto different oxides indicate the formation of structurally similar, i.e. inner-sphere U(VI) surface complexes. This is in accordance to Sylvester et al, who performed EXAFS measurements for the U(VI) alumina sorption system at low and near neutral pH conditions and detected splitting of the equatorial shell into two distinct shells, indicating the formation of an inner-sphere surface complex.

However, in contrast to TiO_2 and SiO_2, only after a short time range, $\upsilon_3(UO_2)$ is distinctly allocated, evidencing that previously used binding sites on γ-Al_2O_3 are occupied and/or are not available for further U(VI) accumulation. Obviously, the band at 927 cm^{-1} presents a weaker bound uranyl(VI) surface species, possibly of outer-sphere character, since the shift of $\upsilon_3(UO_2)$ related to the aqueous species is conspicuously reduced compared to the species presented by the 912 cm^{-1} band.

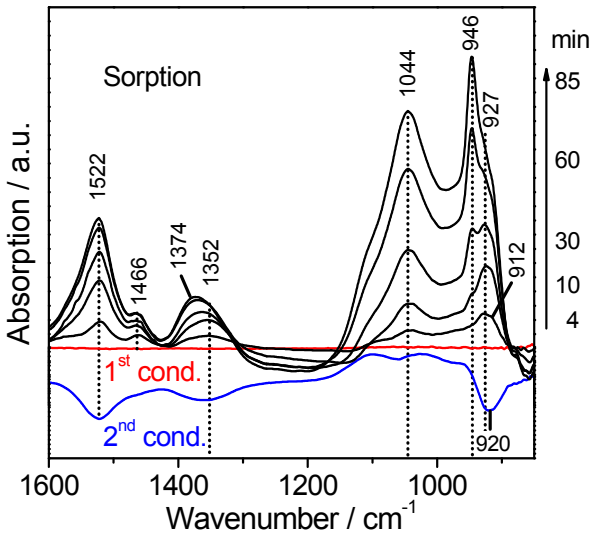

Fig. 5-15: ***In situ*** **time-resolved ATR FT-IR spectra of U(VI) sorption on γ-Al_2O_3. The spectra of the sorption process are recorded at different times after induction as given. The conditioning stages represent the equilibration of the γ-Al_2O_3 film by flushing a blank solution before (1st) and after (2nd) the induced sorption process. Indicated values are in cm^{-1}.**

Outer-sphere complexation leaves the uranyl equatorial hydration structure intact. Pasilis et al investigated uranyl citrate adsorption on γ-Al_2O_3 by ATR FT-IR spectroscopy [176]. The obtained spectrum from the binary U(VI) – γ-Al_2O_3 is of low signal-to-noise ratio, but a broad band concerning $\upsilon_3(UO_2)$ is exhibited at 917 cm^{-1} which is in accordance to an overlapping of the both bands at 912 and 927 cm^{-1} observed here. Moreover, in the same spectrum small broad unassigned bands are shown, at ~ 1530 and ~ 1350 cm^{-1}, also in agreement to the spectral features in Fig. 5-15.

After around 30 minutes of sorption, the development of an additional band centering at 946 cm^{-1} supports a new U(VI) complex. If the surface would have become saturated upon continued U(VI) flux, one may expect surface polymerization and/or precipitation to occur in a next step subsequent to sorption. Consequently, sorption and precipitation are part of a continuous process, reasoning that each adsorbed uranyl ion becomes a sorption site of its own [42].

The band at 946 cm^{-1} fits well with the data of aqueous solutions, where the formation of polymeric and precipitated U(VI) species is presented by $\upsilon_3(UO_2)$ in the frequency range 935 – 950 cm^{-1} (cf. sections 4.1 and 4.2). Precipitates formed and bound onto metal oxide surfaces or surface polymerization may exhibit similar shifts.

However, the formation of colloids in the aqueous solution with subsequent chemical and/or physical sorption on the surface can be ruled out, since the conditions of the sorptive solutions (cf. Fig. 5-1 and Fig. 5-14) are the same in all sorption experiments and this effect has been observed for neither SiO_2 nor TiO_2 samples.

In the previously mentioned EXAFS study, Sylwester et al. found at near-neutral pH a near – neighbor U atom with an average coordination number of approximately 0.4 and tentatively assigned the spectral data to the formation of a polynuclear surface species. The coordination

number of 0.4 is explained by the partial formation of polynuclear complexes along with mononuclear complexes [44].

However, it is also conceivable that upon increased U(VI) accumulation amorphous phases are formed on the γ-Al_2O_3 surface, i.e. hydrated uranyl aluminate. This idea is supported by the spectra obtained from precipitates or colloidal phase from U(VI) solutions of higher concentration and pH (cf. section 4.2.5). Moreover, the narrow band width as well as the frequency range in the ATR FT-IR spectra (cf. Fig. 4-13 and Fig. 5-15) is distinctive for precipitates. Furthermore, the IR spectra of U(VI)-Fe oxide co-precipitation shows strong spectral similarities to schoepite, with respective bands of $\upsilon_3(UO_2)$ occurring at 936 and 933 cm^{-1} [204] supporting the assignment to the formation of an U(VI) surface precipitate.

The lower blue trace in Fig. 5-15 presents the spectrum of the 2nd conditioning. As in case of U(VI) sorption on TiO_2 (cf. Fig. 5-1), the removal of a slightly bound U(VI) species from the surface is expected at this experimental stage. The appearance of the negative band of $\upsilon_3(UO_2)$ at 920 cm^{-1}, suggests that parts of both surface species (912 and 927 cm^{-1}) are removed during flushing the film with blank solution. However, the negative 920 cm^{-1} band is also similar to the monomeric complex dominating the U(VI) speciation at 20 µM U(VI) at pH 6 with absorption maximum at 923 cm^{-1} (cf. Fig. 4-4 and Fig. 4-7). In contrast, the species at 946 cm^{-1} seems to be stable at the surface.

5.4.2 Influence of the U(VI) solution properties on the sorption onto γ-Al_2O_3

In a first step, *in situ* sorption experiments were performed with Cs^+ and Mg^{2+} as representative sorbates for monovalent and divalent cations, respectively. Monoatomic ions like Cs^+ and Mg^{2+} do not show any intrinsic vibrational absorption bands, whereas the UO_2^{2+} ion is identified by its asymmetric stretching vibration υ_3. In fact, the 90 minutes sorption spectra of the Cs(I) and Mg(II) sorption experiment show no bands below 950 cm^{-1} (Fig. 5-16, lower traces), but the U(VI) surface species are observed at 946 and ~919 cm^{-1} in the respective spectrum (Fig. 5-16, upper trace). These findings provide clear evidence for the assignment of these bands to the $\upsilon_3(UO_2)$ mode of the sorbed uranyl species.

However, from these data further information on the mineral-U(VI) surface system is given. In each spectrum, strong overlapping absorption is detected between 1000 and 1150 cm^{-1} independent on the sorbed cation. Moreover, they have never been observed in the numerous ATR FT-IR spectra of U(VI) solutions collected previously for the characterization of the U(VI) speciation at the micromolar concentration level (cf. section 4.1 and 4.2). But, similar bands were observed in the spectra of the sorption of U(VI), Np(V), Cs(I), and Mg(II) onto TiO_2 (cf. section 5.2 and 5.7). Hence, they may represent characteristics, i.e. structural rearrangements, of the oxides surface in relation to sorbing cations.

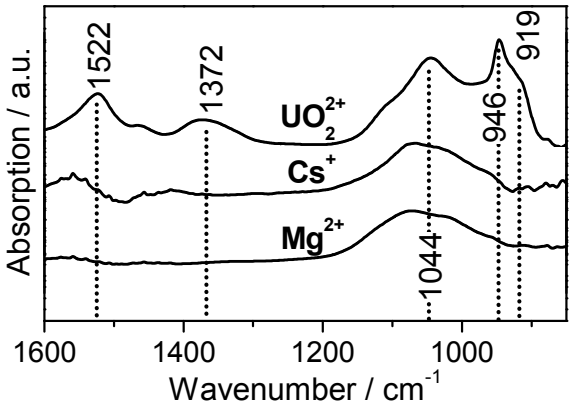

Fig. 5-16: Interaction of different cations at the water- γ-Al_2O_3 interface (20 µM initial cation concentration, 0.1 M NaCl, pH 6, 85 min).

Moreover, the bands at 1522 and 1372 cm^{-1} are clearly related to U(VI) surface complexation, since they are absent in case of Cs(I) and Mg(II). They appear in the characteristic frequency range of carbonate complexation and the formation of U(VI) carbonate complexation is conceivable.

However, ternary U(VI) carbonate surface complexes have already been observed for hematite, Fe_2O_3 [72]. Bargar et al studied the sorption of carbonate on hematite in the absence and presence of U(VI) by monitoring the C-O stretching region. Two bands arising from about 1600 to 1400 cm^{-1} and from 1400 to 1300 cm^{-1} are assigned to the asymmetric and the symmetric $\upsilon_3(CO_3)$ stretching frequency. In the presence of U(VI) the asymmetric υ_3 mode shifts to higher wavenumbers, and the ratio of asymmetric to symmetric band is increased. This is consistent with a bidentate coordination of carbonate anions to U(VI). U(VI) carbonate complexes were found to be the predominant adsorbed U(VI) species at the hematite surface at pH 4.7 – 8.3, that is a much wider pH range than previously postulated based on analogy to aqueous U(VI) carbonate complexes which are trace constituents at $pH < 6$ [72]. Unfortunately, $\upsilon_3(UO_2)$, that could give additional information on the formed species, was not measured within this study. Nevertheless, such complexes may occur also on minerals having surface charging behaviors similar to hematite, such as alumina.

Nevertheless, also in the aqueous U(VI)spectra, bands at 1525 and 1460 cm^{-1} have been detected and were assigned to specially coordinated water molecules of uranyl(VI) hydroxo complexes (cf. section 4.1). Since the contribution of the 1460 cm^{-1} band is very low, their presence in the spectra and therefore, their concurrence to a U(VI) surface species can not be ruled out completely. But, the intense bands at 1522 and 1372 cm^{-1} may most probably be attributed to a ternary carbonate U(VI) complex.

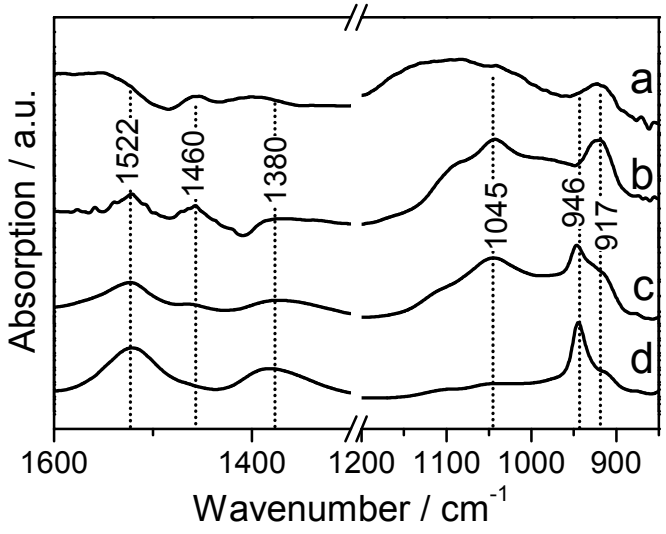

Fig. 5-17: ATR FT-IR spectra of U(VI) sorption onto γ-Al_2O_3. Influence of pH: (a) pH 4; (b) pH 5; (c) pH 6; (d) pH 7 (20 µM initial U(VI), 0.1 M NaCl, 85 min, air). Indicated values are in cm^{-1}.

In a second step, the impact of pH on the sorption of U(VI) onto γ-Al_2O_3 was studied in the range from 4 to 7. The respective spectra, obtained after 85 min sorption, are comparatively presented in Fig. 5-17a-d.

The data show distinct differences in band positions and intensities. At pH 4 U(VI) related bands appear with very low intensity at 917 cm^{-1} and at 1460 cm^{-1} (Fig. 5-17a), indicating very low U(VI) accumulation. Upon increasing pH absorption bands become more intense, indicating increasing U(VI) concentration at the γ-Al_2O_3 surface. At pH 5 further distinct bands are observed at 1044, 1385 and 1522 cm^{-1} (Fig. 5-17b). At pH 6 the band at 917 cm^{-1} obviously undergoes splitting and a new band is developed at 946 cm^{-1} (Fig. 5-17c). Finally, at pH 7, the 946 cm^{-1} band is increased in intensity, while absorption at 917 cm^{-1} appears only as a shoulder. At higher wavenumbers, the band at 1460 cm^{-1} disappears, upon accumulation of the band at 946 cm^{-1} (Fig. 5-17d). The IR spectroscopic data clearly show, that U(VI) sorption depends on pH conditions and confirm the previous complex assignment. Macroscopic studies of U(VI) sorption onto γ-Al_2O_3 in the micromolar range have shown an increasing surface accumulation at pH > 4 which is clearly supported by the spectroscopic findings shown in Fig. 5-17a-d [81].

Furthermore in a third step, the influence of ionic strength in the range from 0.01 to 1 M was investigated on U(VI) sorption onto γ-Al_2O_3. The respective spectra after 85 minutes of sorption are presented in Fig. 5-18.

Upon comparing the data distinct differences are only observed concerning the vibrational mode $\upsilon_3(UO_2)$. At low ionic strength ≤ 0.1 the band at 946 cm^{-1} contributes to the uranyl surface speciation (Fig. 5-18a,b), whereas at higher ionic strength ≥ 0.5 a band centering at 917 cm^{-1} is evident (Fig. 5-18c,d). As suggested in the previous section, the surface species with absorption at 946 cm^{-1} represents a higher sorption level than the 917 cm^{-1} species. The formation of a surface precipitate or a polymeric species is likely. This assumption is in

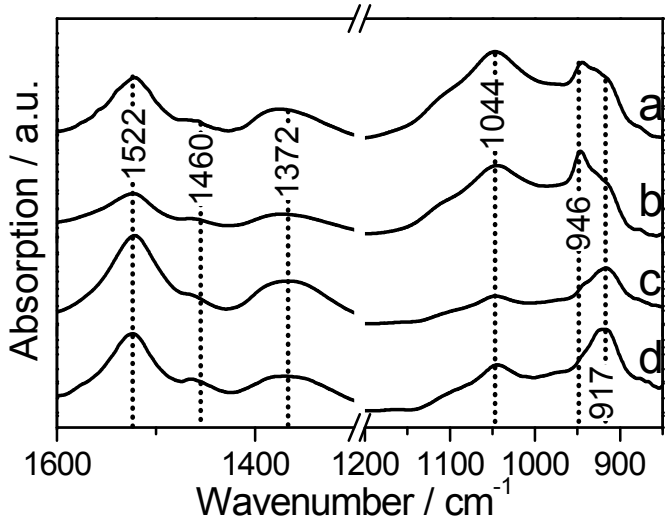

Fig. 5-18: ATR FT-IR spectra of U(VI) sorption onto γ-Al_2O_3. Influence of ionic strength (a) 0.01; (b) 0.1; (c) 0.5 and (d) 1. (20 µM initial U(VI), pH 6, 85 min, air). Indicated values are in cm^{-1}.

agreement with the macroscopic studies of Guo et al., showing insensitivity of ionic strength in the range $0.05 - 0.1$ on U(VI) sorption onto Al_2O_3, while the sorption was slightly decreased with increasing ionic strength from 0.1 to 0.5 [81, 205]. This is also valid for U(VI) sorption on imogolite [97].

In a fourth step, the influence of the solid-liquid ratio, i.e. thickness of the γ-Al_2O_3 film deposited on the ATR crystal in the *in situ* FT-IR experiment was studied. The density of γ-Al_2O_3 particles ranged between 0.02 and 0.4 mg cm^{-2} and the respective spectra of the online monitored U(VI) sorption did not significantly differ.

In a fifth step, the impact of atmospheric carbonate was investigated. In Fig. 5-19, the spectra obtained after 90 minutes of induced sorption from experiments performed at air and inert gas (N_2) atmosphere are illustrated.

Obviously, the spectra show differences in the region above 1200 cm^{-1}. The band at 1044 cm^{-1} and the bands due to $\upsilon_3(UO_2)$ remain unchanged in local maxima and relative intensities. The bands at 1522 and 1377 cm^{-1} disappear in the absence of atmospheric carbonate (Fig. 5-19, lower trace), suggesting that the previously made assignment of asymmetric and the symmetric $\upsilon_3(CO_3)$ stretching is conceivable. From the IR spectroscopic identification of U(VI) species in aqueous solution it is known, that carbonate complexation also influences the vibrational mode of the uranyl(VI) unit, i.e. carbonate complexation led to a red shift of $\upsilon_3(UO_2)$ (cf. section 4.1.4). A similar effect can be expected for the sorption of a ternary uranyl(VI) carbonate complex on a mineral surface [77]. Ho and Miller discerned a U(VI) peak at 910 cm^{-1} in the case of hematite loaded with U(VI) in the absence of carbonate and a peak at 903 cm^{-1} when carbonate was introduced into the system [76]. Wazne et al detected in samples arising from batch experiments a clear peak at 902 cm^{-1} for U(VI) on ferrihydrite which was observed to shift and broaden towards 880 cm^{-1} upon increasing carbonate concentration [77]. However, the $\upsilon_3(UO_2)$ band observed at 946 cm^{-1} in this work is very strong in intensity and may overlap small contributions of possible additional bands.

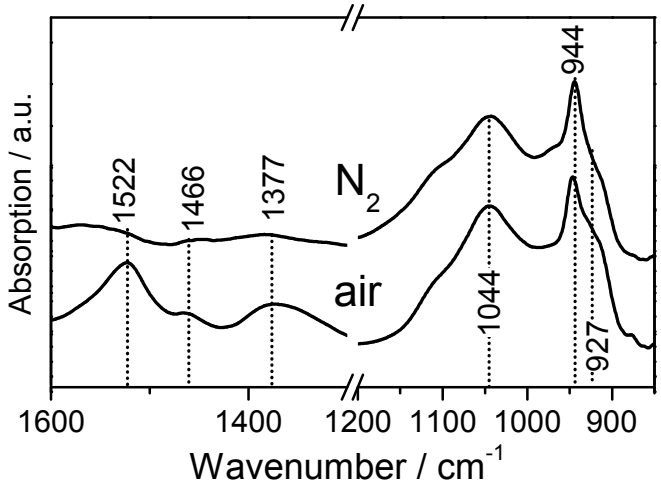

Fig. 5-19: ATR FT-IR spectra of U(VI) sorption onto γ-Al_2O_3. Influence of atmospheric carbonate (20 µM initial U(VI), 0.1 M NaCl, pH 6, 85 min). Indicated values are in cm^{-1}.

Very recently, Foerstendorf et al. performed *in situ* U(VI) sorption experiments in presence and absence of atmospheric carbonate at pH 5.5. All spectra present $\upsilon_3(UO_2)$ at 903 cm^{-1}, and carbonate complexation in bidentate manner upon prolonged sorption is deduced from bands at 1520 and 1396 cm^{-1} corresonding to symmetric and asymmetric $\upsilon_3(CO_3)$ [203]. These results show that ternary surface complexes are formed already at very low carbonate concentrations. Concerning the very similar analysis procedure and the carbonate band maxima occurring at similar frequencies, the formation of ternary uranyl(VI) carbonate complexes on Al_2O_3 is reasonable. In progress are experiments in presence and absence of carbonate, performed at a reduced initial U(VI) level at around 1 µM, representing the lowest detectable concentration in order to avoid fast U(VI) saturation of the alumina surface.

In a last step, the dependence of the flow rate was studied and the obtained spectra at different time ranges of induced sorption are shown in Fig. 5-20.

Upon comparison distinct differences are detected at 0.2 and 0.057 ml min^{-1}. At the reduced flow conditions, splitting of the vibrational mode $\upsilon_3(UO_2)$ is not observed, in fact, only at sorption above 90 minutes the band is slightly red shifted from 912 to ~922 cm^{-1} at 240 minutes (Fig. 5-20 lower traces). In contrast, at a flow rate of 0.2 ml min^{-1} shifting of $\upsilon_3(UO_2)$ happens within the first minutes of induced sorption and becomes even more intensive after around 45 minutes, when the additional band at 946 cm^{-1} occurs (Fig. 5-20 upper traces). From this data, a strong influence of the U(VI) sorption on the flow rate and hence, on the contact time and the availability of dissolved U(VI) species is deduced. Such impact was already observed for TiO_2 (cf. section 5.1.4), although the respective shifts are of lower extent. The bands at 1044 and 1522 cm^{-1} are not varying, whereas the band at 1352 cm^{-1} is shifted to 1377 cm^{-1} upon increasing the flow velocity. The spectra evidence that the shift of 25 cm^{-1} is related to the band occurring at 946 cm^{-1}. This is supported by the time-resolved spectra of the single sorption experiment (cf. Fig. 5-15). Assuming that the band at 946 cm^{-1} refers to a surface precipitate and the bands at 1522 and 1352 cm^{-1} to

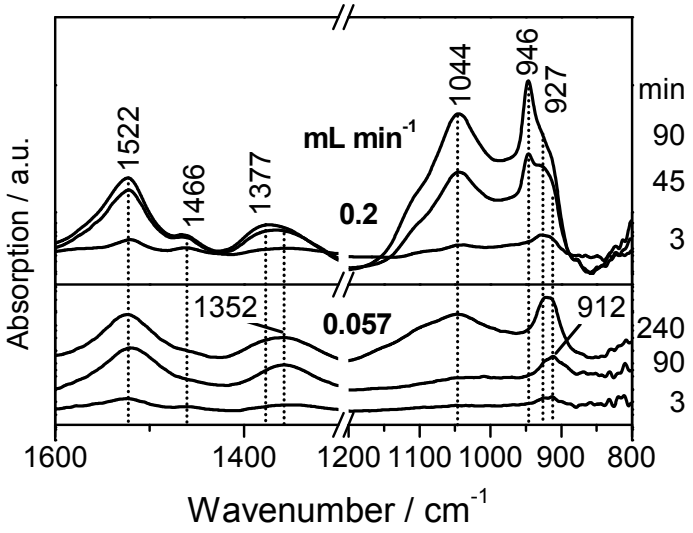

Fig. 5-20: ATR FT-IR spectra of U(VI) sorption onto γ-Al_2O_3. Influence of flow rate. (20 µM initial U(VI), 0.1 M NaCl, pH 6, 5,). Indicated values are in cm^{-1}.

υ_3(CO) of bound carbonate, a relocation of the carbonate ligands upon formation of complex precipitation structures is conceivable. This interpretation is supported by the time-resolved spectra. Although the bands of $\upsilon_3(UO_2)$ are strongly increased upon time, the bands of υ_3(CO) are exhibited almost unchanged in intensity.

5.4.3 Influence of the aluminate mineral phase on U(VI) sorption

In various investigations, the hydration of Al_2O_3 leading to oxy-hydroxide (AlOOH) or trihydroxide ($Al(OH)_3$) was described to be crucial for the study of the reactions occurring ad the alumina-water interface. The presence of bayerite (α-$Al(OH)_3$) in aged γ-Al_2O_3 suspensions has been confirmed by spectroscopic techniques [198-200, 206]. Such phase transformations may affect the surface complexation of U(VI). Therefore, additional experiments have been performed.

In a first series, the γ-Al_2O_3 film on the ATR crystal was flushed for a prolonged time with the blank solution, i.e. 0.1 M NaCl, pH 6. The spectra may provide spectral alterations which are due to changes, e.g. in hydration of the γ-Al_2O_3. The IR spectrum of bayerite exhibits strong absorption bands at 1026 and 976 cm^{-1}, for gibbsite the respective OH bending vibrational modes are observed slightly shifted at 1034 and 980 cm^{-1}, in case of AlOOH they appear at ~1080 cm^{-1} [207]. The spectra in Fig. 5-21 are equally calculated and analyzed as in case of U(VI) sorption, considering a first conditioning for equilibration of the mineral system (cf. section 3.3.2). Hence the spectra, indicated with 10, 30, 60, and 90 minutes in Fig. 5-21a are directly comparable with the spectra obtained after the same time intervals of induced sorption in Fig. 5-15. Obviously, the alumina-water spectra show different spectral characteristics than those of alumina-U(VI) interactions, the signal-to-noise ratio is distinctly reduced which is comparatively demonstrated for the 90 minute spectra of both systems in Fig. 5-21b. In the experiment using the blank solution, no distinct bands below 1000 cm^{-1}, in

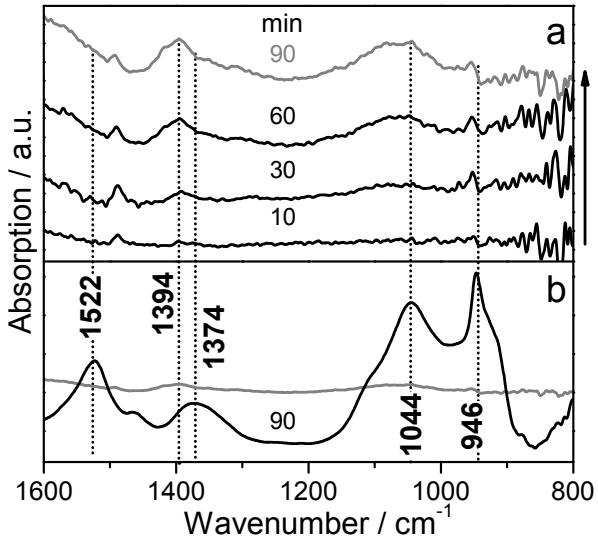

Fig. 5-21: ATR FT-IR spectra of the stability of γ-Al_2O_3 during *in situ* experiments. (a) Standard experiment, but in absence of U(VI); (b) comparison of 90 min spectra in presence (black) and absence (grey) of 20 µM U(VI), equally scaled (0.1 M NaCl, pH 6, 90min). For details see text. Indicated values are in cm^{-1}.

particular at ~980 cm^{-1} which would indicate a certain amount of alumina trihydrate were observed. Nevertheless, broad bands slightly increased in intensity within the flushed time show maxima at 1065 and 1394 cm^{-1}. These wavenumbers do not correspond correctly to the found assignments of bending OH vibrations of alumina mono- and trihydrates [207]. However, the presence of trace amounts of hydrated alumina can not be ruled out with the performed measurements. In future investigations, XRD analysis can be performed with the minerals out of the suspensions used for the ATR film preparation.

In a second series, *in situ* ATR FT-IR sorption measurements of U(VI) have been performed with different aluminate substrates, in order to identify the impact of structural differences on U(VI) sorption. Hence, freshly prepared and 10 months aged suspensions of γ-Al_2O_3 have been utilized in the preparation procedure of thin mineral films on the ATR crystal for standard *in situ* U(VI) sorption studies (Fig. 5-22a,b). Further on, the U(VI) reactions at interfaces of differing aluminates, namely α-Al_2O_3 and γ-$Al(OH)_3$ were investigated (Fig. 5-22c-d).

Comparison of U(VI) sorption onto freshly prepared and 10 months aged samples of γ-Al_2O_3 shows no shifts of the previously described bands at 1522, 1377, 1044 and 946 cm^{-1}, whereas shouldering of the last mentioned band to lower wavenumbers becomes apparent. Though the relative intensities between these bands are changed and the peaks at 1522, 1377 cm^{-1} are increased upon using the aged suspension, the peak at 1044 cm^{-1} and those of $\upsilon_3(UO_2)$ remain the same. If both bands are assigned to $\upsilon_3(CO_2)$ the spectral data evidence that the aging process causes carbonate accumulation on the minerals surface. Since the suspension was aged under oxic conditions, diffusion of atmospheric CO_2 can be responsible for elevated carbonate concentrations.

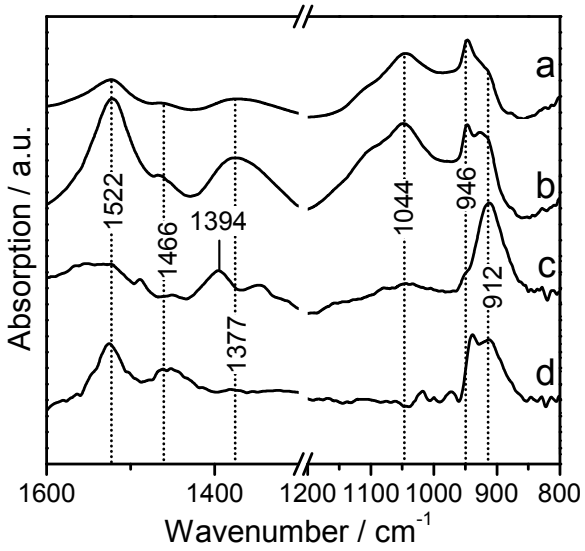

Fig. 5-22: ATR FT-IR spectra of U(VI) sorption onto different aluminates. (a) γ-Al_2O_3 (freshly prepared suspension); (b) the same after 10 months aging; (c) α-Al_2O_3; (d) Merck $Al(OH)_3$; (20 µM initial U(VI), 0.1 M NaCl, pH 6, 90min). Indicated values are in cm^{-1}.

The spectra of U(VI) sorption onto samples of α-Al_2O_3 and γ-$Al(OH)_3$ exhibit interesting differences to γ-Al_2O_3. For α-Al_2O_3 one band centers at 912 cm^{-1} concerning $\upsilon_3(UO_2)$ and in relation, all other bands are considerably reduced in intensity. Moreover, a very small shoulder is found at 946 cm^{-1}. One small additional band is detected at 1394 cm^{-1} which seems to be arising from interactions of the Al_2O_3-water interface, since it was already observed in the spectra of Fig. 5-21a.

The results for α-Al_2O_3, in particular the bands of $\upsilon_3(UO_2)$ agree well with those obtained from TiO_2 and SiO_2. An inner-sphere sorption complex of U(VI) is suggested from the band at 912 cm^{-1}. Since a blue shift and/or splitting of $\upsilon_3(UO_2)$ of the adsorbed U(VI) could not be detected clearly in the ATR FT-IR spectral data, surface precipitation and outer-sphere complexation of U(VI) certainly play only a minor role onto α-Al_2O_3 under the chosen conditions. Furthermore, because of the absence of strong bands in the range 1550 – 1300 cm^{-1}, also the formation of ternary carbonate containing complexes is unlikely.

In a next step, ATR FT-IR sorption experiments of U(VI) were performed with gibbsite, i.e. γ-$Al(OH)_3$. Again, the split band of $\upsilon_3(UO_2)$ with maxima at 912 and ~940 cm^{-1} indicates multi surface species. This is in accordance to results of a previous TRLFS study, when two uranyl(VI) species were identified, one dominating the more acid pH region whereas the second one became gradually more prominent towards higher pH values [82]. Furthermore, small bands are observed in the IR spectrum at ~1000 cm^{-1} which are due to bending vibrational modes of the gibbsite film. Although the spectrum of U(VI) sorption onto gibbsite does not show the strong contribution of the carbonate related bands, the complexation behavior, including at least two different surface species, seems to be similar to that of γ-Al_2O_3.

In summary, the sorption of U(VI) from micromolar solutions onto alumina was investigated in detail by application of *in situ* ATR FT-IR spectroscopy. Under the chosen conditions, the spectroscopic findings substantiate the formation of U(VI) surface complexes onto the aluminum oxides γ- and α-Al_2O_3 and on gibbsite, exemplifying aluminum trihydrate. However, differing sorption complexes are found for α- and γ-Al_2O_3. Most probably both form inner-sphere complexes, but additional surface species, possibly outer-sphere and surface precipitates are characteristic for high U(VI) accumulation on γ-Al_2O_3. At high pH, low ionic strength, and increased contact time the uranyl(VI) concentration on the surface is increased and the formation of surface precipitates is derived. Furthermore, the spectra evidence the formation of ternary U(VI) carbonate surface complexes which have to be studied in more detail. Similarities between the sorption of U(VI) on gibbsite and γ-Al_2O_3 are deduced from the IR spectral data.

5.5 U(VI) sorption onto alumosilicates

In the previous sections comprehensive data for U(VI) sorption onto different metal oxides and under several conditions have been presented. The spectroscopic results clearly show that U(VI) sorption depends strongly on the properties of the mineral surface (type of oxide, surface area, particle size) as well as on the sorptive solution (pH, concentration). Furthermore, it was shown that the degree of surface saturation is decisive for discrimination of different sorption complexes formed during the sorption processes. The obtained data serves as a reference for the investigation of U(VI) surface reactions on more complex mineral systems and for the investigation of further actinyl cations on mineral surfaces.

A first implementation of the obtained spectroscopic data on environmentally relevant minerals, i.e. clay and mica minerals is provided in this section.

Clay minerals are the most important sorbents for metal cations in soils and sediments because of their high abundance in the environment, their large specific surface area, negative surface charge, and reactive surface hydroxyl groups. Kaolinite is a prominent representative of the clay family. It was chosen for the first FT-IR sorption experiments onto a clay mineral because of its contribution to many soils and its relatively simple and well investigated crystal structure. Kaolinite belongs to the class of layered two-sheet alumosilicates. The chemical

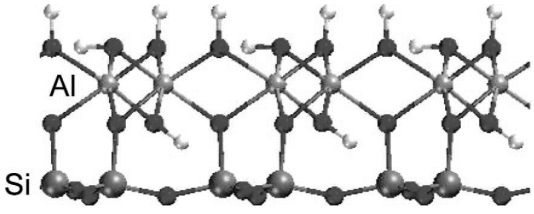

Fig. 5-23: Structure of kaolinite: the atoms of silicon, aluminium, oxygen and hydrogen are in green, pink, red and white, respectively [57].

composition of one such layer can be represented by a unit cell of $Al_2Si_2O_5(OH)_4$ which is overall neutral and consists of a "tetrahedral" Si sheet connected over apical oxygen atoms with an aluminum dioctahedral sheet [119]. Two-sheet layers are connected via hydrogen bonds.

Moreover, the applied kaolinite KGa-1b has been studied previously concerning its retention behavior and mechanisms for U(VI), using macroscopic and spectroscopic measurements [86, 87, 208]. The sorption of U(VI) onto kaolinite is influenced by the pH, presence of CO_2, and by the U(VI) concentration. By application of TRLFS, two bidentate mononuclear uranyl surface complexes differing in the number of water molecules in their coordination environment were identified [86]. From EXAFS studies the formation of inner-sphere surface complexes by edge sharing with aluminum octahedra and/or silicon tetrahedra were derived [87].

The use of granitic rocks for the storage of nuclear wastes increased the number of investigations dealing with the interaction of micas (e.g. biotite, muscovite) with actinide elements [209, 210]. Previously, also coupled sorption-reduction reactions of aqueous U(VI) by ferrous micas were studied. [211, 212]. The micas are a subset of the phyllosilicates in which three of the four oxygen atoms in each silicon tetrahedron are shared with adjacent silicon tetrahedra. Classification of the phyllosilicates is based on their octahedral layers which may be either all filled trioctahedral layers or two-thirds filled dioctahedral layers. For nearly every trioctahedral sheet silicate, there is an analogous dioctahedral sheet silicate.

Muscovite is dioctahedral (ideally, $KAl_2[Si_3AlO_{10}](OH)_2$), and biotite is trioctahedral ($K(Mg,Fe)_3(Si_3Al)O_{10}(OH)_2$), both are common rock-forming minerals. Muscovite is a major constituent of granite and phyllite and thus, a potentially important sorbent of uranium. By application of TRLFS, Arnold et al. found two adsorbed U(VI) surface species on edge surfaces of muscovite, differing in their coordination environment [92].

There are cross structural similarities between clay minerals and micas which make them interesting for the study as model systems. The characteristics of the used samples of kaolinite, biotite, and muscovite are listed in Tab. 5-6.

Tab. 5-6: Characteristics of the used alumosilicate samples.

Sample	Origin	BET in $m^2\ g^{-1}$	Particle size
Kaolinite	Clay Minerals Society Source Clays Repository (Washington County Georgia) KGa-1b	11.8[a]	57.8% < 2 µm 32.0% < 0.5 µm [213]
Muscovite	Dr. F. Krantz Rheinisches Mineralien-Kontor GmbH & Co. KG (Bonn, Germany) X – 01541 (Norwegen)	2.9[a]	< 63 µm[a]
Biotite	Dr. F. Krantz Rheinisches Mineralien-Kontor GmbH & Co. KG (Bonn, Germany) X – 01481 (Norwegen)	2.4[a]	< 63 µm[a]

[a] determined at FZD.

The *in situ* ATR FT-IR experiments of U(VI) sorption on the alumosilicates were performed in analogy to those on γ-Al_2O_3 (cf. Tab. 5-5). The spectra obtained at 90 minutes of induced U(VI) sorption on kaolinite, biotite and muscovite are presented in Fig. 5-24. All spectra show one broad absorption band, centering at 907 cm^{-1}. This band is attributed to the antisymmetric stretching mode $\upsilon_3(UO_2)$. In comparison to the free cation UO_2^{2+}, this vibrational mode is bathochromically shifted by 54 cm^{-1} and the extent is similar to those observed for the investigated oxides of alumina, titania and silicon (cf. section 5.1 and 5.3). Thus, the formation of inner-sphere U(VI) sorption complexes is assumed to occur. This is in accordance to findings for kaolinite and muscovite from different spectroscopic techniques [86, 87, 92]. Furthermore, the spectra show large bandwidths of the uranyl band which was previously found to correspond to the presence of more than one sorbed species. Experiments in progress that evaluate the impact of sorption time, pH and ionic strength, may clarify the number and type of involved species.

All spectra of the U(VI) loaded sorbents show bands at 1525 and 1460 cm^{-1}. These bands have already been observed in the U(VI) spectra of micromolar solutions and sorbent oxides (cf. section 4.1 and 5.1) and were assigned to specially coordinated water in the hydration of U(VI).

In case of kaolinite, an additional shoulder centering at 933 cm^{-1} is observed which is most probably due to vibrations of the mineral phase, since kaolinite provides several bands below 1100 cm^{-1} (cf. Fig. 3-6b). Furthermore, the spectra of kaolinite, muscovite, and biotite show absorption bands in the region from 950 to 1050 cm^{-1}. They are also due to absorption changes at the mineral film, namely assigned to symmetric vibrations of SiO bonding [119].

In summary, in this study the U(VI) speciation at surfaces of kaolinite, muscovite and biotite was investigated by application of ATR FT-IR spectroscopy for the first time. The used substrates can be understood as representatives of complex surfaces as they are found for clay minerals and micas. From the spectra, in particular from shifts of $\upsilon_3(UO_2)$ similar

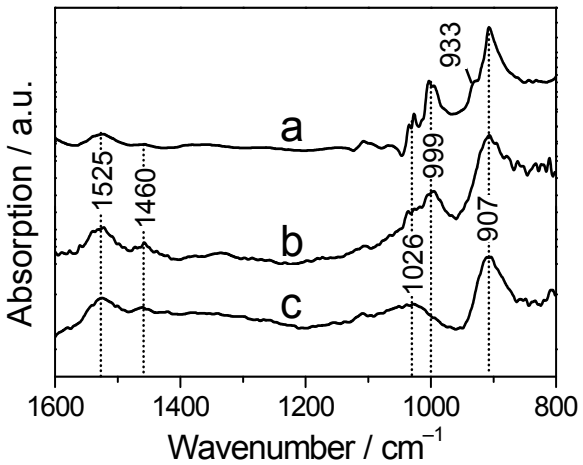

Fig. 5-24: *In situ* ATR FT-IR spectra of U(VI) sorption on (a) kaolinite, (b) muscovite, (c) biotite (20 µM initial U(VI), 0.1 M NaCl, pH 6, 85 min). Indicated values are in cm^{-1}.

complexation of inner-sphere type is assumed. However, only results from future experiments can give detailed descriptions of sorption phenomena on complex minerals

5.6 Introducing remarks on Np(V) sorption onto mineral surfaces

In recent years, the sorption behavior of Np(V) onto synthetic and naturally occurring oxides and hydroxides was intensively studied [98-102, 105-111, 113, 116, 214]. The vast majority of these studies present results of batch experiments investigating the neptunium sorption capacities of the substrates and the effect of selective parameters, such as pH, ionic strength, competing ions, ambient and inert gas atmosphere, on the sorption behavior. Modeling of the sorption was also performed [39, 49, 115, 215]. From these studies, an increased affinity of Np(V) to silanol and aluminol groups was detected at higher pH conditions whereas a decreased sorption was found for silica under aerobic conditions [106]. A similar dependence on pH was also reported for TiO_2, kaolinite, magnetite, hematite, biotite, bentonite, and montmorillonite [98, 101, 102, 114, 115]. Furthermore, due to the very low impact of the ionic strength on the sorption of Np(V) onto TiO_2 and hematite the formation of inner-sphere complexes was suggested [98, 100].

For a better understanding of the sorption mechanisms, spectroscopic experiments are expected to provide structural information of the type of surface complex on a molecular level. There are only few spectroscopic studies of Np(V) sorption on oxides of iron and manganese using XAS and XPS [103, 104, 111, 112]. Vibrational spectroscopy which may provide additional information on the coordination of surface complexes, was not applied up to now. The aim of this work is the *in situ* characterization of Np(V) sorption complexes using ATR FT-IR spectroscopy. A set of pure and well characterized oxides of titanium, silicon and zinc differing in the crystal structure, namely tetragonal TiO_2, tetrahedral γ-Al_2O_3 and SiO_2, and hexagonal ZnO, in specific surface area and in particle size distribution was investigated as model substrates for the elucidation of molecular processes on more complex mineral surfaces. According to reported results from macroscopic measurements, Np(V) sorption experiments are performed in the pH range 4 – 7.6, where pH 7.6 represents maximum sorption condition. The effect of Np(V) loading on the formation of Np(V) surface complexes are considered.

The type of the sorbed species, e.g. inner- and outer-sphere complex, can be elucidated by shifts of the antisymmetric stretching vibration υ_3 of the Np=O bond compared to the aqueous species. Since the frequency of this Np(V) vibrational mode strongly interferes with water absorption at frequencies below 850 cm^{-1}, the sorption experiments have to be performed in heavy water. Due to the isotopic shift of approximately 300 cm^{-1} of D_2O, the signal-to-noise ratio of the spectra is considerably increased allowing an accurate detection of sorbed Np(V) species at a micromolar concentration level [135, 136]. A detailed knowledge of the spectra of

Tab. 5-7: Standard conditions for *in situ* ATR FT-IR experiment of Np(V) sorption on metal oxides.

Mobile phase	Np(V) concentration	50 µM
	Ionic strength (NaCl)	0.1 M
	pH	7.6
	Solvent	D_2O
Stationary phase	Deposited TiO_2 (S1, S6), γ-Al_2O_3, SiO_2 and ZnO	0.1 mg cm^{-2}
		5 layers (each 1 µL of a 2.5 g L^{-1} suspension)
Performance	1st conditioning (Blank)	30 min
	Sorption (Np(V))	60 min
	2nd conditioning (Blank)	30 min
	Atmosphere	Inert gas (N_2)
	Temperature	Room temperature (20 – 23°C)
	Flow velocity	0.1 mL min^{-1}

the aqueous speciation is indispensable for the discrimination of the various species potentially occurring during the sorption processes. Hence, the aqueous Np(V) speciation in micromolar solutions has been investigated using ATR FT-IR and NIR spectroscopy up to neutral conditions (pH ≤ 7.7) and comparison to modeled NEA thermodynamic data of Np(V) evidence the predominance of the free NpO_2^+ species (cf. section 4.4).

The standard conditions, listed in Tab. 5-7 were chosen similar to those for U(VI) (cf. Tab. 5-1), except the use of D_2O in all measurements. The properties of the used mineral phases are listed in Tab. 5-2 (S1, S6) and Tab. 5-4. Because of the high specific radioactivity of ^{237}Np and the cost involved of waste disposal, the flow velocity and the duration of the measurement have been reduced. To exclude fast exchanges between D_2O and H_2O the solutions were prepared and analyzed under nitrogen atmosphere in a glove box. The deposition of the stationary phase was done according to the experiences from the U(VI) sorption experiments (cf. chapters 2 and 5), using five thin layers for the preparation of one film with a density of approximately 0.1 mg cm^{-2}.

5.7 Np(V) sorption on titanium dioxide

5.7.1 Monitoring the Np(V) sorption process onto TiO_2

The course of an *in situ* sorption experiment is illustrated by the spectra shown in Fig. 5-25.

The spectrum referred to as "1st conditioning" reflects the equilibrium state of the TiO_2 film after flushing it with a blank solution for 60 minutes (Fig. 5-25, red trace). No significant absorption changes are observed in the spectral region from 1200 to 700 cm^{-1} within a time period of 30 minutes. Since in this spectral region, in particular below 900 cm^{-1}, absorption bands of TiO_2 can be expected, the absence of bands in this spectrum indicates a sufficient stability of the mineral film on the ATR crystal's surface under the chosen conditions. Similar stabilities have also been confirmed for the oxide layers of alumina, silica and zinc.

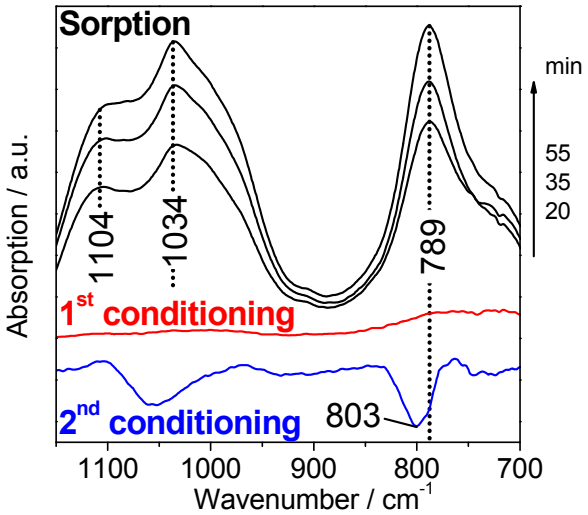

Fig. 5-25: ***In situ*** **time-resolved ATR FT-IR spectra of Np(V) sorption on TiO_2 (S1, 50 µM Np(V), D_2O, 0.1 M NaCl, pH 7.6, N_2). The spectra of the sorption process are recorded at different times after induction as given. The conditioning stages represent the equilibration of the TiO_2 film by flushing a blank solution before (1^{st}) and after (2^{nd}) the induced sorption process. The spectrum of the 2^{nd} conditioning is presented to an enlarged scale (3×). Indicated values are in cm^{-1}.**

The ATR FT-IR difference spectra calculated between the 1^{st} conditioning and after 20, 35, and 55 minutes of the induction of Np(V) sorption are shown in Fig. 5-25 (black traces). These spectra exhibit absorption bands with maxima at 1104, 1034 and 789 cm^{-1}. The intensities of the bands increase during this time of sorption reflecting Np(V) accumulation on the mineral's surface.

The latter absorption band is assigned to the antisymmetric stretching vibration υ_3 of the neptunyl(V) species sorbed on TiO_2. In comparison to the fully hydrated NpO_2^+ species in aqueous solution with absorption at 818 cm^{-1} (cf. Fig. 4-17), the υ_3 mode of the complexed species is shifted by about 30 cm^{-1} to lower wavenumbers. This frequency is due to a decrease of the Np=O force constant as a result of complexation with TiO units of the mineral phase in the equatorial plane.

This work provides *in situ* vibrational data of an actinyl(V) ion sorbed onto a mineral for the first time. Therefore, only a comparison to respective data of actinyl(VI) ions can be given. Upon sorption of U(VI) on different mineral phases, considerable downshifts of the $\upsilon_3(U^{VI}O_2)$ mode up to 50 cm^{-1} were observed [65, 71, 195]. The relative downshift of $\upsilon_3(NpO_2)$ for neptunyl(V) ion observed in our spectra is of the same extent suggesting a similar type of surface complex.

Consequently, such a strong shift to lower frequencies can only be explained by a formation of an inner-sphere surface complex. A coordination of the actinyl ion by electrostatic attraction would not modify the absorption frequency to such an extent [71]. Additionally, previous macroscopic studies demonstrate that the Np(V) sorption onto TiO_2 is independent from the ionic strength in solution using chloride as electrolyte in the millimolar range [98].

These findings support our band assignment to the formation of neptunyl(V) inner sphere complexes onto TiO_2.

The progress of neptunium sorption on the TiO_2 surface can be monitored online by the time-dependent increase of the absorption band at 789 cm^{-1}. After about 55 minutes no further intensity increase was observed, indicating steady state conditions. Moreover, the presence of one band showing a constant frequency maximum and band width throughout the time interval of induced Np(V) sorption indicates the presence of only one type of surface species whose structure does not vary with the sorbed Np(V) quantity.

The bands at 1104 and 1034 cm^{-1} can not be assigned unequivocally up to now. Their assignment to interactions of the background electrolyte, i.e. NaCl, or of heavy water with the TiO_2 can be ruled out, since the blank spectra obtained during the first conditioning stage provide no evidence for any complexation. Different explanations are possible and are discussed together with further results in the following section.

After 60 minutes of sorption, a "2^{nd} conditioning" of the TiO_2 film with blank solution was performed. The respective difference spectrum exhibits a weak negative band at 803 cm^{-1} with low intensity (Fig. 5-25 blue trace, note that the amplitude is enlarged three times for clarity). Because of the negative sign, this band can only represent desorbed neptunyl ions or particles of the mineral film released by the "2^{nd} conditioning". Since TiO_2 particles are not expected to show absorption bands around 820 cm^{-1}, this band has to represent a removal of NpO_2^+ ions from the mineral film which are spectrally different from the species discussed above. Deconvolution of absorption bands can provide additional information for identification of the presence of spectrally distinct species. However, since the intensity of the band at 803 cm^{-1} is very low compared to the band at 789 cm^{-1} (by a factor of approximately 0.1) and the level of noise is considerably high in this spectral region of the spectrum, an adequate deconvolution was found to be uncertain. In any case, the species showing an absorption maximum at 803 cm^{-1} obviously contributes to the Np(V) surface speciation only to a small extent.

The observed frequency at 803 cm^{-1} for this species shows a significantly smaller shift than the sorbed species observed at 789 cm^{-1} compared to the aqueous cation. An electrostatic complexation is expected to show a weak impact on the ion symmetry and on vibrational frequencies of aqueous and surface species [53]. It can be suggested that this species is weakly bound to the titanol groups and may slightly adhere in the pores of the oxide film probably forming outer-sphere complexes. Furthermore, the absence of a negative band at 789 cm^{-1} in the spectrum of the "2^{nd} conditioning" (Fig. 5-25, blue trace) clearly demonstrate the stability of the inner-sphere Np(V) surface species formed during the sorption process.

In conclusion, the first *in situ* vibrational data of Np(V) sorption at the water-mineral interface were obtained by ATR FT-IR spectroscopy on a micromolar concentration level. NpO_2^+ forms stable complexed species, inner-spherical bound to the TiO_2. Outer-spherical complexation may also take place in the TiO_2 pores, but only to a very small amount. From

the time-resolved measurement no differences in the Np(V) surface speciation upon increased loading can be derived.

5.7.2 Influence of the Np(V) solution properties on the sorption onto TiO_2

Since no vibrational spectroscopic data of sorption complexes of pentavalent actinyl ions, namely Np(V), are reported in literature and, thus, no reference data providing structural information are available, a detailed interpretation of the presented sorption spectra at a molecular level remains difficult. Therefore, additional sorption experiments have been performed. The sorption processes of different sorbing cations and the influence of pH on the sorption processes of Np(V) on TiO_2 have been studied for a verification of the band assignments given above (Fig. 5-26).

The verification of the assignment of the band at 789 cm^{-1} to the neptunyl(V) ion was accomplished by *in situ* ATR FT-IR sorption experiments on TiO_2 using Cs^+, Mg^{2+} and UO_2^{2+} as representative sorbates for monovalent, divalent, and divalent actinyl cations, respectively. Due to the fundamentals of IR spectroscopy, monoatomic ions like Cs^+ and Mg^{2+} do not show any intrinsic vibrational absorption bands, whereas the UO_2^{2+} ion which is structurally homologue to the NpO_2^+ ion, is expected to be identified by its asymmetric stretching vibration υ_3 of the surface species. In fact, the spectrum of the Cs(I) sorption experiment shows no bands below 950 cm^{-1} (Fig. 5-26a) and the U(VI) surface species is observed at 911 cm^{-1} in the respective spectrum (Fig. 5-26b). This frequency is in good agreement with infrared spectroscopic data reported recently [65]. These findings provide clear evidence for the assignment of the band at 789 cm^{-1} to the $\upsilon_3(NpO_2^+)$ mode of the sorbed neptunyl species.

Besides ionic strength and cation concentration, the pH value is the most relevant

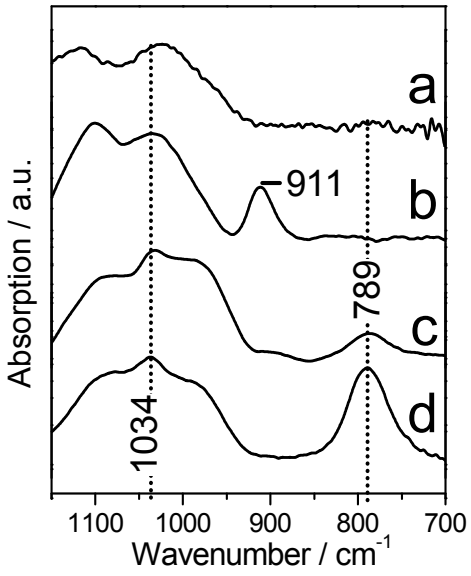

Fig. 5-26: ATR FT-IR sorption spectra of different cations on TiO_2: (a) 50 µM Cs(I) at pH 7.6, (b) 1 µM U(VI) at pH 4, (c) 50 µM Np(V) at pH 4, and (d) at pH 7.6. (S1, D_2O, at 0.1 M NaCl, N_2). Indicated values are in cm^{-1}.

thermodynamic parameter influencing sorption processes of actinyl ions on mineral phases under inert gas atmosphere, potentially allowing the differentiation between different surface complexes. The isoelectric point (IEP) for the investigated TiO_2 sample was determined at pH 5.2 by Lefèvre *et al.* recently [65]. Hence, the overall charge of the TiO_2 surface is negative at a higher pH level which might facilitate outer-sphere complexation of NpO_2^+. We performed *in situ* sorption experiments of 50 µM Np(V) on TiO_2 in the pH range 4 – 7.6 (Fig. 5-26c,d). No significant shifts of the IR band maxima could be observed, indicating the presence of the same type of sorption complex throughout the investigated pH range. However, the relative intensity of the band representing the $\upsilon_3(NpO_2^+)$ at 789 cm^{-1} has considerably increased by a factor of approximately 3 in the spectrum recorded at higher pH (Fig. 5-26d). The enhanced intensity of this band at higher pH reflects an enhanced uptake of Np(V) at higher pH values and is in agreement with previous macroscopic studies [98]. Since sorption of Np(V) already occurs at pH values below the IEP and the absorption frequency of the sorption complex is observed at 789 cm^{-1} irrespective of the pH, the dominance of an outer-sphere complex can be ruled out. The formation of such complexes are expected to show lower frequency shifts compared to the absorption maximum at 818 cm^{-1} of the aqueous complex contributing to the speciation under the prevailing conditions [53, 57].

In the spectral region from 1200 to 900 cm^{-1} all obtained spectra show a similar pattern of broad and overlapping bands. These spectral features are obviously provoked by not yet identified interactions of the cations on the TiO_2 surface. An unequivocal interpretation can not be given at this stage of knowledge. However, with respect to the appearance at very low initial cation concentration (down to 1 µM for U(VI)) and the high reproducibility of these bands, they might represent TiO_2-surface processes correlating with chemical and physical properties of the sorbed cation.

5.8. Comparison of Np(V) sorption onto oxides of titanium, aluminum, silicon and zinc

As mentioned previously, the lack of reference vibrational data of actinyl(V) sorption complexes impedes the unequivocal interpretation of the presented sorption spectra at a molecular level. Hence, a further ATR FT-IR spectroscopic series comprises further oxides as sorbents, i.e. one additional TiO_2, γ-Al_2O_3, ZnO and SiO_2, for comparison of the Np(V)-sorption complexes formed on the mineral phases. The ATR FT-IR spectra of the respective *in situ* experiments after 60 minutes of sorption are shown in Fig. 5-27.

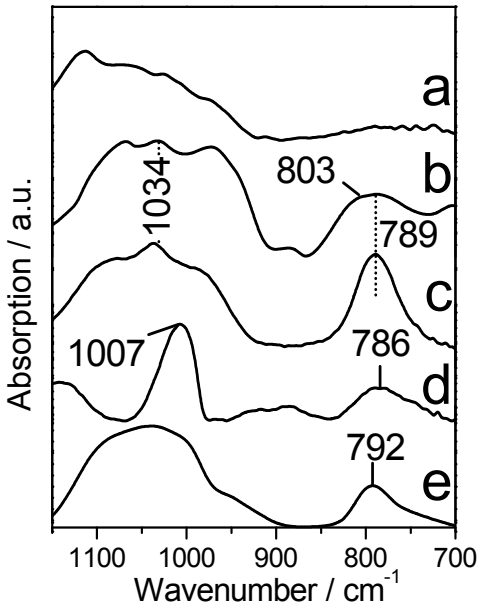

Fig. 5-27: ATR FT-IR spectra of 50 µM Np(V) sorbed on (a) γ-Al_2O_3, (b) TiO_2 (S6), (c) TiO_2 (S1), (d) SiO_2 and (e) ZnO at pH 7.6 (D_2O, at 0.1 M NaCl, N_2). Indicated values are in cm^{-1}.

Since these oxides provide different structures, functionalities and specific surface areas, their impact on Np(V) sorption can be investigated. The oxides of Al, Si and Zn show no sharp absorption bands in the spectral region 850-700 cm^{-1}. The ATR FT-IR spectra obtained after Np(V) uptake on TiO_2, SiO_2 and ZnO at initial 50 µM Np(V) at pH 7.6 are compared in Fig. 5-27. The υ_3 absorption band of the sorbed Np(V) species is observed at nearly the same frequency in all spectra of the different sorbents, i.e. at 789, 786 and 792 cm^{-1} for TiO_2, SiO_2 and ZnO, respectively (Fig. 5-27b-e). The respective band is broader in case of the additional TiO_2 sample (S6), slightly shouldering to higher frequency. Spectral analysis using the second-derivative distinctly clears an additional band at 803 cm^{-1}. In the 2nd conditioning step of the monitoring experiment, the detected negative absorption band centering at the same frequency was assigned to an electrostatic sorption complex. However, this spectral feature was very low in intensity in the respective TiO_2 sample (S1). In contrast its contribution to the surface process seems to be increased in case of the anatase sample S6. Nevertheless, from the investigation of U(VI) surface complexation also slightly differing reactions were proposed for both samples (cf. section 5.1 and [65]). Concerning γ-Al_2O_3, the υ_3 absorption band of the sorbed Np(V) species was not detected in the IR spectral data (Fig. 5-27a).

In conclusion, from the described IR data, the formation of similar Np(V) molecule complexes on TiO_2, SiO_2 and ZnO can be suggested. Furthermore, the coordination type, i.e. monodentate and bidentate, can be elucidated. The impact of a respective mineral phase on the frequency of the actinyl υ_3 mode in a monodentate sorption complex is expected to be lower compared to a bidentate complex because of weaker interactions in the equatorial plane of the actinyl ion. In a bidentate complex the electrostatic characteristics of the mineral phase should generate a kind of fingerprint on the stretching frequency of the heavy metal ion. In recent years, U(VI) sorption onto ferrihydrite, hematite and titanium dioxide was studied by

application of ATR FT-IR spectroscopy, and antisymmetric uranyl(VI) stretching was reported to occur at slightly shifted frequencies, at ~903, 906 and 915 cm^{-1}, respectively [65, 71, 77, 195]. From own experiments, uranyl(VI) stretching was detected at 890 and 917 cm^{-1} for TiO_2 and at 917 and 946 cm^{-1} for γ-Al_2O_3 each depending on the U(VI) surface coverage and respective species (cf. chapter 5.4). Compared to uranyl(VI), the neptunyl(V) stretching vibrations exhibit minor changes upon sorption which is obviously due to the lower force constant of Np(V). Hence, the Np(V) spectral results can be interpreted in analogy to conclusions from structural experiments of uranyl(VI) at mineral interfaces: Since the different sorbents used in this work provide some kind of spectral "fingerprinting", resulting in different absorption maxima from 786 to 792 cm^{-1}, the Np(V) interaction is interpreted as a bidentate complex.

The characteristic vibrational frequency of a functional group is generally influenced by its molecular environment. Therefore, it is conceivable that the different crystal lattices of the different mineral phases are reflected by the different frequencies of the υ_3 mode observed in the infrared spectra. In aqueous actinyl complexes, the lower frequency of the υ_3 mode compared to the fully hydrolyzed ions is due to the presence of electronegative ligands in the equatorial plane of the linear AnO_2^{n+} cation, weakening the An=O bond and, hence, lowering the antisymmetric stretching frequency. In sorption complexes on solid surfaces, the set of parameter controlling the frequency of the υ_3 mode is expected to be much more comprehensive. Therefore, a correlation of the frequency of the υ_3 mode and the crystal structure will be highly speculative at this state of knowledge, in particular with respect to the poor data of Np(V) sorption complex structures and has to be investigated systematically in future times. Only further studies, applying a considerably higher variety of sorbents and of experimental conditions, will show if *in situ* ATR FT-IR spectroscopy provides adequate spectral information for the derivation of detailed molecular structures of actinyl surface complexes.

In conclusion, structurally similar bidentate inner-spherical surface complexes are formed, when Np(V) is sorbed onto ZnO, SiO_2 and TiO_2 surfaces. Np(V) outer-sphere surface complexes on TiO_2 are found to be negligible, since no pH dependence was derived from the ATR FT-IR spectra obtained in the pH range 4 – 7.6. However, their contribution can not be ruled out and completely, and was tentatively assigned in the spectral data of an additional TiO_2 sample.

5.9 Conclusions and Outlook

In this study, the sorption of hexavalent and pentavalent actinyl ions, namely U(VI) and Np(V) on model metal oxides as well as on naturally occurring more complex minerals was investigated on a molecular level using *in situ* ATR FT-IR spectroscopy.

The results have substantiated findings from macroscopic investigations and in parts from structure elucidating spectroscopic studies. Here, the application of the surface sensitive ATR technique provided additional insight into the molecular reactions occurring at different time intervals at the solid-water interface. Using a time resolution in the sub-minute range, the formation of different U(VI) complexes on TiO_2 and Al_2O_3 as a function of surface coverage was elucidated, whereas the formation of only one stable Np(V) complex was found.

The obtained findings present valuable reference data for further *in situ* spectroscopic analysis of sorption and complexation reactions at interfaces. For the study of other pentavalent and hexavalent actinide or mixtures of both, as it is indispensable for multi oxidation state ions, e.g. Pu, the spectra may provide significant structural information on the different complexation behavior of different aqueous species. Furthermore, the data act as a model for the investigation of more complex mineral phases, showing different functionalities.

Future work, using a combination of different techniques may answer the question how U(VI) and Np(V) exactly sorb on model oxide surfaces. Using EXAFS spectroscopy, it might be clarified if U(VI) surface polymerization or unordered precipitation occurs on the surface of γ-Al_2O_3. Furthermore, TRLFS can provide further information on the coordination environment of sorbed U(VI) on aluminates and may capacitate to identify photoreactive U(VI) surface species on semiconducting materials, e.g. TiO_2, ZnO. A combination of ATR FT-IR with microscopic techniques may show possible surface transformations and changes of mineral oxide film characteristics.

6. Materials and methods

6.1 Materials

- All chemicals were of analytical grade.
- The triply-deionized water with a resistivity of 18.2 MΩ/cm was produced by the Milli-RO/Milli-Q-System (Millipore, Schwalbach, Germany). For the experiments performed under inert-gas (N_2) atmosphere, the Milli-Q water was boiled for approximately 90 minutes to remove carbonate. For IR measurements performed with heavy water, D_2O with a purity of ≥ 99.99% from Sigma Aldrich (St. Louis, USA) was used.
- For the adjustment of ionic strength solutions of general 0.1 M were prepared by dissolution of NaCl (Merck, Darmstadt, Germany) in the appropriate volume of MilliQ-water or D_2O.
- The pH adjustments were done by adding small aliquots of 1 M and 0.1 M NaOH / NaOD and HCl / DCl (Merck, Darmstadt / Chemotrade, Leipzig, Germany), respectively.
- To prevent precipitation of uranate salts the non-complexing agent tetramethylammonium hydroxide was used in some experiments carried out at highly alkaline conditions. The hygrophilous TMA-OH (Arcos Organics, New Jersey, USA) was dissolved only at inert gas conditions to prevent rapid dissolution of atmospheric CO_2.
- Reference solutions for ATR FT-IR measurements were prepared by dissolving $CaCl_2.2H_2O$, CsCl, $MgCl_2.6H_2O$ (all from Merck, Darmstadt, Germany) and Eu_2O_3 (Sigma Aldrich, St. Louis, USA) in Milli- Q water or D_2O.
- For the preparation of solutions with extra carbonate, $NaHCO_3$, Na_2CO_3 and $KHCO_3$ (all from Merck, Darmstadt, Germany) and $NaH^{13}CO_3$ (Isotec, Miamisburg, USA) were dissolved in Milli-Q water or D_2O.
- The sorbent materials, listed in Tab. 5-2, Tab. 5-4 and Tab. 5-6 with exception of the TiO_2 samples S2, S5, S6, S7 were used without further purification. The mentioned TiO_2 samples were washed according to the procedure described in section 7.2.13.

6.2 Methods

6.2.1 Thermodynamic data and speciation modeling

Speciation modeling was performed using the updated thermodynamic database of the Nuclear Energy Agency (NEA) [10-12] with minor adaptations according to the Nagra/PSI database [151]. The speciation patterns were computed using the thermodynamic modeling code package EQ3/6 by Wolery [150]. The Davies equation was used to compute activity coefficients, as none of the samples reached ionic strengths above 0.1 M.

6.2.2 Experiments at high actinide concentrations

^{237}Np is a radioactive isotope and an α-emitter. High concentrated stock solutions of Np(V) and Np(VI) were prepared and handled in a reduced pressure box within a laboratory, appropriate for research involving transuranic elements to avoid health risks caused by radiation exposure.

6.2.3 Preparation of actinide solutions

Neptunium (^{237}Np) dioxide was obtained from CEA-Marcoule, France. The solid was dissolved in concentrated nitric acid (65%) under stirring for several days. Then, the pH of the resulting dark brown solution was increased up to pH ~9, and the resulting brownish precipitate was dissolved again in 1 M HCl. This procedure was repeated several times to remove nitrate ions from the Np stock solution. The brownish solution was identified as 0.11 M of 95% Np(VI) and 5% Np(V) by NIR spectroscopy. The radiochemical purity of a 1000 fold dilution was checked by α/γ spectrometry using a semiconductor PIPS (PH450-21-100AM, Canberra) and a High Purity Germanium detector (EGM 2000-20R, Eurysis). Pure Np(V) and Np(VI) stock solution were achieved electrochemically, using the procedure described by Ikeda-Ohno et al.[216]. A cyclic voltammogram (CV) of an aliquot of the mixed Np(V/VI) solution was recorded at room temperature using an AutoLab PGSTAT302 potentiostat/galvanostat (EcoChemie BV) (Fig. 6-1a). A three electrode system consisting of a Pt working electrode, a Pt counter electrode and an Ag/AgCl (in 3 M NaCl with Vycor glass liquid junction) was applied. The sample was deoxygenated by bubbling nitrogen gas prior to the measurement. On the basis of the obtained CV bulk electrolysis was performed, to adjust the oxidation state. The initial potential of the Np(V/VI) solution before electrolysis was between 980 and 990 mV. The mixture was oxidized to a pure Np(VI) solution for 7 hours at 1350 mV and the brownish color remained the same. But, when the mixture was reduced to a pure Np(V) solution at 200 mV for 7.5 hours, the solution turned to bright green (a). The oxidation states were confirmed by NIR spectroscopy (Fig. 6-1b).

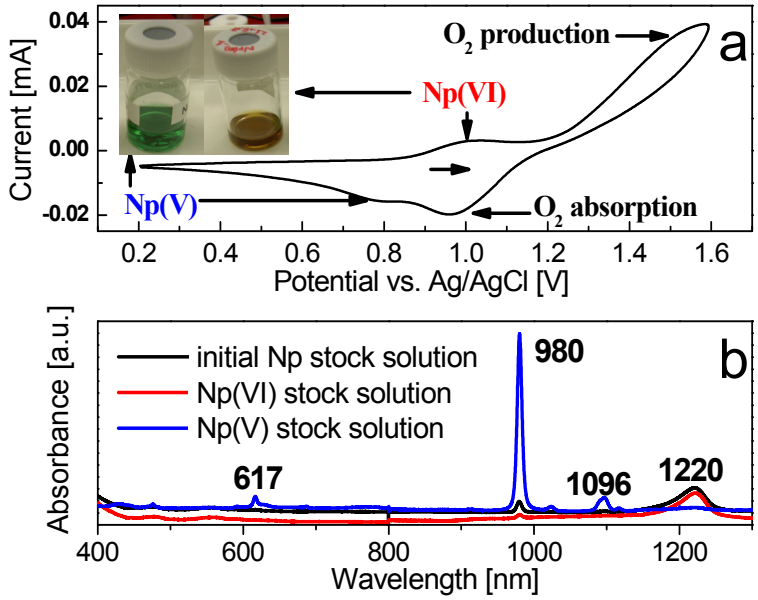

Fig. 6-1: (a) Cyclic voltammogram of Np(VI) in 1 M HCl (Scanrate 200 mV/s) and photographs of stock solutions of Np(V) and Np(VI), (b), UV-Vis-NIR spectra of the stock solutions of Np(V/VI) (1/100 dilutions in 1 M HCl).

To obtain a deuterated Np(V) stock solution, the pH of an aliquot of the initial Np(V) stock solution was increased using concentrated NaOD, the formed Np precipitate was then centrifuged and re-dissolved in 1 M DCl (Chemotrade). This procedure was repeated for five times to eliminate remaining light water. To exclude fast exchanges of D_2O and H_2O the solutions were prepared and analyzed under nitrogen atmosphere in a glove box.

For the U(VI) stock solution $UO_2(NO_3)_2.6H_2O$ (Chemapol, Czech Republic) was converted in a muffle furnace at 320 °C, the resulting UO_3 was dissolved in 1 M HCl [217].

Tab. 6-1: Stock solutions of An(VI/V).

Stock solution	concentration	Solvent
U(VI)	0.05 M	1 M HCl
U(VI)	0.01 M	1 M DCl
Np(VI)	0.11 M	1 M HCl
Np(V)	0.11 M	1 M HCl
Np(V)	0.02 M	1 M DCl

6.2.4 Preparation of diluted solutions

The diluted solutions of Np(VI) and U(VI) were freshly prepared using stock solutions of 0.11 M NpO_2Cl_2 and 0.05 M UO_2Cl_2 and Milli-Q water with a resistivity of 18.2 MΩ/cm. Ionic strength was in general 0.1 M NaCl, pH was adjusted by adding aliquots of 1 M and 0.1 M NaOH and HCl.

For the preparation of the micromolar concentrated Np(V) sample solutions the obtained deuterated 0.02 M NpO_2Cl_2 stock solution and D_2O (≥99.99%, Sigma Aldrich) were used. In this work pH values determined using an electrode standardized in light water are given. The

concerning values of pD can be calculated by the equation pD = pH + 0.4 [218]. The adjustments were done by adding small aliquots of 1 M and 0.1 M NaOD and DCl, respectively.

6.2.5 Check for colloids in sample solutions

Several experiments have been performed to check the prepared actinide(V/VI) solutions for precipitation and formation of colloids. Photon correlation spectroscopy (PCS, Brookhaven Instr. 90) in combination with ATR FT-IR spectroscopy were applied to several solutions containing and excluding precipitation. Furthermore, freshly prepared actinyl(VI) solutions were ultracentrifuged (Beckmann Coulter, Optima XL-100K) using a SW32Ti rotor for 1 hour at 40,000 rpm (2,850,000 x g at the maximum RCF). Then, PCS, ICP-MS and ATR FT-IR measurements were applied to the supernatant and the remaining solution at the bottom of the centrifugation tube.

6.2.6 ATR FT-IR spectroscopic measurements

Detailed information on the used experimental setup is given in section 3.3.

6.2.7 NIR absorption spectroscopy

NIR spectra of the micromolar Np(V/VI) solutions were recorded from 200 to 1400 nm in 0.1 nm interval steps using a Varian Cary 5G UV-vis-NIR spectrometer at 25 °C. Source change was set at 350 nm and detector change at 900 nm. Quartz cells with a path length of 1 cm and a sample holder for radioactive samples were used.

6.2.8 Laser-induced fluorescence spectroscopy

The LIFS system consist of an Inlite laser (Continuum) generating a wavelength of 266 nm which was used for the excitation of the samples. The spectra were recorded with an ICCD-camera (Princeton Instruments) in the wavelength range from 421 to 593 nm with a resolution of 0.17 nm. The delay time after the excitation laser pulse was 2 µs and the pulse energy 0.5 mJ. For each spectrum 25 laser shots were averaged for three times.

6.2.9 Analysis of uranium and neptunium concentration

Liquid scintillation counting (LSC) and Inductively coupled plasma – mass spectrometry (ICP-MS) were applied to verify the ^{237}Np and ^{238+}U concentrations in the samples, respectively. The U(VI) concentration in solution was determined using the Perkin Elmer model ELAN 6000. All U(VI) samples were previously acidified with hundredth volume units of concentrated high purity HNO_3. For Np analysis LSC measurements were carried out

using the Perkin Elmer instrument Wallac Win Spectral 1414. A quantity of general 50 µL to1 mL of the sample was mixed with 15 mL of the scintillation cocktail Ultima Gold (Perkin Elmer).

6.2.10 Measurement of pH values

The pH value of the samples were determined and adjusted using laboratory pH-Meter inoLab pH 720 (WTW, Weilheim, Germany) with BlueLine 16pH microelectrode (Schott Instruments, Mainz, Germany). The calibration was performed by means of standard buffers (WTW, Weilheim, Germany). Measuring accuracy was ±0.05 pH units.

6.2.11 TiO_2 digestion analysis

Digestion coupled with ICP-MS and graphite furnace atomic absorption spectroscopy, (AAS-GF, Analysentechnik Jena, Germany) of the sorbent samples were done to control the amount of the following cations: Na, Mg, Al, Si, K, Ca, Cr, Mn, Fe, Co, Ni, Cu, Zn, Ga, Rb, Sr, Zr, Nb, Mo, Ag, Ba, Ta, W, Tl, Pb, La, Sn, before and after the washing procedure. The microwave digestion was done using 50 mg solid sample and 5 mL of a solvent mixture, containing HNO_3, HF and HCl (3:1:1).

6.2.12 Determination of the Specific Surface Area

The surface areas of the used sorbent materials were determined from the amount of adsorbed nitrogen at monolayer coverage from a BET (Brunauer-Emmet-Teller) plot of sorption isotherm data using a Beckman Coulter analyzator SA 3100. Prior to the measurement the samples of biotite and muscovite were heated at 150 °C for 120 minutes. The TiO_2 samples were heated at 300 °C for 480 minutes.

6.2.13 Washing procedure of the TiO_2 samples

In a collaborative study two different washing procedures, a slight one at the IRC and a more aggressive one at the ANSTO were performed to some of the TiO_2 samples For the slightly washing several steps were performed consecutively, using S2, S5, S6 and S7, similar to the procedure described by Lefèvre et al. [181]. Each step was conducted with a solid liquid ratio of 2.5 g of TiO_2 in 50 mL reagent in an overhead shaker at 4 rpm for 24 h with subsequent centrifugation for the separation of solid and liquid. Firstly, for the removal of anions 0.1 M NaOH was used, then 0.1 M HCl for two times was applied to eliminate cations and carbonate. In a third step the samples were shaken for five or six times with Milli-Q water until the conductivity of the supernatant solution after centrifugation did not change significantly. The solids were dried at 50 C for three days and ball-milled for approximately

10 minutes. At ANSTO the more aggressive washing was done for the TiO_2 samples S2 and S7 according to the procedure described by Kosmulski and Matijevic, using 5 M NaOH, 5 M HNO_3, and Milli-Q water at a solid to liquid ratio of approximately 1:5 for 3 hours under occasional stirring [184].

6.2.14 Experiments at inert gas atmosphere

The experiments at inert gas atmosphere to exclude on one hand the dissolution of atmospheric carbon dioxide and on the other fast exchanges of D_2O and H_2O hand in case of heavy water solutions, were performed in a glove box (MBraun, Inertgas-Systeme GmbH, Garching, Germany) with nitrogen atmosphere (O_2 < 0.1 ppm). For the ATR FT-IR analysis of the prepared solutions a small N_2 box was utilized (Dinkelberg analytics).

6.2.15 AFM measurements

The AFM measurements were performed using an Asylum Research instrument (Santa Barbara, USA). The dimensions of the ATR crystal did not allow a direct analysis of the mineral film prepared on the diamond surface. Hence, a silicon wafer was used and the mineral film was prepared in homology to the ATR FT-IR experiments. The micrographs were taken in AC mode which is a resonant intermittent contact. An AC240 Cantilever with a middle resonant frequency of 75 kHz was used.

7. References

[1] T. Brasser, J. Droste, I. Müller-Lyda, J. Neles, M. Sailer, G. Schmidt, M. Steinhoff, "Endlagerung wärmeentwickelnder radioaktiver Abfälle in Deutschland. GRS-247", Gesellschaft für Anlagen und Reaktorsicherheit (GRS) mbH and Öko-Institut e.V., Braunschweig / Darmstadt, 2008.

[2] G. Meinrath, P. Volke, C. Helling, E.G. Dudel, B.J. Merkel, "Determination and interpretation of environmental water samples contaminated by uranium mining activities", *Fresenius Journal of Analytical Chemistry* 364 (1999) 191-202.

[3] A. Meinrath, P. Schneider, G. Meinrath, "Uranium ores and depleted uranium in the environment, with a reference to uranium in the biosphere from the Erzgebirge/Sachsen, Germany", *Journal of Environmental Radioactivity* 64 (2003) 175-193.

[4] M.L. Wilson, J.H. Gauthier, R.W. Barnard, G.E. Barr, H.A. Dockery, E. Dunn, R.R. Eaton, D.C. Guerin, N. Lu, M.J. Martinez, R. Nilson, C.A. Rautman, T.H. Robey, B. Ross, E.E. Ryder, A.R. Schenker, S.A. Shannon, L.H. Skinner, W.G. Halsey, J.D. Gansemer, L.C. Lewis, A.D. Lamont, I.R. Triay, A. Meijer, D.E. Morris, "Total-system performance assessment for Yucca Mountain-SNL second iteration. Report SAND93-2675", Sandia National Laboratories, Albuquerque, New Mexico, 1994.

[5] N. Chapman, D. Hodgkinson, P. Maul, "The scientific and regulatory basis for the geological disposal of radioactive waste", in: D. Savage, Wiley, Chichester, 1995.

[6] J.P. Kaszuba, W.H. Runde, "The aqueous geochemistry of neptunium: Dynamic control of soluble concentrations with applications to nuclear waste disposal", *Environmental Science & Technology* 33 (1999) 4427-4433.

[7] P.A. O'Day, "Molecular environmental geochemistry", *Reviews of Geophysics* 37 (1999) 249-274.

[8] OECD/NEA, "Physics and Safety of Transmutation Systems - A Status Report (NEA No. 6090)", Paris, 2006.

[9] R. Guillaumont, "Radiochemical approaches to the migration of elements from a radwaste repository", *Radiochimica Acta* 66-7 (1994) 231-242.

[10] I. Grenthe, J. Fuger, R.J. Lemire, A.B. Muller, C. Nguyen-Trung, H. Wanner, Chemical Thermodynamics of Uranium., Elsevier Science Publishers B. V., Amsterdam, 1992.

[11] R. Guillaumont, T. Fanghänel, J. Fuger, I. Grenthe, V. Neck, D.A. Palmer, M.H. Rand, Update on the chemical thermodynamics of U, Np, Pu, Am and Tc, Elsevier, Amsterdam, 2003.

[12] R.J. Lemire, J. Fuger, K. Spahiu, H. Nitsche, J.C. Sullivan, W.J. Ullman, P. Potter, P. Vitorge, M.H. Rand, H. Wanner, J. Rydberg, Chemical thermodynamics of neptunium and plutonium, Elsevier, Amsterdam, 2001.
[13] V. Brendler, A. Vahle, T. Arnold, G. Bernhard, T. Fanghänel, "RES$_3$T-Rossendorf expert system for surface and sorption thermodynamics", *Journal of Contaminant Hydrology* 61 (2003) 281-291.
[14] R.J. Silva, H. Nitsche, "Actinide environmental chemistry", *Radiochimica Acta* 70-1 (1995) 377-396.
[15] J.J. Katz, G.T. Seaborg, L.R. Morss, The chemistry of the actinide elements Chapman and Hall, New York, 1986.
[16] I. Grenthe, J. Drozdzynski, T. Fujino, E.C. Buck, T.E. Albrecht-Schmitt, S.F. Wolf, "Uranium", in: L.R. Morss, N.M. Edelstein, J. Fuger, "The chemistry of the actinide and transactinide elements", Springer, 2006.
[17] Z. Yoshida, S.G. Johnson, T. Kimura, J.R. Krsul, "Neptunium", in: L.R. Morss, N.M. Edelstein, J. Fuger, "The chemistry of the actinide and transactinide elements", Springer, 2006.
[18] G. Choppin, J. Rydberg, J.O. Liljenzin, Radiochemistry and Nuclear Chemistry, Butterworth-Heinemann, London, 1995.
[19] L.H. Jones, R.A. Penneman, "Infrared Spectra and Structure of Uranyl and Transuranium(V) and(VI) Ions in Aqueous Perchloric Acid Solution", *Journal of Chemical Physics* 21 (1953) 542-544.
[20] G.R. Choppin, "Trace analysis-methods for actinides in aqueous systems", *Analytical Sciences* 11 (1995) 143-147.
[21] G.R. Choppin, "Actinide speciation in the environment", *Journal of Radioanalytical and Nuclear Chemistry* 273 (2007) 695-703.
[22] W. Runde, "The Chemical Interactions of Actinides in the Environment", *Los Alamos Science* 26 (2000).
[23] N. Takeno, "Atlas of Eh-pH diagrams. Intercomparison of thermodynamic databases. Geological Survey of Japan Open File Report No.419", National Institute of Advanced Industrial Science and Technology. Research Center for Deep Geological Environments, Japan, 2005.
[24] D.L. Clark, D.E. Hobart, M.P. Neu, "Actinide Carbonate Complexes and Their Importance in Actinide Environmental Chemistry", *Chemical Reviews* 95 (1995) 25-48.
[25] G.R. Choppin, "Solution chemistry of the actinides", *Radiochimica Acta* 32 (1983) 43-53.
[26] J. Fuger, "Thermodynamic properties of actinide aqueous species relevant to geochemical problems", *Radiochimica Acta* 58-9 (1992) 81-91.
[27] K. Müller, V. Brendler, H. Foerstendorf, "Aqueous Uranium(VI) Hydrolysis Species Characterized by Attenuated Total Reflection Fourier-Transform Infrared Spectroscopy", *Inorganic Chemistry* 47 (2008) 10127-10134.
[28] F. Quilès, A. Burneau, "Infrared and Raman spectra of uranyl(VI) oxo-hydroxo complexes in acid aqueous solutions: a chemometric study", *Vibrational Spectroscopy* 23 (2000) 231-241.
[29] D.L. Clark, S.D. Conradson, S.A. Ekberg, N.J. Hess, D.R. Janecky, M.P. Neu, P.D. Palmer, C.D. Tait, "A multi-method approach to actinide speciation applied to pentavalent neptunium carbonate complexation", *New Journal of Chemistry* 20 (1996) 211-220.
[30] D.L. Clark, S.D. Conradson, S.A. Ekberg, N.J. Hess, M.P. Neu, P.D. Palmer, W. Runde, C.D. Tait, "EXAFS studies of pentavalent neptunium carbonate complexes.

Structural elucidation of the principal constituents of neptunium in groundwater environments", *Journal of the American Chemical Society* 118 (1996) 2089-2090.

[31] V. Neck, T. Fanghänel, J.I. Kim, "Mixed hydroxo-carbonate complexes of neptunium(V)", *Radiochimica Acta* 77 (1997) 167-175.

[32] L. Ciavatta, "The specific interaction theory in equilibrium-analysis - some empirical rules for estimating interaction coefficients of metal-ion complexes", *Annali Di Chimica* 80 (1990) 255-263.

[33] C. Moulin, I. Laszak, V. Moulin, C. Tondre, "Time-resolved laser-induced fluorescence as a unique tool for low-level uranium speciation", *Applied Spectroscopy* 52 (1998) 528-535.

[34] G. Meinrath, "Speciation of uranium (VI) by advanced spectroscopic and data treatment techniques", Technische Universität, Bergakademie, Freiberg, 2000.

[35] A. Kirishima, T. Kimura, O. Tochiyama, Z. Yoshida, "Speciation study on uranium(VI) hydrolysis at high temperatures and pressures", *Journal of Alloys and Compounds* 374 (2004) 277-282.

[36] V. Eliet, G. Bidoglio, N. Omenetto, L. Parma, I. Grenthe, "Characterisation of hydroxide complexes of uranium(VI) by Time-resolved Fluorescence Spectroscopy", *Journal of the Chemical Society - Faraday Transactions* 91 (1995) 2275-2285.

[37] A. Cassol, G. Tomat, Portanov.R, L. Magon, "Soluble intermediates in hydrolysis of neptunium(VI) and comparison with other actinides(VI)", *Inorganic Chemistry* 11 (1972) 515-519.

[38] L. Maya, "Carbonate complexation of dioxoneptunium(VI) at 25°C - Its effect on the Np(V)/Np(VI) potential", *Inorganic Chemistry* 23 (1984) 3926-3930.

[39] OECD/NEA, "NEA Sorption Project; Phase II: Interpretation and prediction of radionuclide sorption onto substrates relevant for radioactive waste disposal using thermodynamic sorption models (NEA No. 5992)", Paris, 2005.

[40] G.R. Choppin, B.E. Stout, "Actinide behavior in natural waters", *Science of the Total Environment* 83 (1989) 203-216.

[41] M.A. Blesa, A.D. Weisz, P.J. Morando, J.A. Salfity, G.E. Magaz, A.E. Regazzoni, "The interaction of metal oxide surfaces with complexing agents dissolved in water", *Coordination Chemistry Reviews* 196 (2000) 31-63.

[42] G.A. Parks, "Surface energy and adsorption at mineral-water interfaces: An introduction", in: M.F. Hochella Jr., A.F. White, "Mineral-Water Interface Geochemistry", Mineralogical Society of America, Washington D.C., 1990.

[43] G.E. Brown, "Spectroscopic Studies of Chemisorption Reaction Mechanisms at Oxide-Water Interfaces", in: M.F. Hochella Jr., A.F. White, "Mineral-Water Interface Geochemistry", Mineralogical Society of America, Washington D.C., 1990.

[44] E.R. Sylwester, E.A. Hudson, P.G. Allen, "The structure of uranium(VI) sorption complexes on silica, alumina, and montmorillonite", *Geochimica Et Cosmochimica Acta* 64 (2000) 2431-2438.

[45] T. Wu, S. Amayri, J. Drebert, L.R. Van Loon, T. Reich, "Neptunium(V) sorption and diffusion in opalinus clay", *Environmental Science & Technology* 43 (2009) 6567-6571.

[46] M. Fedoroff, G. Lefevre, M. Duc, S. Milonjic, C. Neskovic, "Sorption mechanisms and sorption models", Trans Tech Publications Ltd, Zurich-Uetikon, 2004.

[47] J.A. Davis, D.B. Kent, "Surface complexation modeling in aqueous geochemistry", in: M.F. Hochella Jr., A.F. White, "Mineral-Water Interface Geochemistry", Mineralogical Society of America, Washington D.C., 1990.

[48] D.R. Turner, F.P. Bertetti, R.T. Pabalan, "Applying surface complexation modeling to radionuclide sorption", in: J. Lützenkirchen, "Surface Complexation Modeling", Elsevier, Amsterdam, 2006.

[49] P. Wang, A. Anderko, D.R. Turner, "Thermodynamic modeling of the adsorption of radionuclides on selected minerals. I: Cations", *Ind. Eng. Chem. Res.* 40 (2001) 4428-4443.

[50] G. Sposito, "Distinguishing Adsorption from Surface Precipitation", *ACS Symposium Series* 323 (1986) 217-228.

[51] G. Geipel, "Some aspects of actinide speciation by laser-induced spectroscopy", *Coordination Chemistry Reviews* 250 (2006) 844-854.

[52] C. Den Auwer, E. Simoni, S. Conradson, C. Madic, "Investigating actinyl oxo cations by X-ray absorption spectroscopy", *European Journal of Inorganic Chemistry* (2003) 3843-3859.

[53] G. Lefevre, "In situ Fourier-transform infrared spectroscopy studies of inorganic ions adsorption on metal oxides and hydroxides", *Advances in Colloid and Interface Science* 107 (2004) 109-123.

[54] J.R. Bargar, J.D. Kubicki, R. Reitmeyer, J.A. Davis, "ATR-FTIR spectroscopic characterization of coexisting carbonate surface complexes on hematite", *Geochimica Et Cosmochimica Acta* 69 (2005) 1527-1542.

[55] R. Drot, J. Roques, E. Simoni, "Molecular approach of the uranyl/mineral interfacial phenomena", *Comptes Rendus Chimie* 10 (2007) 1078-1091.

[56] E. Veilly, J. Roques, M.C. Jodin-Caumon, B. Humbert, R. Drot, E. Simoni, "Uranyl interaction with the hydrated (001) basal face of gibbsite: A combined theoretical and spectroscopic study", *Journal of Chemical Physics* 129 (2008) 10.

[57] A. Kremleva, S. Kruger, N. Rosch, "Density functional model studies of uranyl adsorption on (001) surfaces of kaolinite", *Langmuir* 24 (2008) 9515-9524.

[58] D.M. Sherman, C.L. Peacock, C.G. Hubbard, "Surface complexation of U(VI) on goethite (α-FeOOH)", *Geochimica Et Cosmochimica Acta* 72 (2008) 298-310.

[59] L. Gagliardi, B.O. Roos, "Coordination of the neptunyl ion with carbonate ions and water: A theoretical study", *Inorganic Chemistry* 41 (2002) 1315-1319.

[60] G. Schreckenbach, P.J. Hay, R.L. Martin, "Theoretical study of stable trans and cis isomers in $[UO_2(OH)_4]^{2-}$ using relativistic density functional theory", *Inorganic Chemistry* 37 (1998) 4442-4451.

[61] S. Tsushima, A. Rossberg, A. Ikeda, K. Muller, A.C. Scheinost, "Stoichiometry and structure of uranyl(VI) hydroxo dimer and trimer complexes in aqueous solution", *Inorganic Chemistry* 46 (2007) 10819-10826.

[62] S. Tsushima, Y. Uchida, T. Reich, "A theoretical study on the structures of $UO_2(CO_3)_3^{4-}$, $Ca_2UO_2(CO_3)_3^{0}$, and $Ba_2UO_2(CO_3)_3^{0}$", *Chemical Physics Letters* 357 (2002) 73-77.

[63] S. Tsushima, U. Wahlgren, I. Grenthe, "Quantum chemical calculations of reduction potentials of AnO_2^{2+}/AnO_2^{+} (An = U, Np, Pu, Am) and Fe^{3+}/Fe^{2+} couples", *Journal of Physical Chemistry A* 110 (2006) 9175-9182.

[64] L. Maya, "Sorbed uranium(VI) species on hydrous titania, zirconia, and silica gel", *Radiochimica Acta* 31 (1982) 147-151.

[65] G. Lefèvre, J. Kneppers, M. Fédoroff, "Sorption of uranyl ions on titanium oxide studied by ATR-IR spectroscopy", *Journal of Colloid and Interface Science* 327 (2008) 15-20.

[66] C. Den Auwer, R. Drot, E. Simoni, S.D. Conradson, M. Gailhanou, J.M. de Leon, "Grazing incidence XAFS spectroscopy of uranyl sorbed onto TiO_2 rutile surfaces", *New Journal of Chemistry* 27 (2003) 648-655.

[67] J. Vandenborre, R. Drot, E. Simoni, "Interaction mechanisms between uranium(VI) and rutile titanium dioxide: From single crystal to powder", *Inorganic Chemistry* 46 (2007) 1291-1296.

[68] Z.J. Guo, Z.Y. Yan, Z.Y. Tao, "Sorption of uranyl ions on TiO_2: Effects of contact time, ionic strength, concentration and humic substance", *Journal of Radioanalytical and Nuclear Chemistry* 261 (2004) 157-162.

[69] N.K. Pandey, "Effect of pH on adsorption of U(VI) ions on TiO_2, γ-Al_2O_3 and SiO_2 surface from aqueous solution", *Oxidation Communications* 29 (2006) 698-707.

[70] H. Perron, C. Domain, J. Roques, R. Drot, E. Simoni, H. Catalette, "Periodic density functional theory investigation of the uranyl ion sorption on the TiO_2 rutile (110) face", *Inorganic Chemistry* 45 (2006) 6568-6570.

[71] G. Lefèvre, S. Noinville, M. Fedoroff, "Study of uranyl sorption onto hematite by in situ attenuated total reflection-infrared spectroscopy", *Journal of Colloid and Interface Science* 296 (2006) 608-613.

[72] J.R. Bargar, R. Reitmeyer, J.A. Davis, "Spectroscopic confirmation of uranium(VI)-carbonato adsorption complexes on hematite", *Environmental Science & Technology* 33 (1999) 2481-2484.

[73] T.D. Waite, J.A. Davis, T.E. Payne, G.A. Waychunas, N. Xu, "Uranium(VI) adsorption to ferrihydrite - Application of a surface complexation model", *Geochimica Et Cosmochimica Acta* 58 (1994) 5465-5478.

[74] M. Walter, T. Arnold, T. Reich, G. Bernhard, "Sorption of uranium(VI) onto ferric oxides in sulfate-rich acid waters", *Environmental Science & Technology* 37 (2003) 2898-2904.

[75] J.G. Catalano, T.P. Trainor, P.J. Eng, G.A. Waychunas, G.E. Brown, "CTR diffraction and grazing-incidence EXAFS study of U(VI) adsorption onto alpha-Al_2O_3 and alpha-Fe_2O_3 ($11\bar{0}2$) surfaces", *Geochimica Et Cosmochimica Acta* 69 (2005) 3555-3572.

[76] C.H. Ho, N.H. Miller, "Adsorption of uranyl species from bicarbonate solution onto hematite particles", *Journal of Colloid and Interface Science* 110 (1986) 165-171.

[77] M. Wazne, G.P. Korfiatis, X.G. Meng, "Carbonate effects on hexavalent uranium adsorption by iron oxyhydroxide", *Environmental Science & Technology* 37 (2003) 3619-3624.

[78] A.J. Dent, J.D.F. Ramsay, S.W. Swanton, "An EXAFS study of uranyl ion in solution and sorbed onto silica and montmorillonite clay colloids", *Journal of Colloid and Interface Science* 150 (1992) 45-60.

[79] T. Reich, H. Moll, T. Arnold, M.A. Denecke, C. Hennig, G. Geipel, G. Bernhard, H. Nitsche, P.G. Allen, J.J. Bucher, N.M. Edelstein, D.K. Shuh, "An EXAFS study of uranium(VI) sorption onto silica gel and ferrihydrite", *Journal of Electron Spectroscopy and Related Phenomena* 96 (1998) 237-243.

[80] E. Guibal, R. Lorenzelli, T. Vincent, P. Lecloirec, "Application of silica-gel to metal-ion sorption - static and dynamic removal of uranyl ions", *Environmental Technology* 16 (1995) 101-114.

[81] Z.L. Guo, F.H. Guo, Z.Y. Tao, "Effects of phosphate and ionic strength upon uranium(VI) sorption onto alumina as a function of pH", *Radiochimica Acta* 94 (2006) 223-228.

[82] N. Baumann, V. Brendler, T. Arnold, G. Geipel, G. Bernhard, "Uranyl sorption onto gibbsite studied by time-resolved laser-induced fluorescence spectroscopy (TRLFS)", *Journal of Colloid and Interface Science* 290 (2005) 318-324.

[83] J.D. Prikryl, R.T. Pabalan, D.R. Turner, B.W. Leslie, "Uranium Sorption on α-Alumina - Effects of pH and surface area / solution-volume ratio", *Radiochimica Acta* 66/67 (1994) 291-296.

[84] T. Yamaguchi, S. Nakayama, T. Yoshida, "Interactions between anionic complex species of actinides and negatively charged mineral surfaces", *Radiochimica Acta* 92 (2004) 677-682.

[85] M.A. Denecke, J. Rothe, K. Dardenne, P. Lindqvist-Reis, "Grazing incidence (GI) XAFS measurements of Hf(IV) and U(VI) sorption onto mineral surfaces", *Physical Chemistry Chemical Physics* 5 (2003) 939-946.

[86] A. Krepelova, V. Brendler, S. Sachs, N. Baumann, G. Bernhard, "U(VI)-kaolinite surface complexation in absence and presence of humic acid studied by TRLFS", *Environmental Science & Technology* 41 (2007) 6142-6147.

[87] A. Krepelova, T. Reich, S. Sachs, J. Drebert, G. Bernhard, "Structural characterization of U(VI) surface complexes on kaolinite in the presence of humic acid using EXAFS spectroscopy", *Journal of Colloid and Interface Science* 319 (2008) 40-47.

[88] T.E. Payne, J.A. Davis, G.R. Lumpkin, R. Chisari, T.D. Waite, "Surface complexation model of uranyl sorption on Georgia kaolinite", *Applied Clay Science* 26 (2004) 151-162.

[89] C. Hennig, T. Reich, R. Dahn, A.M. Scheidegger, "Structure of uranium sorption complexes at montmorillonite edge sites", *Radiochimica Acta* 90 (2002) 653-657.

[90] C. Chisholm-Brause, S.D. Conradson, C.T. Buscher, P.G. Eller, D.E. Morris, "Speciation of uranyl sorbed at multiple binding sites on montmorillonite", *Geochimica Et Cosmochimica Acta* 58 (1994) 3625-3631.

[91] C.J. Chisholm-Brause, J.M. Berg, K.M. Little, R.A. Matzner, D.E. Morris, "Uranyl sorption by smectites: spectroscopic assessment of thermodynamic modeling", *Journal of Colloid and Interface Science* 277 (2004) 366-382.

[92] T. Arnold, S. Utsunomiya, G. Geipel, R.C. Ewing, N. Baumann, V. Brendler, "Adsorbed U(VI) surface species on muscovite identified by laser fluorescence spectroscopy and transmission electron microscopy", *Environmental Science & Technology* 40 (2006) 4646-4652.

[93] E.S. Chardon, D. Bosbach, N.D. Bryan, I.C. Lyon, C. Marquardt, J. Romer, D. Schild, D.J. Vaughan, P.L. Wincott, R.A. Wogelius, F.R. Livens, "Reactions of the feldspar surface with metal ions: Sorption of Pb(II), U(VI) and Np(V), and surface analytical studies of reaction with Pb(II) and U(VI)", *Geochimica Et Cosmochimica Acta* 72 (2008) 288-297.

[94] G. Geipel, T. Reich, V. Brendler, G. Bernhard, H. Nitsche, "Laser and X-ray spectroscopic studies of uranium-calcite interface phenomena", *Journal of Nuclear Materials* 248 (1997) 408-411.

[95] P. Thakur, R.C. Moore, G.R. Choppin, "Sorption of U(VI) species on hydroxyapatite", *Radiochimica Acta* 93 (2005) 385-391.

[96] A. Krestou, A. Xenidis, D. Panias, "Mechanism of aqueous uranium(VI) uptake by hydroxyapatite", *Minerals Engineering* 17 (2004) 373-381.

[97] Y. Arai, M. McBeath, J.R. Bargar, J. Joye, J.A. Davis, "Uranyl adsorption and surface speciation at the imogolite-water interface: Self-consistent spectroscopic and surface complexation models", *Geochimica Et Cosmochimica Acta* 70 (2006) 2492-2509.

[98] A.M. Jakobsson, Y. Albinsson, "Sorption of NpO_2^+ and Co^{2+} onto TiO_2", *Radiochimica Acta* 82 (1998) 257-262.

[99] O. Tochiyama, S. Endo, Y. Inoue, "Sorption of neptunium(V) on various iron oxides and hydrous iron oxides", *Radiochimica Acta* 68 (1995) 105-111.

[100] D.C. Girvin, L.L. Ames, A.P. Schwab, J.E. McGarrah, "Neptunium adsorption on synthetic amorphous iron oxyhydroxide", *Journal of Colloid and Interface Science* 141 (1991) 67-78.

[101] K. Nakata, T. Fukuda, S. Nagasaki, S. Tanaka, A. Suzuki, T. Tanaka, S. Muraoka, "Sorption of neptunium on iron-containing minerals", *Czechoslovak Journal of Physics* 49 (1999) 159-166.

[102] A. Jain, N. Rawat, S. Kumar, B.S. Tomar, V.K. Manchanda, S. Ramanathan, "Effect of humic acid on sorption of neptunium on hematite colloids", *Radiochimica Acta* 95 (2007) 501-506.

[103] A.Y. Teterin, K.I. Maslakov, Y.A. Teterin, S.N. Kalmykov, K.E. Ivanov, L. Vukcevic, A.B. Khasanova, N.S. Shcherbina, "Interaction of neptunyl with goethite (alpha-FeOOH), maghemite (γ-Fe_2O_3), and hematite (α-Fe_2O_3) in water as probed by X-ray photoelectron spectroscopy", *Russian Journal of Inorganic Chemistry* 51 (2006) 1937-1944.

[104] J.M. Combes, C.J. Chisholmbrause, G.E. Brown, G.A. Parks, S.D. Conradson, P.G. Eller, I.R. Triay, D.E. Hobart, A. Meijer, "EXAFS spectroscopic study of neptunium(V) sorption at the alpha-FeOOH water interface", *Environmental Science & Technology* 26 (1992) 376-382.

[105] M. Kohler, B.D. Honeyman, J.O. Leckie, "Neptunium(V) sorption on hematite (α-Fe_2O_3) in aqueous suspension: The effect of CO_2", *Radiochimica Acta* 85 (1999) 33-48.

[106] W.J. Li, Z.Y. Tao, "Comparative study on Np(V) sorption on oxides of aluminum and silicon: effects of humic substance and carbonate in solution", *Journal of Colloid and Interface Science* 267 (2003) 25-31.

[107] M. Del Nero, A. Assada, B. Made, R. Barillon, G. Duplatre, "Surface charges and Np(V) amorphous sorption Al and Fe on silicates", *Chemical Geology* 211 (2004) 15-45.

[108] O. Tochiyama, H. Yamazaki, T. Mikami, "Sorption of neptunium(V) on various aluminum oxides and hydrous aluminum oxides", *Radiochimica Acta* 73 (1996) 191-198.

[109] T. Wu, S. Amayri, T. Reich, "Neptunium(V) sorption onto gibbsite", *Radiochimica Acta* 97 (2009) 99-103.

[110] P.N. Pathak, G.R. Choppin, "Sorption of neptunyl(V) cations on suspended silicate: Effects of pH, ionic strength, complexing anions, humic acid, and metal ions", *Journal of Radioanalytical and Nuclear Chemistry* 274 (2007) 53-60.

[111] P.A. Wilk, D.A. Shaughnessy, R.E. Wilson, H. Nitsche, "Interfacial interactions between Np(V) and manganese oxide minerals manganite and hausmannite", *Environmental Science & Technology* 39 (2005) 2608-2615.

[112] Y. Arai, P.B. Moran, B.D. Honeyman, J.A. Davis, "In situ spectroscopic evidence for neptunium(V)-carbonate inner-sphere and outer-sphere ternary surface complexes on hematite surfaces", *Environmental Science & Technology* 41 (2007) 3940-3944.

[113] S. Aksoyoglu, W. Burkart, W. Goerlich, "Sorption of Neptunium on Clays", *Journal of Radioanalytical and Nuclear Chemistry* 149 (1991) 119-122.

[114] M.N. Sabodina, S.N. Kalmykov, Y.A. Sapozhnikov, E.V. Zakharova, "Neptunium, plutonium and Cs-137 sorption by bentonite clays and their speciation in pore waters", *Journal of Radioanalytical and Nuclear Chemistry* 270 (2006) 349-355.

[115] D.R. Turner, R.T. Pabalan, F.P. Bertetti, "Neptunium(V) sorption on montmorillonite: An experimental and surface complexation modeling study", *Clays and Clay Minerals* 46 (1998) 256-269.

[116] M. Zavarin, S.K. Roberts, N. Hakem, A.M. Sawvel, A.B. Kersting, "Eu(III), Sm(III), Np(V), Pu(V), and Pu(IV) sorption to calcite", *Radiochimica Acta* 93 (2005) 93-102.

[117] R.C. Moore, K. Holt, H.T. Zhao, A. Hasan, N. Awwad, M. Gasser, C. Sanchez, "Sorption of Np(V) by synthetic hydroxyapatite", *Radiochimica Acta* 91 (2003) 721-727.
[118] P. Thakur, R.C. Moore, G.R. Choppin, "$Np(V)O_2^+$ sorption on hydroxyapatite-effect of calcium and phosphate anions", *Radiochimica Acta* 94 (2006) 645-649.
[119] J.B. Dixon, S.B. Weed, Minerals in soil environments, Soil Science Soc. of America, Madison, Wisc., 1989.
[120] G.E. Brown, V.E. Henrich, W.H. Casey, D.L. Clark, C. Eggleston, A. Felmy, D.W. Goodman, M. Gratzel, G. Maciel, M.I. McCarthy, K.H. Nealson, D.A. Sverjensky, M.F. Toney, J.M. Zachara, "Metal oxide surfaces and their interactions with aqueous solutions and microbial organisms", *Chemical Reviews* 99 (1999) 77-174.
[121] C. Koretsky, "The significance of surface complexation reactions in hydrologic systems: a geochemist's perspective", *Journal of Hydrology* 230 (2000) 127-171.
[122] R. Drot, E. Simoni, M. Alnot, J.J. Ehrhardt, "Structural environment of uranium(VI) and europium(III) species sorbed onto phosphate surfaces: XPS and optical spectroscopy studies", *Journal of Colloid and Interface Science* 205 (1998) 410-416.
[123] N. Eglizaud, F. Miserque, E. Simoni, M. Schlegel, M. Descostes, "Uranium(VI) interaction with pyrite (FeS_2): Chemical and spectroscopic studies", *Radiochimica Acta* 94 (2006) 651-656.
[124] S.J. Hug, "*In situ* fourier transform infrared measurements of sulfate adsorption on hematite in aqueous solutions", *Journal of Colloid and Interface Science* 188 (1997) 415-422.
[125] A.R. Hind, S.K. Bhargava, A. McKinnon, "At the solid/liquid interface: FTIR/ATR - the tool of choice", *Advances in Colloid and Interface Science* 93 (2001) 91-114.
[126] A. Rossberg, K.U. Ulrich, S. Weiss, S. Tsushima, T. Hiemstra, A.C. Scheinostt, "Identification of uranyl surface complexes an ferrihydrite: Advanced EXAFS data analysis and CD-MUSIC modeling", *Environmental Science & Technology* 43 (2009) 1400-1406.
[127] S. Stumpf, T. Stumpf, K. Dardenne, C. Hennig, H. Foerstendorf, R. Klenze, T. Fanghanel, "Sorption of Am(III) onto 6-line- ferrihydrite and its alteration products: Investigations by EXAFS", *Environmental Science & Technology* 40 (2006) 3522-3528.
[128] M. Walter, T. Arnold, G. Geipel, A. Scheinost, G. Bernhard, "An EXAFS and TRLFS investigation on uranium(VI) sorption to pristine and leached albite surfaces", *Journal of Colloid and Interface Science* 282 (2005) 293-305.
[129] J. Rothe, M.A. Denecke, K. Dardenne, T. Fanghanel, "The INE-beamline for actinide research at ANKA", *Radiochimica Acta* 94 (2006) 691-696.
[130] K. Großmann, T. Arnold, E. Krawczyk-Barsch, S. Diessner, A. Wobus, G. Bernhard, R. Krawietz, "Identification of fluorescent U(V) and U(VI) microparticles in a multispecies biofilm by confocal laser scanning microscopy and fluorescence spectroscopy", *Environmental Science & Technology* 41 (2007) 6498-6504.
[131] S.J. Hug, B. Sulzberger, "*In-Situ* fourier-transform infrared spectroscopic evidence for the formation of several different surface complexes of oxalate on TiO_2 in the aqueous-phase", *Langmuir* 10 (1994) 3587-3597.
[132] K. Müller, V. Brendler, H. Foerstendorf, G. Bernhard, "Sorption of Np(V) onto TiO_2, SiO_2, and ZnO: An *in situ* ATR FT-IR spectroscopic study", *Environmental Science &Technology* 43 (2009) 7665-7670.
[133] F.M. Mirabella, "Internal reflection spectroscopy", *Applied Spectroscopy Reviews* 21 (1985) 45-178.

[134] J.W. Strojek, J. Mielczarski, P. Nowak, "Spectroscopic investigations of the solid-liquid interface by the ATR technique", *Advances in Colloid and Interface Science* 19 (1983) 309-327.
[135] R.C. Gore, R.B. Barnes, E. Petersen, "Infrared absorption of aqueous solutions of organic acids and their salts", *Analytical Chemistry* 21 (1949) 382-386.
[136] S.Y. Venyaminov, F.G. Prendergast, "Water (H_2O and D_2O) molar absorptivity in the 1000-4000 cm^{-1} range and quantitative infrared spectroscopy of aqueous solutions", *Analytical Biochemistry* 248 (1997) 234-245.
[137] V. Neck, J.I. Kim, B.S. Seidel, C.M. Marquardt, K. Dardenne, M.P. Jensen, W. Hauser, "A spectroscopic study of the hydrolysis, colloid formation and solubility of Np(IV)", *Radiochimica Acta* 89 (2001) 439-446.
[138] H. Moll, T. Reich, Z. Szabo, "The hydrolysis of dioxouranium(VI) investigated using EXAFS and 17-O NMR", *Radiochimica Acta* 88 (2000) 411-415.
[139] C. Zscherp, A. Barth, "Reaction-induced infrared difference spectroscopy for the study of protein reaction mechanisms", *Biochemistry* 40 (2001) 1875-1883.
[140] W. Mäntele, "Reaction-Induced Infrared Difference Spectroscopy for the Study of Protein Function and Reaction-Mechanisms", *Trends in Biochemical Sciences* 18 (1993) 197-202.
[141] C.B. Mendive, T. Bredow, M.A. Blesa, D.W. Bahnemann, "ATR-FTIR measurements and quantum chemical calculations concerning the adsorption and photoreaction of oxalic acid on TiO_2", *Physical Chemistry Chemical Physics* 8 (2006) 3232-3247.
[142] A.J. McQuillan, "Probing solid-solution interfacial chemistry with ATR-IR spectroscopy of particle films", *Advanced Materials* 13 (2001) 1034-+.
[143] G. Lefèvre, M. Fedoroff, "Sorption of sulfate ions onto hematite studied by attenuated total reflection-infrared spectroscopy: Kinetics and competition with other ions", *Physics and Chemistry of the Earth* 31 (2006) 499-504.
[144] D. Peak, R.G. Ford, D.L. Sparks, "An in situ ATR-FTIR investigation of sulfate bonding mechanisms on goethite", *Journal of Colloid and Interface Science* 218 (1999) 289-299.
[145] A. Voegelin, S.J. Hug, "Catalyzed oxidation of arsenic(III) by hydrogen peroxide on the surface of ferrihydrite: An in situ ATR-FTIR study", *Environmental Science & Technology* 37 (2003) 972-978.
[146] C.M. Su, D.L. Suarez, "In situ infrared speciation of absorbed carbonate on aluminum and iron oxide", *Clays and Clay Minerals* 45 (1997) 814-825.
[147] E.J. Elzinga, D.L. Sparks, "Phosphate adsorption onto hematite: An in situ ATR-FTIR investigation of the effects of pH and loading level on the mode of phosphate surface complexation", *Journal of Colloid and Interface Science* 308 (2007) 53-70.
[148] C. Hennig, J. Tutschku, A. Rossberg, G. Bernhard, A.C. Scheinost, "Comparative EXAFS investigation of uranium(VI) and -(IV) aquo chloro complexes in solution using a newly developed spectroelectrochemical cell", *Inorganic Chemistry* 44 (2005) 6655-6661.
[149] K. Müller, H. Foerstendorf, S. Tsushima, V. Brendler, G. Bernhard, "Direct spectroscopic characterization of aqueous actinyl(VI) species: A comparative study of Np and U", *Journal of Physical Chemistry A* 113 (2009) 6626-6632.
[150] T.J. Wolery, "EQ3/6. A software package for the geochemical modeling of aqueous systems: Package Overview and Installation Guide", Lawrence Livermore National Laboratory, California, USA, 1992.
[151] W. Hummel, U. Berner, E. Curti, F.J. Pearson, T. Thoenen, "Nagra/PSI chemical thermodynamic data base 01/01", Universal Publishers, Parkland, Florida, 2002.

[152] I. Grenthe, J. Fuger, R.J.M. Konings, R.J. Lemire, A.B. Muller, C. Nguyen-Trung Cregu, H. Wanner, Chemical thermodynamics of uranium, OECD Nuclear Energy Agency, Issy-les-Moulineaux, France, 1992.

[153] R. Guillaumont, T. Fanghänel, J. Fuger, I. Grenthe, V. Neck, D.A. Palmer, M.H. Rand, Update on the Chemical Thermodynamics of Uranium, Neptunium, Plutonium, Americium and Technetium, Elsevier, Amsterdam, 2003.

[154] C. Nguyen-Trung, G.M. Begun, D.A. Palmer, "Aqueous uranium complexes. 2. Raman spectroscopic study of the complex formation of the dioxouranium(VI) ion with a variety of inorganic and organic ligands", *Inorganic Chemistry* 31 (1992) 5280-5287.

[155] C. Nguyen-Trung, D.A. Palmer, G.M. Begun, C. Peiffert, R.E. Mesmer, "Aqueous uranyl complexes. 1. Raman spectroscopic study of the hydrolysis of uranyl(VI) in solutions of trifluoromethanesulfonic acid and/or tetramethylammonium hydroxide at 25 °C and 0.1 MPa", *Journal of Solution Chemistry* 29 (2000) 101-129.

[156] L. Maya, G.M. Begun, "A Raman spectroscopic study of hydroxo and carbonato species of the uranyl (VI) ion", *Journal of Inorganic & Nuclear Chemistry* 43 (1981) 2827-2832.

[157] K.I.M. Ingram, L.J.L. Häller, N. Kaltsoyannis, "Density functional theory investigation of the geometric and electronic structures of $[UO_2(H_2O)_m(OH)_n]^{2-n}$ (n+m=5)", *Dalton Transactions* (2006) 2403-2414.

[158] U. Wahlgren, H. Moll, I. Grenthe, B. Schimmelpfennig, L. Maron, V. Vallet, O. Gropen, "Structure of uranium(VI) in strong alkaline solutions. A combined theoretical and experimental investigation", *Journal of Physical Chemistry A* 103 (1999) 8257-8264.

[159] G. Geipel, A. Brachmann, V. Brendler, G. Bernhard, H. Nitsche, "Uranium(VI) sulfate complexation studied by time-resolved laser-induced fluorescence spectroscopy (TRLFS)", *Radiochimica Acta* 75 (1996) 199-204.

[160] E. Selli, V. Eliet, M.R. Spini, G. Bidoglio, "Effects of humic acids on the photoinduced reduction of U(VI) in the presence of semiconducting TiO_2 particles", *Environmental Science & Technology* 34 (2000) 3742-3748.

[161] M. Kakihana, T. Nagumo, M. Okamoto, H. Kakihana, "Coordination structures for uranyl carboxylate complexes in aqueous-solution studied by IR and C-13 NMR-Spectra", *Journal of Physical Chemistry* 91 (1987) 6128-6136.

[162] P.G. Allen, J.J. Bucher, D.L. Clark, N.M. Edelstein, S.A. Ekberg, J.W. Gohdes, E.A. Hudson, N. Kaltsoyannis, W.W. Lukens, M.P. Neu, P.D. Palmer, T. Reich, D.K. Shuh, C.D. Tait, B.D. Zwick, "Multinuclear NMR, Raman, EXAFS, and X-Ray-Diffraction Studies of Uranyl Carbonate Complexes in near-Neutral Aqueous-Solution - X-Ray Structure of $[C(NH_2)_3]_6[(UO_2)_3(CO_3)_6]_6.5H_2O$", *Inorganic Chemistry* 34 (1995) 4797-4807.

[163] Z. Szabó, H. Moll, I. Grenthe, "Structure and dynamics in the complex ion $(UO_2)_2(CO_3)(OH)_3^-$", *Journal of the Chemical Society-Dalton Transactions* (2000) 3158-3161.

[164] G. Meinrath, Y. Kato, T. Kimura, Z. Yoshida, "Solid-aqueous phase equilibria of uranium(VI) under ambient conditions", *Radiochimica Acta* 75 (1996) 159-167.

[165] N.A. Budantseva, A.M. Fedosseev, A.A. Bessonov, M.S. Grigoriev, J.C. Krupa, "Synthesis and spectroscopic properties of neptunium(VI) and plutonium(VI) oxoanion compounds", *Radiochimica Acta* 88 (2000) 291-295.

[166] W.C. Waggener, "Measurement of the absorption spectra of neptunium ions in heavy water solution from 0.35 to 1.85 μ", *Journal of Physical Chemistry* 62 (1958) 382-383.

[167] L.R. Morss, N.M. Edelstein, J. Fuger, The chemistry of the actinide and transactinide elements, Springer, 2006.
[168] C. Nguyen-Trung, D.A. Palmer, G.M. Begun, C. Peiffert, R.E. Mesmer, "Aqueous uranyl complexes 1. Raman spectroscopic study of the hydrolysis of uranyl(VI) in solutions of trifluoromethanesulfonic acid and/or tetramethylammonium hydroxide at 25 °C and 0.1 MPa", *Journal of Solution Chemistry* 29 (2000) 101-129.
[169] C. Madic, G.M. Begun, D.E. Hobart, R.L. Hahn, "Raman spectroscopy of neptunyl and plutonyl ions in aqueous solution - Hydrolysis of Np(VI) and Pu(VI) and Disproportionation of Pu(V)", *Inorganic Chemistry* 23 (1984) 1914-1921.
[170] S.D. Reilly, M.P. Neu, "Pu(VI) hydrolysis: Further evidence for a dimeric plutonyl hydroxide and contrasts with U(VI) chemistry", *Inorganic Chemistry* 45 (2006) 1839-1846.
[171] G.A. Shamov, G. Schreckenbach, "Density functional studies of actinyl aquo complexes studied using small-core effective core potentials and a scalar four-component relativistic method", *Journal of Physical Chemistry A* 109 (2005) 10961-10974.
[172] H. Zänker, K.U. Ulrich, K. Opel, V. Brendler, "Influence of colloids on uranium transport in nuclear waste repositories and abandoned uranium mines - A critical comparison", *Geochimica Et Cosmochimica Acta* 70S (2006) A731-A731.
[173] H. Zänker, G. Huttig, T. Arnold, H. Nitsche, "Formation of iron-containing colloids by the weathering of phyllite", *Aquatic Geochemistry* 12 (2006) 299-325.
[174] R. Sjoblom, J.C. Hindman, "Spectrophotometry of neptunium in perchloric acid solutions", *Journal of the American Chemical Society* 73 (1951) 1744-1751.
[175] S. Tsushima, S. Nagasaki, S. Tanaka, A. Suzuki, "A Raman spectroscopic study of uranyl species adsorbed onto colloidal particles", *Journal of Physical Chemistry B* 102 (1998) 9029-9032.
[176] S.P. Pasilis, J.E. Pemberton, "Spectroscopic investigation of uranyl(VI) and citrate coadsorption to Al_2O_3", *Geochimica Et Cosmochimica Acta* 72 (2008) 277-287.
[177] O. Carp, C.L. Huisman, A. Reller, "Photoinduced reactivity of titanium dioxide", *Progress in Solid State Chemistry* 32 (2004) 33-177.
[178] A.R. Milnes, R.W. Fitzpatrick, "Titanium and zirconium minerals", in: J.B. Dixon, S.B. Weed, "Minerals in soil environments", Soil Science Soc. of America, Madison, Wisc., 1989.
[179] A.v. Hippel, R.G. Breckenridge, F.G. Chesley, L. Tisza, "High dielectric constant ceramics", *Industrial and Engineering Chemistry* 38 (1946) 1097-1109.
[180] S. Lebrette, C. Pagnoux, P. Abelard, "Fabrication of titania dense layers by electrophoretic deposition in aqueous media", *Journal of the European Ceramic Society* 26 (2006) 2727-2734.
[181] G. Lefèvre, M. Duc, M. Fedoroff, "Accuracy in the determination of acid-base properties of metal oxide surfaces", in: J. Lützenkirchen, "Surface Complexation Modeling", Elsevier, Amsterdam, 2006.
[182] M.K. Ridley, V.A. Hackley, M.L. Machesky, "Characterization and surface-reactivity of nanocrystalline anatase in aqueous solutions", *Langmuir* 22 (2006) 10972-10982.
[183] M. Kosmulski, J.B. Rosenholm, "High ionic strength electrokinetics of anatase in the presence of multivalent inorganic ions", *Colloids and Surfaces A-Physicochemical and Engineering Aspects* 248 (2004) 121-126.
[184] M. Kosmulski, E. Matijevic, "Zeta-potential of anatase (TiO_2) in mixed solvents", *Colloids and Surfaces* 64 (1992) 57-65.

[185] H. Wijnja, C.P. Schulthess, "Carbonate adsorption mechanism on goethite studied with ATR-FTIR, DRIFT, and proton coadsorption measurements", *Soil Science Society of America Journal* 65 (2001) 324-330.

[186] V. Eliet, G. Bidoglio, "Kinetics of the laser-induced photoreduction of U(VI) in aqueous suspensions of TiO_2 particles", *Environmental Science & Technology* 32 (1998) 3155-3161.

[187] R. Amadelli, A. Maldotti, S. Sostero, V. Carassiti, "Photodeposition of uranium-oxides onto TiO_2 from aqueous uranyl solutions", *Journal of the Chemical Society-Faraday Transactions* 87 (1991) 3267-3273.

[188] M.I. Litter, "Heterogeneous photocatalysis - Transition metal ions in photocatalytic systems", *Applied Catalysis B-Environmental* 23 (1999) 89-114.

[189] J. Yu, X. Zhao, Q. Zhao, "Effect of surface structure on photocatalytic activity of TiO_2 thin films prepared by sol-gel method", *Thin Solid Films* 379 (2000) 7-14.

[190] T. Kawahara, T. Ozawa, M. Iwasaki, H. Tada, S. Ito, "Photocatalytic activity of rutile-anatase coupled TiO_2 particles prepared by a dissolution-reprecipitation method", *Journal of Colloid and Interface Science* 267 (2003) 377-381.

[191] I. Billard, E. Ansoborlo, K. Apperson, S. Arpigny, M.E. Azenha, D. Birch, P. Bros, H.D. Burrows, G. Choppin, L. Couston, V. Dubois, T. Fanghanel, G. Geipel, S. Hubert, J.I. Kim, T. Kimura, R. Klenze, A. Kronenberg, M. Kumke, G. Lagarde, G. Lamarque, S. Lis, C. Madic, G. Meinrath, C. Moulin, R. Nagaishi, D. Parker, G. Plancque, F. Scherbaum, E. Simoni, S. Sinkov, C. Viallesoubranne, "Aqueous solutions of uranium(VI) as studied by time-resolved emission spectroscopy: A round-robin test", *Applied Spectroscopy* 57 (2003) 1027-1038.

[192] K. Grossmann, T. Arnold, A. Ikeda-Ohno, R. Steudtner, G. Geipel, G. Bernhard, "Fluorescence properties of a uranyl(V)-carbonate species $[U(V)O_2(CO_3)_3]^{5-}$ at low temperature", *Spectrochimica Acta Part A-Molecular and Biomolecular Spectroscopy* 72 (2009) 449-453.

[193] A. Kirishima, T. Kimura, O. Tochiyama, Z. Yoshida, "Luminescence study of tetravalent uranium in aqueous solution", *Chemical Communications* (2003) 910-911.

[194] A. Kirishima, T. Kimura, R. Nagaishi, O. Tochiyama, "Luminescence properties of tetravalent uranium in aqueous solution", *Radiochimica Acta* 92 (2004) 705-710.

[195] K.U. Ulrich, A. Rossberg, H. Foerstendorf, H. Zanker, A.C. Scheinost, "Molecular characterization of uranium(VI) sorption complexes on iron(III)-rich acid mine water colloids", *Geochimica Et Cosmochimica Acta* 70 (2006) 5469-5487.

[196] T. Brasser, J. Droste, I. Müller-Lyda, J. Neles, M. Sailer, G. Schmidt, M. Steinhoff, "Endlagerung wärmeentwickelnder radioaktiver Abfälle in Deutschland", Gesellschaft für Anlagen- und Reaktorsicherheit (GRS) mbH Braunschweig / Darmstadt, 2008.

[197] G.V. Franks, Y. Gan, "Charging behavior at the alumina-water interface and implications for ceramic processing", *Journal of the American Ceramic Society* 90 (2007) 3373-3388.

[198] C. Dyer, P.J. Hendra, W. Forsling, M. Ranheimer, "Surface hydration of aqueous gamma-Al_2O_3 studied by fourier-transform Raman and infrared-spectroscopy .1. Initial results", *Spectrochimica Acta Part A-Molecular and Biomolecular Spectroscopy* 49 (1993) 691-705.

[199] G. Lefèvre, M. Duc, P. Lepeut, R. Caplain, M. Fedoroff, "Hydration of γ-alumina in water and its effects on surface reactivity", *Langmuir* 18 (2002) 7530-7537.

[200] X. Carrier, E. Marceau, J.F. Lambert, M. Che, "Transformations of gamma-alumina in aqueous suspensions 1. Alumina chemical weathering studied as a function of pH", *Journal of Colloid and Interface Science* 308 (2007) 429-437.

[201] D.H. Lee, R.A. Condrate, "An FTIR spectral investigation of the structural species found on alumina surfaces", *Materials Letters* 23 (1995) 241-246.
[202] S. Desset, O. Spalla, P. Lixon, B. Cabane, "Variation of the surface state of alpha-alumina through hydrothermal treatments", *Colloids and Surfaces a-Physicochemical and Engineering Aspects* 196 (2002) 1-10.
[203] H. Foerstendorf, K. Heim, "Spectroscopic identification of ternary carbonate complexes upon U(VI) sorption onto ferrihydrite", *Geochimica Et Cosmochimica Acta,* 73 (2009) A386.
[204] M.C. Duff, J.U. Coughlin, D.B. Hunter, "Uranium co-precipitation with iron oxide minerals", *Geochimica Et Cosmochimica Acta* 66 (2002) 3533-3547.
[205] Z.J. Guo, C. Yan, J. Xu, W.S. Wu, "Sorption of U(VI) and phosphate on gamma-alumina: Binary and ternary sorption systems", *Colloids and Surfaces A-Physicochemical and Engineering Aspects* 336 (2009) 123-129.
[206] E. Laiti, P. Persson, L.O. Ohman, "Balance between surface complexation and surface phase transformation at the alumina/water interface", *Langmuir* 14 (1998) 825-831.
[207] L.D. Frederickson, "Characterization of hydrated aluminas by infrared spectroscopy - application to study of bauxite ores", *Analytical Chemistry* 26 (1954) 1883-1885.
[208] A. Krepelova, "Influence of humic acid on the sorption of uranium(VI) and americium(III) onto kaolinite", TU Dresden, 2007.
[209] P. Misaelides, A. Godelitsas, "Interaction of actinides with natural microporous materials: A review", *Czechoslovak Journal of Physics* 49 (1999) 167-174.
[210] L.L. Ames, J.E. McGarrah, B.A. Walker, "Sorption of uranium and radium by biotite, muscovite, and phlogopite", *Clays and Clay Minerals* 31 (1983) 343-351.
[211] E.S. Ilton, A. Haiduc, C.O. Moses, S.M. Heald, D.C. Elbert, D.R. Veblen, "Heterogeneous reduction of uranyl by micas: Crystal chemical and solution controls", *Geochimica Et Cosmochimica Acta* 68 (2004) 2417-2435.
[212] S.Y. Lee, M.H. Baik, Y.B. Lee, "Adsorption of uranyl ions and microscale distribution on Fe-bearing mica", *Applied Clay Science* 44 (2009) 259-264.
[213] R.J. Pruett, H.L. Webb, "Sampling and analysis of KGa-1b well-crystallized kaolin source clay", *Clays and Clay Minerals* 41 (1993) 514-519.
[214] Z.Y. Tao, T.W. Chu, W.J. Li, J.Z. Du, X.X. Dai, Y.J. Gu, "Cation adsorption of NpO_2^+, UO_2^{2+}, Zn^{2+}, Sr^{2+}, Yb^{3+}, and Am^{3+} onto oxides of Al, Si, and Fe from aqueous solution: ionic strength effect", *Colloids and Surfaces A* 242 (2004) 39-45.
[215] M.H. Bradbury, B. Bayens, "Modelling sorption data for the actinides Am(III), Np(V) and Pa(V) on montmorillonite", *Radiochimica Acta* 94 (2006) 619-625.
[216] A. Ikeda-Ohno, C. Hennig, A. Rossberg, H. Funke, A.C. Scheinost, G. Bernhard, T. Yaita, "Electrochemical and complexation behavior of neptunium in aqueous perchlorate and nitrate solutions", *Inorganic Chemistry* 47 (2008) 8294-8305.
[217] K. Opel, S. Weiss, S. Hubener, H. Zanker, G. Bernhard, "Study of the solubility of amorphous and crystalline uranium dioxide by combined spectroscopic methods", *Radiochimica Acta* 95 (2007) 143-149.
[218] P.K. Glasoe, F.A. Long, "Use of glass electrodes to measure acidities in deuterium oxide", *Journal of Physical Chemistry* 64 (1960) 188-190.